TP 8275E

DEVELOPMENT OF A METHOD FOR ESTIMATING SHIP PERFORMANCE CAPABILITIES AND IDENTIFYING LIMITING CONDITIONS WHEN TRANSITING ICE RIDGES

prepared for
Transportation Development Centre
Transport Canada

May 1987

by

John T. Stubbs
Richard Wiefelspuett
Stefan Gordin
John Fowlis

Wartsila Arctic Inc.

DISCLAIMER The contents of this report reflect the views of the authors and not necessarily the official view or opinions of the Transportation Development Centre of Transport Canada.

Un sommaire en francais de ce rapport est inclus avant la Table des matieres.

Transport Canada Transports Canada

Development Développement

REPORT DOCUMENTATION FORM

1. Transport Canada Report No.
TP 8275E

2. TDC Project No.
6669/70

3. Recipient's Catalogue No.

4. Title and Subtitle
Development of a Method for Estimating Ship Performance Capabilities and Identifying Limiting Conditions when Transiting Ice Ridges

5. Report Date
May 1987

6. Performing Organization Report No.

7. Author(s)
John T. Stubbs, Richard Wiefelspuett, Stefan Gordin and John Fowlis

8. Transport Canada File No.
D1460-234

9. Performing Organization Name and Address
Wartsila Arctic Inc.
Suite 201
1684 West 8th Avenue
Vancouver, B.C. V6J 1V4

10. DSS File No.
09SD.T8200-6-6500

11. DSS or Transport Canada Contract No.
T8200-6-6500/01-SB

12. Sponsoring Agency Name and Address
Transportation Development Centre (TDC)
200 Dorchester Blvd. West
Suite 601, West Tower
Montreal, Quebec H2Z 1X4

13. Type of Report and Period Covered
Final

14. Sponsoring Agency Code

15. Supplementary Notes

16. TDC Project Officer
N.R. Gore, C. Nowicki

17. Abstract

Ship performance capabilities when transiting first year ridges are evaluated. Performance limits are established as a function of ship main particulars and principal ice characteristics. A literature search and assessment of public material define the state-of-the-art. Field test data of ridge profiles are analyzed and a functional relation between ridge parameters is identified. The analyses of public and proprietary ridge full scale penetration tests lead to a formulation for the prediction of ridge resistance. Theoretical evaluations and consideration of model and full scale tests are utilized to develop a formula for the prediction of ridge extraction forces.

In a systematic analysis employing computer simulations, performance capabilities of a family of ships are tested. The influence of ship power, ship size and form on penetration resistance and extraction forces is investigated using the prediction models. The significance of particular findings for practical design applications is interpreted. Finally, recommendations for further R&D applicable to regulations regarding navigation in Arctic waters are made.

18. Key Words
Ship, Vessel, Icebreaking, Performance, Ice Ridges

19. Distribution Statement
Limited number of copies available from the Transportation Development Centre

20. Security Classification (of this report)
Unclassified

21. Security Classification (of this page)
Unclassified

22. No. of Pages
168

23. Price

Canada

Canada Canada

Développement Development

FORMULE DOCUMENTAIRE DU RAPPORT

1. Nº du rapport Transports Canada **TP 8275E**	2. Nº de l'étude — CDT 6669/70	3. Nº de catalogue du destinataire

4. Titre et sous-titre **Development of a Method for Estimating Ship Performance Capabilities and Identifying Limiting Conditions when Transiting Ice Ridges**	5. Date du rapport Mai 1987 6. Nº du rapport de l'organisme exécutant
7. Auteur(s) **John T. Stubbs, Richard Wiefelspuett, Stefan Gordin et John Fowlis**	8. Nº de dossier Transports Canada D1460-234
9. Nom et adresse de l'organisme exécutant Wartsila Arctic Inc. Suite 201 1684 West 8th Avenue Vancouver (Colombie-Britannique) V6J 1V4	10. Nº de dossier — ASC 09SD.T8200-6-6500 11. Nº de contrat — ASC ou Transports Canada T8200-6-6500/01-SB
12. Nom et adresse de l'organisme parrain Centre de développement des transports (CDT) 200 ouest, boul. Dorchester Suite 601, tour ouest Montréal (Québec) H2Z 1X4	13. Genre de rapport et période visée Final 14. Code de l'organisme parrain
15. Remarques additionnelles	16. Agent de projet — CDT **N.R. Gore, C. Nowicki**

17. Résumé

Le présent rapport concerne l'aptitude des navires à franchir des crêtes de première année, en fonction des principales caractéristiques du navire considéré et des propriétés de glaces rencontrées. Un tour d'horizon documentaire du domaine a été accompli, suivi de l'évaluation des données tombées dans le domaine public. Les résultats de campagnes de mesurage qui visaient à reconnaître les nombreux profils de crête existants sont analysés et une formule fonctionnelle reliant les divers paramètres caractéristiques est proposée. Les résultats des essais de franchissement en vraie grandeur faits par les secteurs privé et public sont analysés et débouchent sur une formule de prévision de la résistance des crêtes au franchissement. Enfin, intégrant le résultat de travaux théoriques, d'essais sur modèles réduits et d'essais en vraie grandeur, une formule est donnée, qui permet de calculer la force nécessaire à un navire pour se dégager d'une crête.

L'aptitude de familles de navires à franchir des crêtes de glace a été déterminée grâce à une analyse systématique de la question par la méthode des simulations informatiques. En se basant sur les modèles de prévision élaborés, les conditions opérationnelles limites des navires sont données en fonction de leur puissance installée, de leur taille et de la forme de leur proue. L'importance de certaines conclusions est discutée dans l'optique d'une application pratique. Enfin, des recommandations sont formulées sur la poursuite de la recherche et sur la réglementation de la navigation dans les eaux arctiques.

18. Mots-clés Navire, brise-glace, performances, crêtes de glace.	19. Diffusion Le Centre de développement des transports dispose d'un nombre limité d'exemplaires.

20. Classification de sécurité (de ce rapport) non classifié	21. Classification de sécurité (de cette page) non classifiée	22. Nombre de pages 168	23. Prix

CDT TDC 79-005
Rev 86

SUMMARY

1. INTRODUCTION

Based on an unsolicited proposal submitted to the Transportation Development Centre of Transport Canada in 1985, Wartsila Arctic Inc. was asked to develop a method for estimating ship performance capabilities and limitations for operations in first year ice ridges.

2. OBJECTIVES

The present study forms part of a long-term research and development program geared to improve reliability and cost effectiveness of Arctic marine transportation.

The objective of the work is to systematically study Arctic ship performance capabilities in transiting first year ridges and establish performance limits as a function of ship main particulars.

3. SCOPE OF WORK

To achieve the stated objective, the following tasks were completed:

- comprehensive literature search and assessment of state of the art in terms of ship transit through ridges;
- compilation of proprietary and public domain ship test data relevant to the subject matter in a sizeable data base;
- analysis and interpretation of ridge parameters relative to ship performance capabilities;
- analysis of full scale ridge penetration tests and identification of the most significant ship size and geometry parameters;
- development of an analytical model describing the major components during the extraction phase; and,
- establishment of criteria applicable to the performance limits of ships in first year ridges.

The following sections summarize the principal results of the individual tasks.

4. RESULTS

4.1 Definition of Ridges

The investigation of 136 ridge profiles measured during field tests highlighted distinct differences in the geometry of ridges. Ridges with equivalent sail heights (h_s) differed significantly in terms of the corresponding cross sectional area (CSA). The ratio of average ridge thickness (h_r) and ridge width (W_r) was found to be a significant parameter distinguishing ridges from different regions. The following values were established:

Area	h_r/W_r
Baltic Sea	0.02 - 0.06
Beaufort Sea	0.05 - 0.07
Bering Sea	0.08 - 0.09

To facilitate the determination of ridge CSA as a function of h_s, a functional relation with h_r/W_r as parameter was derived in the following form:

$$\mathrm{CSA} = 1310 \times \tanh(h_s) \times \left(\frac{\tanh(h_s)}{500 \times (1 - \tanh^2(h_s))} \right)^{(150 \times (hr/Wr - .02)^2)} \tag{1}$$

4.2 Ridge Penetration Analysis

The analytical work in this section focused entirely on full scale ridge penetration tests. The total energy required to penetrate ridges was derived from 51 separate tests. Linear functions expressing penetration energy as a function of CSA and correspondingly average penetration resistance as a function of h_r were developed for the tested ships.

In a comprehensive sensitivity analysis, the ship hull size and geometry parameters of most significant influence on the resistance were identified. For the purpose of practical applications the identified parameters were combined in a formula expressing the average penetration resistance as a function of the average ridge thickness h_r and the ship parameters:

$$R_{ridge} = .0886 \cdot h_r \cdot [B^2 \, B/d \cdot 1/\cos\varphi \;\; 1/\tan\alpha \;\; 1/\sin\beta \; + \mu_d \cdot L_m \, (0.61B + .45d)] \tag{2}$$

where:

B = Breadth
d = Draft

α = 1/2 angle of entrance
β = Angle between section and vertical plane
φ = Buttock angle to horizontal
μ_d = Dynamic friction coefficient
L_m = Length of vessel's midbody

For a parametric series of icebreaking ships, the limits of continuous transit through first year ridges were determined. The investigated ships are illustrated in the following table:

TABLE 1 Ship Parameter

Block Coefficient C_b		.56		
B/d		3.3		
Displacement	[t]:	5,000	15,000	30,000
Thrust Levels in Bollard Condition	[t]:			
	Low:	40	150	300
	Medium:	95	275	550
	High:	150	400	800
Corresponding Main Particulars [m]:				
	B:	20.0	25.0	30.0
	d:	6.0	7.5	9.0
	L_{CWL}:	75.0	120.0	135.0
Bow Geometries:				
	Conventional:	$\psi = 43^\circ$		
	Medium:	$\psi = 35^\circ$		
	Extreme:	$\psi = 29^\circ$		

Ridge sail height, ice thickness and consolidated thickness within the ridges were varied in the following ranges:

TABLE 2 Ice Parameters

Parameter	Minimum	Maximum
h_s (m)	0.10	3.70
h_{ice} (m)	0.10	1.80
h_c/h_{ice}	0	2

A computer simulation model was applied for each ship and each ice condition (h_{ice}, h_c); the sail height of the limiting ridge which stopped the ship was determined.

The results are summarized in Table 3. The table permits, within the tested range of ship particulars, determination of the limiting ice conditions, i.e. a combination of h_{ice} and h_c, with installed power and main particulars as parameters.

4.3 Ridge Extraction

The analysis of extraction was restricted to the break-out force at the moment the ship starts to move after getting stopped in a ridge. Although the resistance in the broken channel, when the ship moves astern, influences the speed of advance of the ship, this situation usually does not form the limiting condition and was therefore not studied in this project.

Based on a combination of theoretical work, model test results and full scale results, the following formulation for the extraction force of a ship totally embedded in a ridge was derived:

$$F_E = q_M \left(\mu_s L_P + C_E L_E/2 \right) \qquad (3)$$

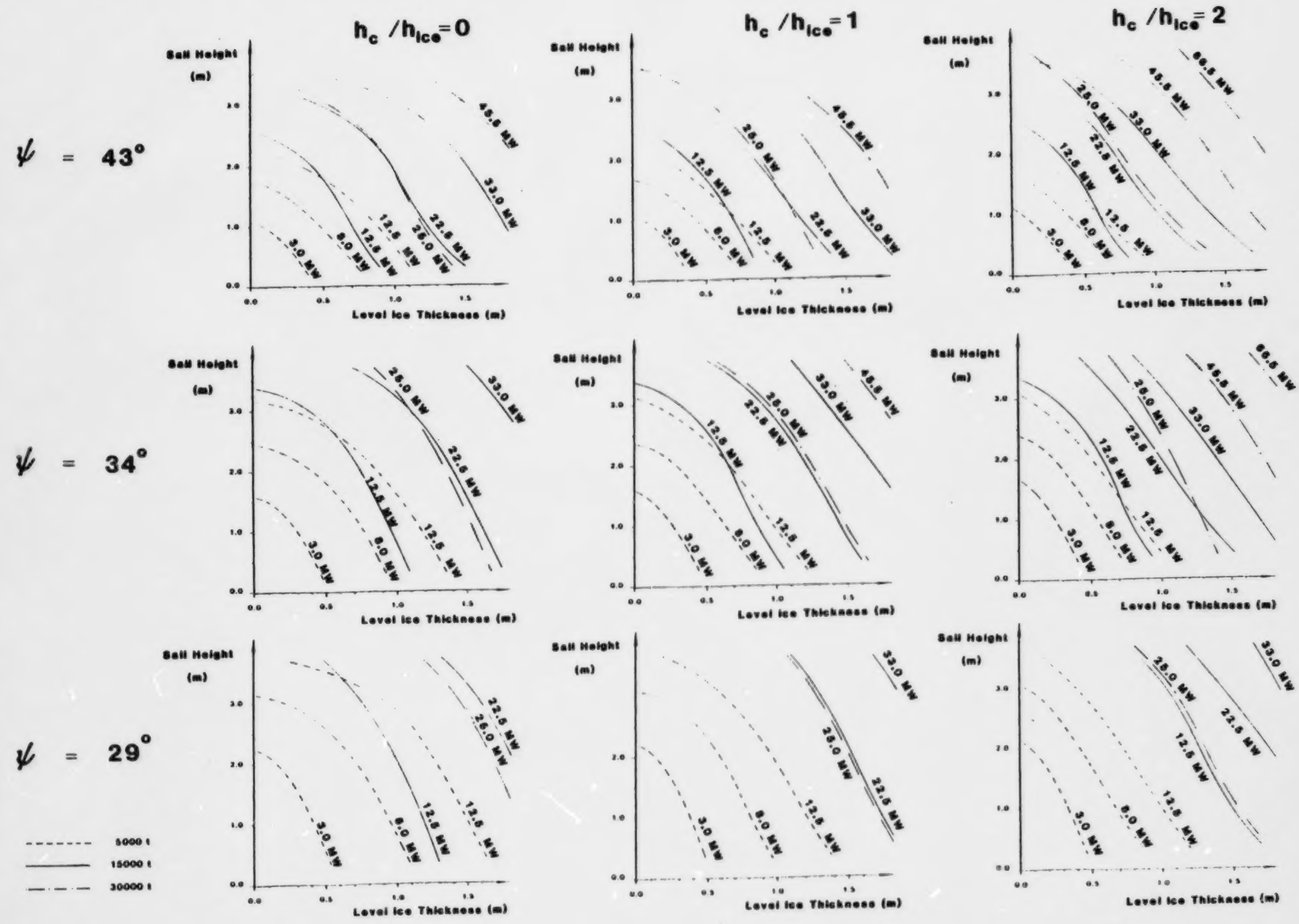

Table 3 Limiting Ice Conditions for Continuous Mode of Operation

where:

$$q_M = h_r\,[0.68\ B\ (1 - 0.11\ d/h_r) + 0.39\ d\ (1 + 0.15\ d/h_r)]\quad (\mathrm{kN/m})$$

valid for $d/hr < 3$

μ_s = static friction coefficient between ship hull and ridge mass
L_p = length of parallel midbody
C_E = $\mu_s - (0.4 + 5 \sin\psi)\ \alpha_s/1000$ with α_s in degrees
L_E = entrance length
B = ship breadth
d = ship draft
h_r = average ridge thickness
ψ = angle between horizontal plane and hull in a section perpendicular to the waterline
α_s = half waterline angle at stem, however, disregarding abrupt changes very close to the centerline

This formula, as applied to the parametric ship series described in the previous section, results in the following approximate power requirements:

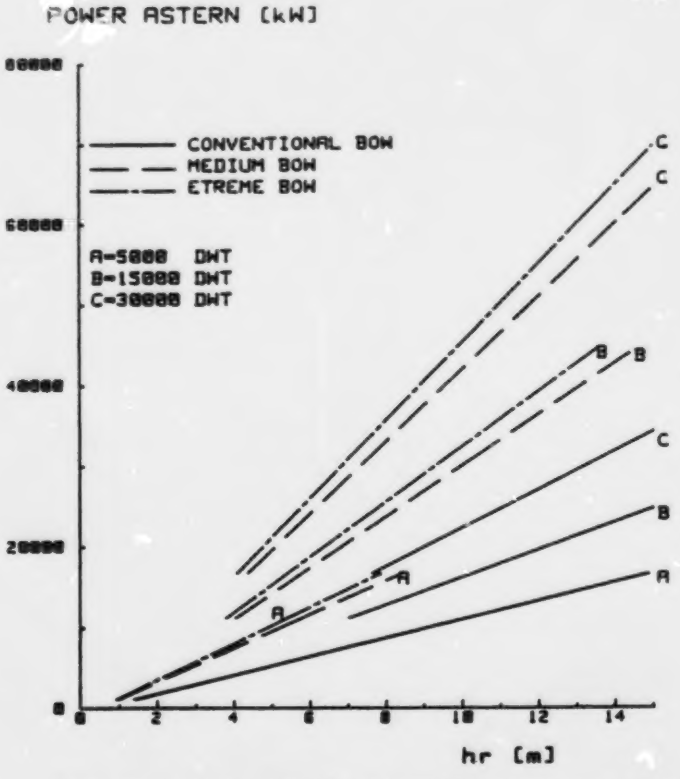

Figure 1 Approximate Power Requirements for Vessels Totally Embedded in a Ridge.

For vessel particulars, see Section 4.2.

5. CONCLUSIONS

With reference to the three major aspects of the preceeding investigations, the following principal conclusions were derived.

5.1 First Year Ridges

- The ice mass of a ridge, i.e. the cross sectional area, can be defined through the height of the ridge sail in combination with a selected value for the ridge aspect ratio hr/Wr; and,
- The cross sectional area increases with the sail height. An upper limit for CSA = 1300 m^2 exists for single ridges. The corresponding sail height is about 3.7 m.

5.2 Ridge Penetration Analysis

- The most significant ship size parameter in terms of ridge penetration resistance was found to be B^2;
- For a given midship section area a minimized B/d ratio increases the performance capabilities in ridges; and,
- The optimum bow form for the passage through ridges features large waterline angles, large flare angles and shallow stem and buttock angles.

5.3 Ridge Extraction Analysis

- The influence of ship breadth is clearly dominant compared to the draft;
- In isolation a short bow with large half waterline angle is beneficial. However, for constant displacement, such a bow requires a longer midbody and the total extraction force may be larger for a ship with this type of bow; and,
- The extraction force with long bows is very sensitive to friction. For vessels with short bows and long midbodies the relationship is close to linear.

6. RECOMMENDATIONS

In view of the overall long-term objective to develop design criteria relevant for ship transit in ice covered waters and applicable to regulations governing operation in Arctic waters of Canadian interest, the following principal requirements for further research were outlined:

- The scope of the data base for ridge parameters relevant to ship transit performance and in areas of Canadian interest is to be increased;

- Dedicated full scale tests with ships of different size and form will aid in the further development of the prediction formulas derived for the prediction of penetration and extraction performance; and

- The effects of randomly distributed sizes and spacing of ridges on the overall speed of advance have to be investigated to establish criteria for minimum performance requirements.

SOMMAIRE

1. INTRODUCTION

Donnant suite à une proposition spontanée soumise en 1985, le Centre de développement des transports de Transports Canada a confié à la firme Wartsila Arctic Inc. la tâche d'étudier une méthode de prévision de l'aptitude d'un navire à franchir des crêtes de première année et des limites opérationnelles devant lui être fixées.

2. OBJECTIFS

La présente recherche entre dans le cadre d'un programme de R&D de longue haleine visant à relever la fiabilité et la rentabilité de la navigation maritime arctique.

Cette recherche a eu pour but d'étudier systématiquement l'aptitude d'un navire de cote arctique à franchir le type de crêtes visé et de déterminer les limites opérationnelles à fixer en fonction des principales caractéristiques du navire.

3. PORTÉE

Afin de réaliser l'objectif ci-dessus, les travaux suivants ont été accomplis:

- recherche documentaire complète sur la question et évaluation de l'état de la technique dans le domaine concerné;

- compilation d'une base de données de grande envergure renfermant les résultats des essais faits par les secteurs tant public que privé dans ce même domaine;

- analyse et interprétation des paramètres caractéristiques d'une crête par rapport aux performances des navires;

- analyse du résultat des essais de franchissement en vraie grandeur et détermination des paramètres architecturaux déterminants du navire - dimensions et forme;

- élaboration d'un modèle analytique comportant les principaux éléments dont il faut tenir compte pour décrire le processus de dégagement;

- élaboration de critères définissant les limites opérationnelles d'un navire devant franchir des crêtes de première année.

Les sections qui suivent présentent un résumé des principaux résultats de ces travaux.

4. RÉSULTATS

4.1 Définition des crêtes

L'étude des 136 profils en travers obtenus par une campagne de mesurage in situ a mis en évidence d'importantes différences dans les caractéristiques géométriques des crêtes considérées. À hauteur h_s comparable, les profils en travers des crêtes ont varié considérablement en superficie. Un autre paramètre important distinctif a été l'allongement, rapport de l'épaisseur h_r à la largeur W_r, dont voici les valeurs selon la région:

Région	h_r/W_r
Baltique	0,02 - 0,06
Mer de Beaufort	0,05 - 0,07
Mer de Béring	0,08 - 0,09

Pour rendre plus aisée la détermination de la superficie du profil en travers en fonction de la hauteur h_s, une relation fonctionnelle faisant intervenir l'allongement parmi les éléments pris en compte a été obtenue sous la forme suivante:

$$\text{Superficie du profil} = 1310 \times \text{th}\,(h_s) \times \left(\frac{\text{th}\,(h_s)}{500 \times (1 - \text{th}^2(h_s))}\right)^{\left(150 \times (h_r/W_r - 0{,}02)^2\right)} \quad (1)$$

4.2 Résistance au franchissement

La recherche analytique dont il est question ici s'est concentrée exclusivement sur des essais de franchissement en vraie grandeur. Le calcul de l'énergie totale mise en oeuvre pour franchir une crête a été fait à partir des résultats de 51 essais distincts. De plus, à l'égard des navires soumis aux essais, des relations linéaires ont été établies où l'énergie nécessaire est fonction de la superficie du profil en travers et où, corrélativement, la résistance moyenne au franchissement est fonction de l'épaisseur h_r.

Une analyse de sensibilité exhaustive a permis de mettre en évidence les paramètres architecturaux du navire ayant le plus d'impact sur la résistance, à savoir les dimensions de la coque et la forme de la proue. Pour les fins de déterminations pratiques, une formule a été élaborée où la résistance moyenne est fonction de l'épaisseur h_r moyenne de la crête et des paramètres ci-dessus. Ainsi,

$$R_{\text{crête}} = 0{,}0886 \cdot h_r \left[B^2 . B/d \cdot 1/\cos\varphi \cdot 1/\tan\alpha \cdot 1/\sin\beta + \mu d \cdot L_m (0{,}61B + 0{,}45d)\right] \quad (2)$$

où:

B = largeur du navire

d = tirant d'eau

α = demi-angle d'acuité

β = angle d'une section transversale par rapport à la verticale

φ = angle d'une section longitudinale par rapport à l'horizontale

μd = coefficient de frottement dynamique

L_m = longueur de la partie médiane du navire.

Une étude paramétrique d'un certain nombre de navires brise-glace a permis de déterminer les conditions opérationnelles limites à la marche continue dans des crêtes de première année. La gamme des paramètres caractéristiques étudiés est explicitée dans le **tableau 1** ci-dessous:

Tableau 1 Paramètres caractéristiques - Navires

Coefficient de remplissage	0,56		
Rapport B/d	3,3		
Déplacement (t)	5 000	15 000	30 000
Poussée au point fixe (t)			
Faible puissance	40	150	300
Puissance moyenne	95	275	550
Puissance élevée	150	400	800
Caractéristiques dimensionnelles (m)			
B	20,0	25,0	30,0
d	6,0	7,5	9,0
Longueur hors tout à la flottaison	75,0	120,0	135,0
Proue de forme			
classique	$\psi = 43°$		
intermédiaire	$\psi = 35°$		
avancée	$\psi = 29°$		

$$\psi = \text{Arc tg} \frac{(\text{tg}\varphi)}{(\sin\alpha)}$$

Quant aux glaces, elles ont présenté des variations dans les paramètres caractéristiques de hauteur de crête h_s, d'épaisseur h_{glace} et d'épaisseur consolidée h_c, s'inscrivant dans l'enveloppe indiquée dans le **tableau 2**:

Tableau 2 Paramètres caractéristiques - Glaces

Paramètre	**Valeur minimale**	**Valeur maximale**
h_s (m)	0,10	3,70
h_{glace} (m)	0,10	1,80
h_c/h_{glace}	0	2

Un modèle de simulation informatique a été utilisé pour l'analyse systématique de l'effet des paramètres caractéristiques des navires et dans diverses combinaisons de h_{glace} et h_c, ce qui a débouché sur la détermination de la hauteur de crête limite que peut franchir chacun des navires considérés.

Les résultats de cette étude paramétrique sont présentés dans le **tableau 3**. Il donne, à l'intérieur du domaine expérimental fixé, les conditions glacielles limites exprimées en termes de h_{glace} et de h_c en fonction de la puissance installée et des paramètres caractéristiques des navires.

4.3 Dégagement

L'analyse du processus de dégagement du navire a été confinée à la détermination de la force en jeu au moment précis où le navire commence à faire marche arrière pour se dégager. Bien qu'à ce moment précis la résistance des glaces dans le chenal ouvert soit un facteur influant sur la vitesse du navire, elle ne représente normalement pas une condition limite. C'est pourquoi il n'a pas été jugé utile de s'y attarder.

Intégrant le résultat de travaux théoriques, d'essais sur modèles réduits et d'essais en vraie grandeur, la relation suivante permet de calculer la force qu'un navire totalement enfoncé dans une crête doit mettre en oeuvre pour se dégager:

$$F_E = q_M \, (\mu s \; L_p + C_E \; L_E/2) \qquad (6\text{-}22)$$

où:

$q_M = h_r[0{,}68 \; B \; (1 - 0{,}11 \; d/h_r) + 0{,}39 \; d \; (1 + 0{,}15 \; d/h_r)]$ (kN/m)

valable pour des valeurs de d/h_r inférieures à 3

μs = coefficient de frottement statique entre la coque et la crête

L_p = longueur de la partie médiane à flancs parallèles du navire

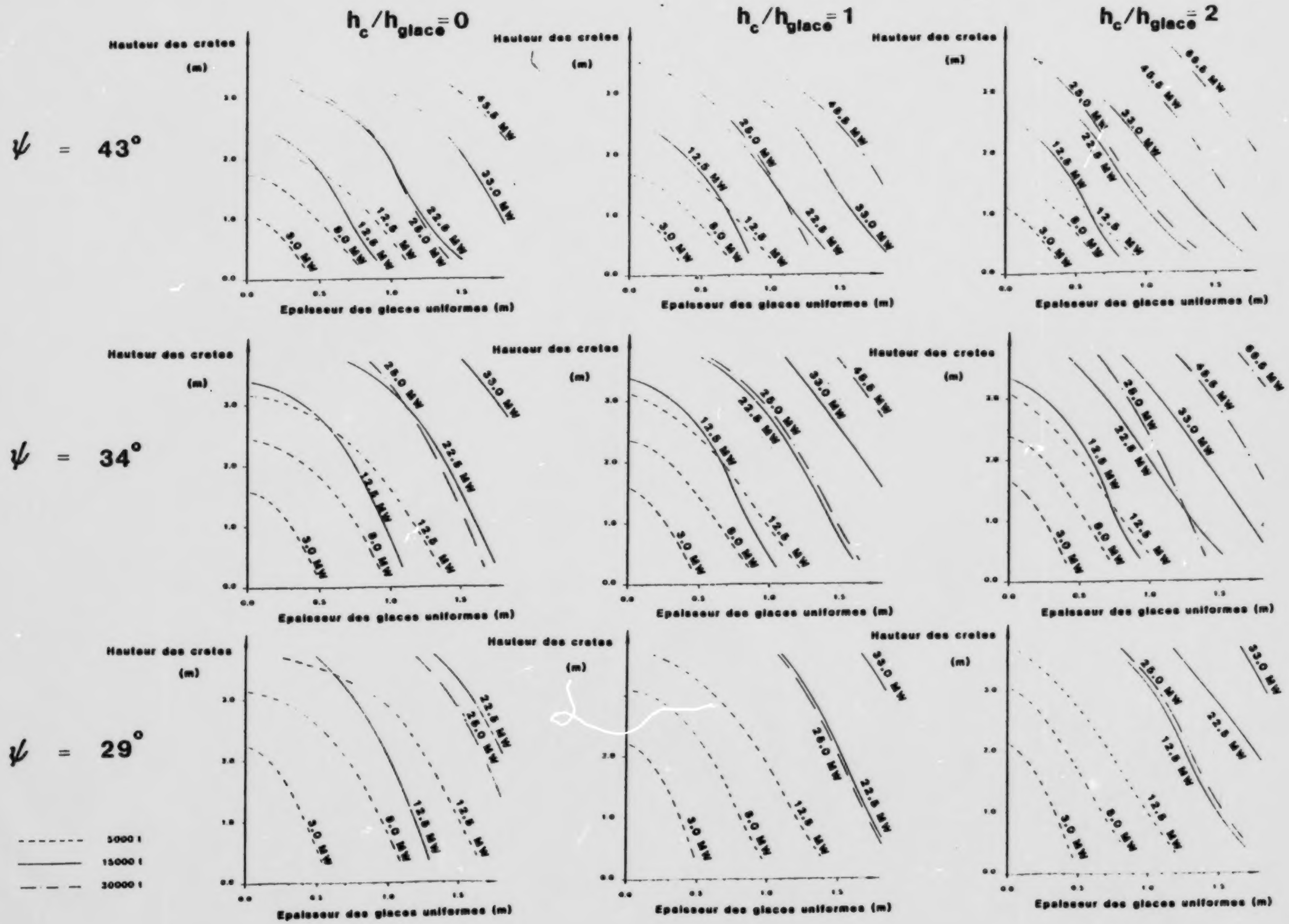

Tableau 3 Valeurs limites des hauteurs franchissables en marche continue

C_E = $\mu_s - (0{,}4+5 \sin\psi)\ \alpha_s/1000$

α_s étant exprimé en degrés

L_E = profondeur de pénétration

B = largeur du navire

d = tirant d'eau

h_r = épaisseur moyenne de crête

ψ = angle de la coque vue en section normale à la flottaison par rapport à l'horizontale

α_s = demi-angle d'acuité à l'étrave; il n'a toutefois pas été tenu compte des changements abrupts de forme tout près de l'axe longitudinal.

Utilisant l'équation 6-22, l'étude paramétrique des navires a débouché sur la détermination approchée des niveaux de puissance à mettre en oeuvre:

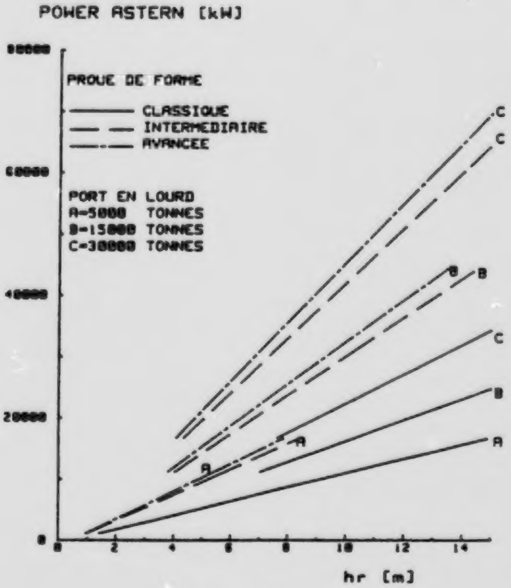

Figure 1 Détermination approchée des niveaux de puissance à mettre en oeuvre pour qu'un navire totalement enfoncé dans une crête puisse se dégager (pour les paramètres caractéristiques des navires, voir 4.2)

5. CONCLUSIONS

Concernant les trois grands aspects de la recherche décrite dans les pages précédentes, les principales conclusions pouvant être tirées sont les suivantes:

5.1 Crêtes de première année

- La masse d'une crête, qui est fonction de la superficie de son profil en travers, peut être déterminée directement de la hauteur de la crête à une valeur d'allongement h_r/W_r donnée.

- La superficie du profil en travers croît avec la hauteur de crête jusqu'à une valeur limite de 1300 m^2 dans le cas des crêtes simples. La hauteur de crête correspondante est de quelque 3,7 m.

5.2 Analyse paramétrique de l'aptitude au franchissement

- Le paramètre dimensionnel le plus important pour ce qui est de la résistance au franchissement est celui du carré de la largeur du navire.

- Pour un superficie donnée de la partie médiane du navire, l'aptitude au franchissement des crêtes croît inversement au rapport B/d.

- La forme de proue qui optimise cette aptitude doit présenter des valeurs élevées d'angle d'acuité et de dévers et des valeurs faibles d'angle α à l'étrave, et d'angle α (sections longitudinales par rapport à l'horizontale).

5.3 Analyse paramétrique de l'aptitude au dégagement

- La largeur du navire est un paramètre nettement plus important que le tirant d'eau.

- Considérée isolément, une proue de courte longueur avec un demi-angle d'acuité ouvert donne un effet bénéfique. Cependant, à déplacement égal, un tel choix se traduit par une partie médiane de longueur excessive nécessitant une puissance totale de dégagement plus élevée.

- La puissance à mettre en oeuvre pour dégager un navire équipé d'une proue de grande longueur est étroitement liée au frottement. Dans le cas d'un navire équipé d'une courte proue, mais avec une partie médiane longue, la relation puissance-frottement est quasi linéaire.

6. RECOMMANDATIONS

Considérant l'objectif à long terme qui est d'élaborer des critères régissant la conception de navires de cote arctique et la réglementation de la navigation dans les eaux arctiques canadiennes, la poursuite de la recherche devra être axée sur ce qui suit:

- Enrichir les connaissances sur les paramètres caractéristiques des crêtes dans l'optique de la présente recherche, et étendre la base de données à toutes les eaux d'intérêt pour le Canada.

- Lancer des essais spécialisés en vraie grandeur avec des navires de taille et de forme variables dans le but de mettre au point les modèles de prévision de l'aptitude d'un navire à franchir les crêtes et à s'en dégager.

- Étudier l'influence sur la vitesse de marche d'une distribution aléatoire des crêtes tant par leur taille que par leur espacement, de manière à pouvoir déterminer les performances minimums à exiger.

TABLE OF CONTENTS

		Page
1.	INTRODUCTION	1
2.	STUDY OBJECTIVES	3
3.	BACKGROUND	3
	3.1 Ridge Morphology	4
	3.2 Influence of Friction	6
	3.3 Penetration	8
	3.3.1 Analytical Work	8
	3.3.2 Full Scale Test Data	10
	3.3.3 Model Test Penetration Data	11
	3.4 Extraction Considerations	12
4.	RIDGE DEFINITION	14
	4.1 Data Transformation	14
	4.2 Results	15
5.	PENETRATION ANALYSIS	20
	5.1 Data Base	20
	5.2 Analysis of Test Data	23
	5.3 Sensitivity Analysis	25
	5.4 Ridge Resistance Formula	35
6.	EXTRACTION ANALYSIS	37
	6.1 Approach	38
	6.2 Ice Distribution Around Ship Cross Section	38
	6.3 Derivation of Midbody Extraction Force	39
	6.4 Derivation of Midbody Resistance	42
	6.5 Calibration to Model Tests	42
	6.6 Derivation of Bow Extraction Force	43
	6.7 Additional Consideration	51
	6.8 Calibration to Full Scale Tests	52
	6.9 Final Formulations	52

Page

7. PARAMETRIC INVESTIGATION 54
  7.1 Penetration 54
    7.1.1 Assumptions 54
    7.1.2 Systematic Analysis 54
    7.1.3 Results 56
    7.1.4 Discussions of Results and Limitations 57
  7.2 Extraction 62
    7.2.1 Approach 62
    7.2.2 Results 62
    7.2.3 Discussion of Results 68

8. CONCLUSIONS 69
  8.1 First Year Ridges 69
  8.2 Ridge Penetration Analysis 69
  8.3 Ridge Extraction Analysis 72

9. RECOMMENDATIONS 73
  9.1 Ridge Particulars 73
  9.2 Ridge Penetration Resistance 73
  9.3 Ridge Extraction 74
  9.4 Speed of Advance 74

10. REFERENCES 75

11. BIBLIOGRAPHY 80

APPENDIX A - Principles of Isostatic Equilibrium Calculations

APPENDIX B -
  B.1 - Significance and Sensitivity of Hull Main Particulars
  B.2 - Significance and Sensitivity of Bow Geometry Parameters and Combinations Thereof
  B.3 - Significance and Sensitivity of Hull Main Particulars and Bow Geometry Parameters
  B.4 - Sensitivity of Ridge Resistance Formula to Changes in H_R

APPENDIX C - Computer Simulations

NOMENCLATURE

A - Area
A_B - Cross section area of ridge under ship bottom
Am - Midship section area of a ship
B - Breadth
C_i - Ridge dependent coefficient
C_E - Bow form friction coefficient
CSA - Ridge cross sectional area
d - Draught
E - Ridge penetration energy
F_{EP} - Extraction force due to parallel midbody
F_{EB} - Extraction force due to bow
F_E - Extraction force
h_r - Average ridge thickness
h_b - Ridge thickness of side of ship
h_c - Thickness of consolidated layer
h_i - Thickness of level ice
h_k - Depth of keel of a ridge
h_s - Height of a ridge sail
L - Length
L_E - Distance between aft end of bow shoulder and point at bow where friction force equals pushing force
L_{wl} - Ship length on water line
L_A - Ship length of vessels run
L_E - Ship length of vessels entrance
L_M - Ship length of vessels midbody
L_P - Ship length of vessels parallel midbody
R - Ship resistance
r - Correlation coefficient
q_M - Force per unit length
q_{MB} - Bottom component of q_M
q_{MS} - Side component of q_M
s - Standard error of estimate
v - Velocity
W_r - Width of a ridge
α - 1/2 angle of entrance (see Figure 5.1)
α_S - 1/2 angle of entrance at stem
β - Angle between section and vertical plane
λ - Scale factor
μ - Coefficient of friction
μ_B - Porosity of ridge
μ_s - Static friction coefficient
ν - Poisson's Ratio
ρ - Density
ρ_W - Density of water
ρ_i - Density of ice
η - Form coefficient
φ - Stem or buttock angle to horizontal (see Figure 5.1)
ψ - Angle of attack (see Figure 5.1)

1. INTRODUCTION

In 1985, Wartsila Arctic Inc. submitted an unsolicited proposal to the Transportation Development Centre of Transport Canada, and Supply and Services Canada, Science and Professional Services Directorate, Reference UP-W-263. This study has been undertaken as a result of this submission under Supply and Services, Canada contract award 8SB.T8200-6-6500, dated July 1986.

The scope of the investigation covers particular aspects of ship performance in first year ice ridges. It is unique from the perspective that the approach taken to develop this investigation has been to study from ship test data. An attempt has been made to identify the governing parameters influencing ship transit through ridges. The work scope particularly focuses on the penetration phase as the ship goes through a ridge and the extraction forces required to back out in the event that the ship is stopped in a ridge.

The contents should be viewed as an initial step in the complex investigation of ship passage through ice ridges. Review of existing analytical techniques shows just how complex this is and how many parameters must be quantified for application purposes with some degree of accuracy. This work is intended to result in the development of methods suitable for estimating ship performance in first year ice ridges.

The results are summarized in a practical form which is useful for designers to undertake feasibility assessment and sensitivity analysis of ship design parameters. Because full scale data has been used to develop the study results, the authors feel that these can be used and applied with greater confidence than in the past. The ultimate objective of this work is, of course, to improve the reliability and cost effectiveness of shipping in ice covered waters.

2.0 STUDY OBJECTIVES

The overall long term objective of this work is to develop a scientific data base and methods for the design and operation of ice transiting vessels through first year ridges.

The objective of this study is to establish criteria applicable to regulations regarding navigation in Arctic waters of Canadian interest. This is regarded of significant importance as ice ridges represent a major obstacle to shipping and little research has been performed to date.

The work to achieve the stated objective requires evaluation of ship performance capabilities in transiting ridges for the purpose of identifying performance limits as a function of ship and ridge principal particulars. This involves systematically studying icegoing ship performance capabilities as a function of ship main particulars and principle ice characteristics.

3.0 BACKGROUND

Over the past twenty years, much research and development has been conducted on the subject of ships transiting in ice. The results of this work have provided the marine community with an initial understanding of some of the parameters that influence vessel transit through ice.

Most of this research work has focused on the performance of ships in level ice, and most icebreaking ships are still designed based on the maximum level ice thickness they are intended to break. In practice the ability of a ship to operate in a given geographical area is, however, limited by its capability to penetrate ridges rather than by its performance in level ice. There is therefore a discrepancy between current know-how and practices relative to one of the main factors known to limit ship transit in ice.

This disparity arises from the fact that ridges are very complex in relation to the study of ships in level ice. It is important to improve our knowledge in this respect as significant delays and lost efficiency are incurred as ships transit, and at times get stuck in first year ridges. The gains that have been obtained in level ice performance in terms of reduced powering requirements increase the need to better understand ridge performance.

Wartsila has been a forerunner as regards research on the performance of ships in ice ridges. After some initial work in the sixties, systematic work on this subject was pursued in the early seventies. In addition to analytical work, investigations have also included a large number of full scale tests in ridges in the Baltic and the high Arctic. Such tests have been made both with icebreakers and cargo ships. Similar tests in model scale have also been extensively carried out in the Wartsila Arctic Research Centre.

A comprehensive literature search and technical assessment of material relating to ridge transit has been performed. The related bibliographies listed in Section 11 of this study have formed the basis for identifying public domain information. In addition, the data base of Wartsila has been reviewed and appropriate references are cited in Section 10 of this report.

It is noteworthy that recent work sponsored by the Canadian Government has produced many comprehensive bibliographies that have been very useful in identifying applicable references in the course of this study.

The review of published and proprietary information has been performed under the following headings:

- Ridge Morphology;
- Influence of Friction;
- Analytical Study of Ridge Penetration;
- Ridge Penetration Test Data;
- Model Test Penetration Data; and,
- Extraction Considerations.

The state of the art in terms of ship performance in first year ridges and the extent of the data base for performing this study are identified and discussed in the following sections.

3.1 Ridge Morphology

The purpose of investigating ridge morphology is to define, analyse and quantify the ice conditions in a manner meaningful to ship designers.

Review of bibliographies shows that extensive research has been conducted on ridges. The list of references is in the hundreds. Much of this work is very scientific in nature and very detailed in relation to our current knowledge relative to the objectives of this study.

For this reason the scope of investigation in this study encompasses consideration of ridge data which has been gathered in conjunction with ship tests in first year ice ridges.

Existing analytical results of field measurements of ridges have been identified in the course of this work and include:

1. The test voyages of the USCGC POLAR STAR in the greater Bering Sea region (see 1)[*].
2. The typical structure of Beaufort Sea ridges (see 2).
3. Detailed investigations of ice ridges in the Baltic Sea performed by Keinonen (see 3 and 4).

The data, from which the foregoing models have been derived, and the ice data on ridges which have been identified for study in the course of this project, are summarized on Table 3.1.

For orientation purposes, the following are the measurements of first year ridges which are identified as fundamental to the study of ship transit through ridges and which have been investigated:

- sail height;
- top side profile measurement;
- consolidation thickness;
- ridge width;
- keel depth;
- cross sectional area;
- porosity; and,
- snow cover thickness.

---

[*] Numbers in brackets designate references listed at the end of the report.

REFERENCE	YEAR	NAME	SHIP TYPE	# OF RIDGE PROFILES	PENETRATION TESTS	EXTRACTION TESTS	TEST AREA
1	1980	USCGC POLAR SEA	ICEBREAKER	40	–	–	SOUTH BERING SEA
5	1981	USCGC POLAR SEA	ICEBREAKER	4	–	–	SOUTH BERING SEA
6	1982	USCGC POLAR SEA	ICEBREAKER	26	10	–	SOUTH BERING SEA
7	1981	MV ARCTIC	BULK CARRIER	1	1	–	LAKE MELVILLE
8	1982	MV ARCTIC	BULK CARRIER	–	–	–	LAKE MELVILLE
9	1982	MV ARCTIC	BULK CARRIER	–	–	–	LAKE MELVILLE
10	1982	MV ARCTIC	BULK CARRIER	–	–	–	LAKE MELVILLE
11	1982	MV ARCTIC	BULK CARRIER	–	–	–	LAKE MELVILLE
12	1982	MV ARCTIC	BULK CARRIER	–	–	–	LAKE MELVILLE
13	1982	MV ARCTIC	BULK CARRIER	–	–	–	LAKE MELVILLE
14	1974	SHIP 'A'	TANKER	1	1	–	BALTIC SEA
15	1974	SHIP 'B'	ICEBREAKER	11	0	–	BALTIC SEA
16	1975	SHIP 'M'	ICEBREAKER	11	11	–	BALTIC SEA
17	1976	SHIP 'C'	ICEBREAKER	8	0	–	BALTIC SEA
18	1977	SHIP 'D'	ICEBREAKER	5	5	5	BLACK SEA
19	1978	SHIP 'E'	ICEBREAKER	6	6	–	BALTIC SEA
20	1977	SHIP 'F'	TANKER	1	1	–	BALTIC SEA
21	1979	SHIP 'G'	BULK CARRIER	1	1	–	BALTIC SEA
22	1983	SHIP 'H'	ICEBREAKER	9	9	–	BALTIC SEA
23	1984	SHIP 'I'	TANKER	5	5	7	BALTIC SEA
24	1985	SHIP 'K'	TEST BOW	3	3	–	BALTIC SEA
25	1986	SHIP 'J'	ICEBREAKER	4	4	–	BALTIC SEA
				$\Sigma = 136$	$\Sigma = 51$	$\Sigma = 12$	

TABLE 3.1 FULL SCALE TEST DATA BASE

Initial investigation and comparison of ridge properties revealed substantial differences between data gathered in various geographic regions. For this reason, the matter has been investigated as a separate task and is presented in Section 4 of this Report.

3.2 Influence of Friction

Prior to investigating resistance and extraction of ships in ridges, it is important to consider the significance of the frictional component of ice resistance which has an important bearing on the total ice resistance of all icebreaking vessels. The frictional component is dependent upon several interrelated factors considering both the ship and its immediate surroundings. Work has been done to quantify the significance of friction, and recently much emphasis has been placed to reduce ship-ice friction. This work has led to an understanding of the important determining factors and the development of low friction surface coatings and friction reducing auxillary systems to improve ship performance.

Investigations have been carried out to determine the friction coefficient between the surface of the ship's hull and ice. Results show that values of the friction coefficient can vary significantly because friction depends upon:

- contact pressure;
- contact area;
- hull surface conditions;
- auxiliary devices;
- physical conditions of the ice surface such as temperature, degree of snow cover, etc.; and,
- static or dynamic condition.

The sensitivity to contact pressure is illustrated in Figure 3.1 which has been extracted from reference (26). As pressure increases the friction coefficient becomes smaller. In a ridge mass, the ice contact pressure distribution along the hull varies leading to substantial variations in frictional contact forces in the various regions of the hull. It is therefore difficult to isolate this parameter for both the penetration and extraction conditions.

The surface condition of the hull surface also affects resistance. A hull surface that is left untreated will become badly pitted by corrosion and friction will increase. To overcome this, solvent-free epoxy coatings and stainless steel hull surfaces have been developed to maintain a low friction surface condition.

Another significant parameter is the physical condition of the ice itself. As can been seen in Figure 3.1 a large amount of snow on the ice surface will dramatically increase the coefficient of friction. Also influencing the friction is temperature, salinity, and cohesion. In order to reduce the influence of snow and temperature related friction dependency systems such as bubblers and water lubrication devices have been developed.

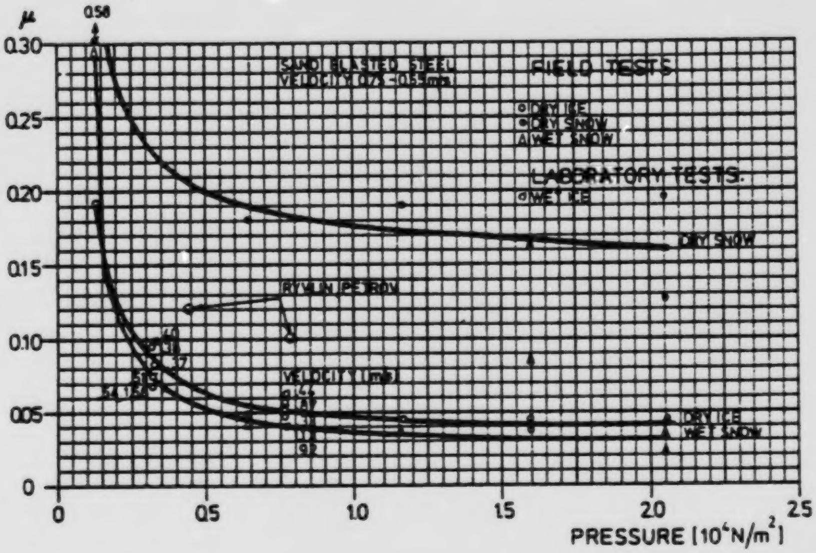

Figure 3.1 Variations in μ as a Function of Pressure from Reference (26)

The static or dynamic condition establishes the order of magnitude of the coefficient. The static condition has a value approximately 2.5 times that of the dynamic condition.

In his thesis Enkvist (see 26) reviews and summarizes the work done on establishing the coefficient of friction between hull surface and ice up until about 1972. This data and results of further research published since 1972 are presented in Table 3.2. As illustrated in the table a broad range for the friction coefficient has been recorded in various tests. This range of values reflects the sensitivity of the coefficient to environmental conditions, hull surface conditions and test conditions.

As illustrated in Table 3.2 the values for dynamic friction between a hull surface and ice can range from .02 - .4. Enkvist, (see 34), in recent research results, establishes a range of .08 - .1 in a dynamic condition, for a modern low friction hull surface. This work and further on-going work by Wartsila indicates that these are reasonable values to use in association with modern ship hulls. For the purpose of this study, the dynamic coefficient used is of the order of 0.1.

With respect to establishing representative values of the static coefficient, Reference (28) and Reference (31) give values that are approximately 2.5 times the values of dynamic friction, which are acceptable. The static value used herein is for the development of the extraction formula and is of importance in that respect, however no definite values for static friction can be found in current publications.

With reference to (26) the factor of μ static being 2.5 times the dynamic value shall be used to establish a range for μ static in the order of 0.25 - 0.3.

3.3 Penetration

Prior work on the derivation of ship resistance in first year ridges has been investigated from three possible perspectives:

1 - resistance estimated by analytical methods;
2 - resistance derived from full scale ship tests; and
3 - resistance derived from model scale tests.

Each of the three above methods are discussed in the following sections.

3.3.1 Analytical Work

Analytical work suitable for application has been conducted by Keinonen (see 34, 35, 36), Malmberg (see 37) and Mellor (see 38). Common to their work is the application of soil mechanical principles to derive at failure criteria of the ridged ice mass under the impact of the ship. The resulting formulations express ridge resistance as a linear function of ship parameters and ridge particulars.

The most exhaustive investigation is performed by Keinonen (see 34). In summary the results of his work are expressed as follows:

$$R_{tot} = R\gamma_1 + R\gamma_2 + R_\epsilon + R_{PB} + R_{PS} \qquad (3\text{-}1)$$

where

$R\gamma_1$: resistance components due to shear plan breaking of the ice rubble mass; $R\gamma_1 \approx 80\%$ of R_{tot};
$R\gamma_2$: component due to second lower breaking plane;
R_ϵ : component due to shear in end plate;
R_{PB} : component due to bottom friction; and,
R_{PS} : component due to side friction.

The derivation of the individual components is complex and requires a series of assumptions related to the following ridge physical characteristics:

- ice density;
- ridge porosity;
- inner friction of ridge mass;
- cohesion of ridge mass; and,
- hull-ice friction.

A resistance component due to the acceleration of the ice mass in the

SOURCE	REFERENCE	YEAR	TEST TYPE	DYNAMIC	STATIC	SURFACE TYPE
ENKVIST	26	1972	LABRATORY FIELD TESTS	.03-.11 ICE .1-.3 SNOW	2.5X DYNAMIC	VARIOUS STEEL SURFACES
GILL ET AL	27	1981	NO TESTS	.1-.2	-------	STEEL
POLAR STAR	30	1981	FULL SCALE	.2-.4	-------	STEEL HULL & LOW FRICTION COATING
R CLASS	28	1981	FIELD &FULL SCALE TESTS	SNOW & ICE .19 .12	.3 .07	STEEL HULL & LOW FRICTION COATING
POZNYAK	29	1981	MODEL	.04-.13	-------	
POLAR STAR	30	1981	FIELD TESTS	.031-.086	-------	VARIOUS STEEL SURFACES
KATMAI BAY	31	1981	FIELD TESTS	.02-.145 .05-.17	.037-.24 .08-.48	LOW FRICTION COATING STEEL PLATE
ENKVIST	32	1983	NO TESTS	.08 .16	------- -------	LOW FRICTION COATING STEEL HULL
FORLAND	33	1984	LABRATORY	.03	-------	STEEL & LOW FRICTION COATING
ENKVIST	34	1986	FULL SCALE	.045-.13 .157-.255	------- -------	HIGH PRESSURE PLATE LOW PRESSURE PLATE

TABLE 3.2 RECORDED VALUES OF THE COEFFICIENT OF FRICTION FROM FIELD AND LABORATORY TESTS

penetration phase is acknowledged by Keinonen (see 34). The final results of the reference however reflect the quasi-static penetration model.

Comparison of the formula with full scale test data leads to the introduction of a semi-empirical correction coefficient of 0.51, thus:

$$R_{tot,\ corr} = 0.51 * R_{tot} \qquad (3\text{-}2)$$

While the analytically derived resistance formulas differ in the degree of detail they all work with idealizations and simplifications of randomly distributed ridge characteristics. In view of the difficulties in determining the necessary ice parameters they can be considered a suitable tool for highlighting qualatitive effects of design variations on ridge resistance.

Their complex character renders them impractical for the designer involved in the quantative assessment of ridge performance capabilities.

3.3.2. Full Scale Test Data

The basic principles and procedures of full scale testing of ships in natural ridges were established with the work of Makinen, Keinonen and Laine in 1974 (see 39). Consecutive tests worldwide have applied essentially the same methods of testing with occasional modifications in individual components of the procedure. Full scale ridge tests consist of the following main components:

- survey of ridge profile;
- measurement of ship performance parameters during the penetration phase; and,
- calculation of ridge resistance.

The determination of the ridge profile is most commonly done by measurement of the ridge sail and consecutive calculation of the keel ice mass distribution according to the principles of isostatic equilibrium (see 4). Alternative methods involve vertical drilling into the ice feature and in the case of the USCGC POLAR SEA trials (see 1, 5, 6) submerged echo sounding equipment to determine the ridge keel profile. These methods are time intensive and despite the high level of effort provide no measurable increase in accuracy.

Ridge resistance is generally determined on the basis of the recorded ship performance parameters. Most analyses idealize the ship's motion during the penetration as truly horizontal. Effects of trimming and swaying on the resistance are neglected. The ridge performance analysis of POLAR SEA tests (see 6, 62) involves a complex computer model and takes vertical and lateral accelerations into account.

Table 3.1 shows the scope of full scale test data available for the present work. More full scale tests have been carried out particularly in the Canadian Beaufort Sea (see 40) and with experimental design concepts (see 41), but the data from these tests is of proprietary nature and is not available for the present work.

Data from M/V ARCTIC has also been considered. The ramming performance was analysed in great detail (see 7, 8, 10, 13) in tests done in level ice fields. The performance prediction for ridges are obtained by extrapolation of level ice results. Numerical information on ridge performance is obtained from (7) and provides one data point for the assessment of ridge breaching capabilities.

The results obtained from full scale trials are typically presented as in Figure 3.2 (see 42) and express ridge resistance as a linear function of ridge thickness.

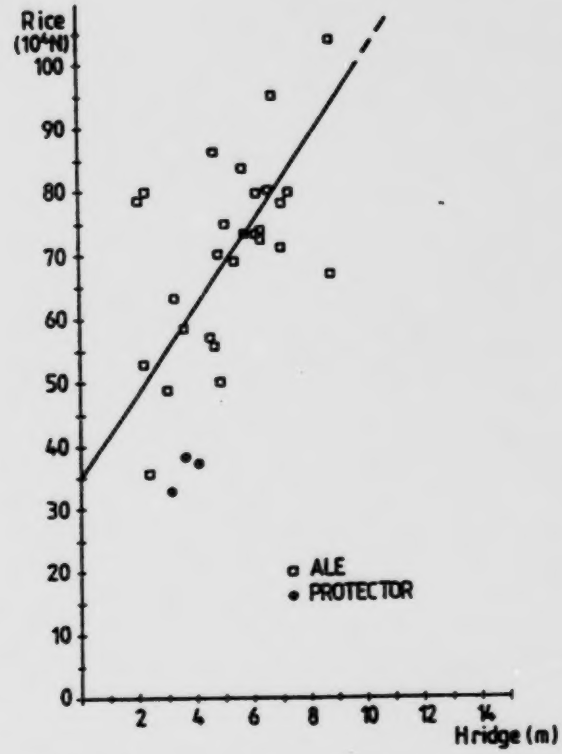

Figure 3.2. Full Scale Ridge Penetration Results (see 42)

3.3.3 Model Test Penetration Data

A great range of ship models has been tested in homogeneous ridge fields in Wartsila's model test tank facilities (see 43 to 57). The results of model tests support the linear relationship between ridge resistance and ridge thickness. Ridge model tests constitute a good qualitative measure of resistance when the influence of several design alternatives is under investigation.

For the quantitative assessment of ridge resistance in full scale, the interpretation of model test results relies on information obtained from full scale correlation tests. Therefore the detailed analysis of ridge performance capabilities in the following sections applies only full scale data.

The findings of the penetration analysis, on the other hand, can be used to improve the model scale predictions in future investigations.

3.4 Extraction Considerations

One of the most critical elements in the overall capability of an icebreaking vessel is the risk of getting stuck in ridges. Level ice and broken channels will influence the advance of the vessel, but will not prevent it from operating unless the ice conditions are significantly beyond the design values of the ship. However, a single ridge formation in otherwise moderate ice conditions may prevent the ship from any further advance. Even highly ice capable ships have, reportedly, been stuck for days.

In view of the importance of extraction in ridges, the limited effort in research is notable. There are several reasons for this:

- in the early days of icebreaking research, level ice was the governing factor. The ships were not capable enough to even contemplate entering heavily ridged areas;

- the complex nature of ridges make it difficult to define them accurately, in physical terms;

- the proper measurement of a single ridge is a tedious undertaking, resulting in high testing costs;

- the extraction force is very sensitive to a number of factors which are difficult to control. This includes the dynamic behaviour of the ice if the ramming speed is high, the washing effect of the propeller stream, the use of rudder during and after a ram, and the sensitivity to time and load of ice-ship friction; and,

- icebreaking cargo ships are more vulnerable to getting stuck than actual icebreakers due to their hull form and typically lower power. Such ships have only been in commercial use for about a decade and consequently the need for knowledge on ridge penetration has increased considerably during this period.

There are only a few references available related to extraction in ridges. A theoretical approach, without experimental verification was taken by Popov and Kashteljan (see 58). Relevant parts of research on ridge penetration, especially as regards to midbody resistance, can be applied taking into account the differences between the dynamic nature of penetration and the static nature of extraction. Such research is covered e.g. by Keinonen (see 34) and Malmberg (see 37). Beyond these, most sources of information are proprietary.

Likewise, the data base on extraction is very limited. Full scale tests have been made on about a dozen ships. However, in many cases the tests have been made in a simplified manner or without proper measurements and documentation on ridge characteristics. All relevant data is proprietary, but such tests made by Wartsila have been used to calibrate and verify the extraction formulations developed analytically in this project.
Model tests specifically on extraction are not available. Wartsila model tests in ridges are often done in a manner which allows us to separately determine the bow and midbody resistance components. These tests have been used for the development of the midbody resistance; an important element in extraction.

The derivation of extraction forces in this study is limited to the actual break-out force after the ship has stopped and got stuck. The broken channel resistance astern once the ship is in motion naturally influences the time needed for getting into position for the next ram, but will not be the limiting factor in the ship's capability to penetrate a ridge and has not been investigated. Thus, the expression "extraction" in this report specifically refers to the situation at the moment when the ship starts to move.

4.0 RIDGE MORPHOLOGY

Ridge morphology is examined in the context of this study for the purpose of establishing a method of characterizing first year ice ridges in terms relevant and compatible with ship transit analysis.

In this study, data from several sources identified in Section 3.1 have been applied. It is of primary importance that in characterizing the ridges, the data be compatible for analysis purposes.

Ridge data for the Bering Sea has been extracted from References (1, 5, 6). Ridges profiled in this work cover a large area of the Bering Sea from the Bering Strait to St. Lawrence Island. In total 70 ridge profiles from this region were included in the data base.

Baltic Sea ridge data originates from profile measurements taken during Wartsila full scale ship tests performed over a period of the last twelve years. This data base represents a large sample taken over a wide area. There are in total 65 data points.

Beaufort Sea information for the purpose of defining ridge morphology is available in analysed form as presented in Reference (2).

4.1 Data Transformation

Applicable parameters have been identified and methods for analysis have been established in prior work by Makinen (see 39), and Keinonen (see 4, 35). These methods and assumptions have been applied by many researchers and remain a valid basis for analyzing data in the context of this study.

Ridge characterization is determined from topside profile and other measurements. The underwater characteristics of ridges can be measured by sonar and drilling. Measurement results using these methods, however, show considerable differences. Methods used by Wartsila to determine the underbody's profile and size apply the principle of Isostatic Equilibrium. This approach makes use of the topside profile data from which other parameters are derived. By using this method and checking against what was measured originally ridge data available from varied sources can be rationalized on a common basis and applied.

$$\frac{H_B}{H_A} = \frac{\mu_A \times \rho_I}{\mu_B \times (\rho_W - \rho_I)} \qquad (4\text{-}1)$$

Formula for Isostatic Equlibrium (see 4).

where:

H_B = height of bottom profile point
H_A = height of sail profile point
μ_A = coefficient of permeability for sail
μ_B = coefficient of permeability for keel

ρ_W = density of water
ρ_I = density of ice

To ensure that this principle was correct values for cross sectional area of the ridge as given by the above formula were checked against the keel profiles and areas as recorded in the separate data bases. Validation of this method is shown in Figure. 4.1. Details describing the application and assumptions of this formula are described in Appendix A.

The Wartsila data was originally determined by this formula and as such were not re-analyzed for this study.

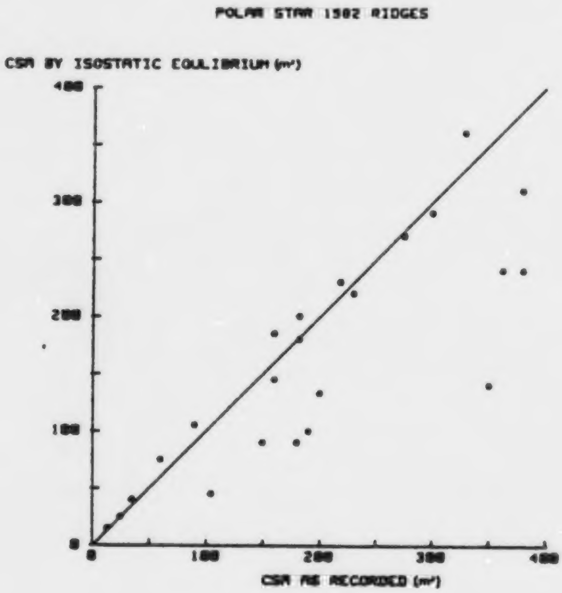

Figure 4.1 Validation of Isostatic Method

4.2 Results

Using this compiled data base, characteristics are plotted to assess their importance in discribing ridges. Figure 4.2 is a plot of sail height (hs) versus the cross sectional area of the ridge (CSA).

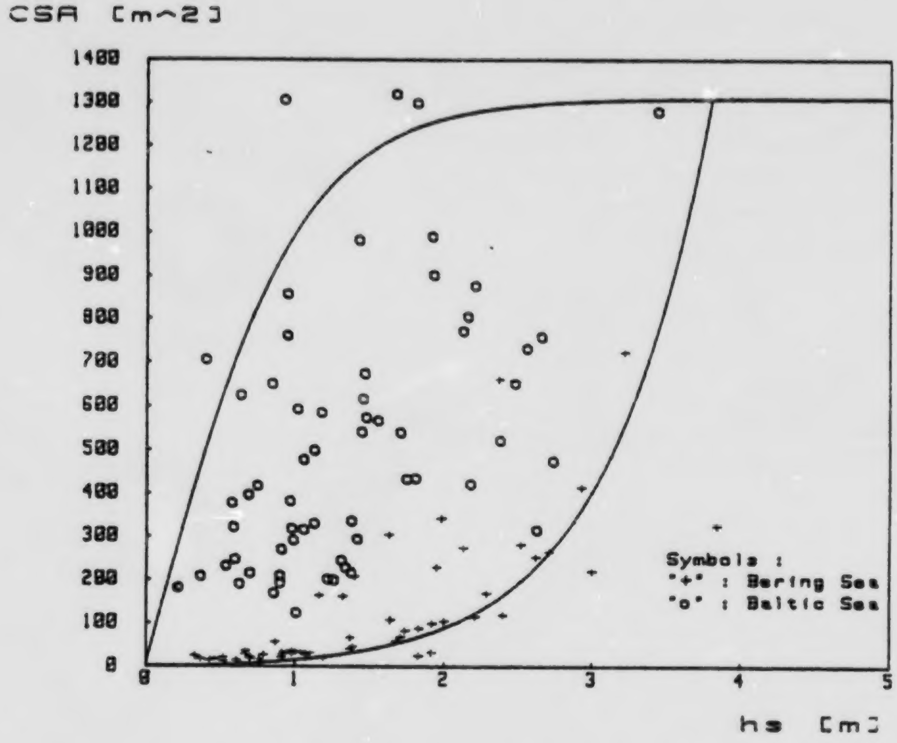

Figure 4.2 Envelope of CSA/h_s - Data from Full Scale Measurements

As the data points on the graph show there is considerable scatter in the data. However, under close observation the following points become apparent.

- The ridges for the Bering See are concentrated at the bottom of the graph;

- The Baltic data has comparatively larger CSA and shows wider scatter; and,

- The data indicates a limit to the size of a single identifiable ridge.

The data on the graph shows that a ridge with a certain sail height can have a large range of cross sectional area thus indicating that sail height alone will not enable prediction of the ridge ice mass. Figure 4.3 shows three ridges of equal cross sectional area, however, their widths-keel depths and sail heights are quite different. It is necessary to link these parameters such that a method to describe them can be obtained.

It was found that the ridge sail height and width (Wr) are linked to the cross sectional area by the aspect ratio of the ridge. This is a dimensionless ratio,

$$\text{Aspect Ratio} = \frac{hr}{Wr}$$

which qualifies the average mass per unit length of the ridge. Analysis of the aspect ratio of ridges found in the Bering and Baltic Seas, and the standard Beaufort Sea ridge (see 2) indicates a predominance of the aspect ratio in the following ranges.

- Bering Sea	.08 - .09
- Beaufort Sea	.05 - .07
- Baltic Sea	.02 - .06

The following functional relationship between h_s and CSA was formulated with the aspect ratio as parameter:

$$\text{CSA} = 1310 \times \tanh(h_s) \times \left(\frac{\tanh(h_s)}{500 \times (1 - \tanh^2(h_s))} \right)^{(150 \times (hr/Wr - .02)^2)} \qquad (1)$$

The Equation (4.2) describes an envelope of possible ridge configurations as shown in ridge configurations as shown in Figure 4.2. This envelope is, however, not all encompassing as the graph suggests. There are definite ranges for the Bering, Beaufort and Baltic Seas that exist for each sea within the total range. The range shown is finite and the data Fig. 4.4 provides a guidance tool to the user for the ascertation of ridge size on the basis of recorded sail heights.

Dependant on the selection of an Aspect Ratio, the severity of the predicted ridges can be adjusted. The ranges of the Aspect Ratio, established in this report for the separate geographical areas, will result in representative ice conditions. These values do not cover the extreme ice features possible in all areas.

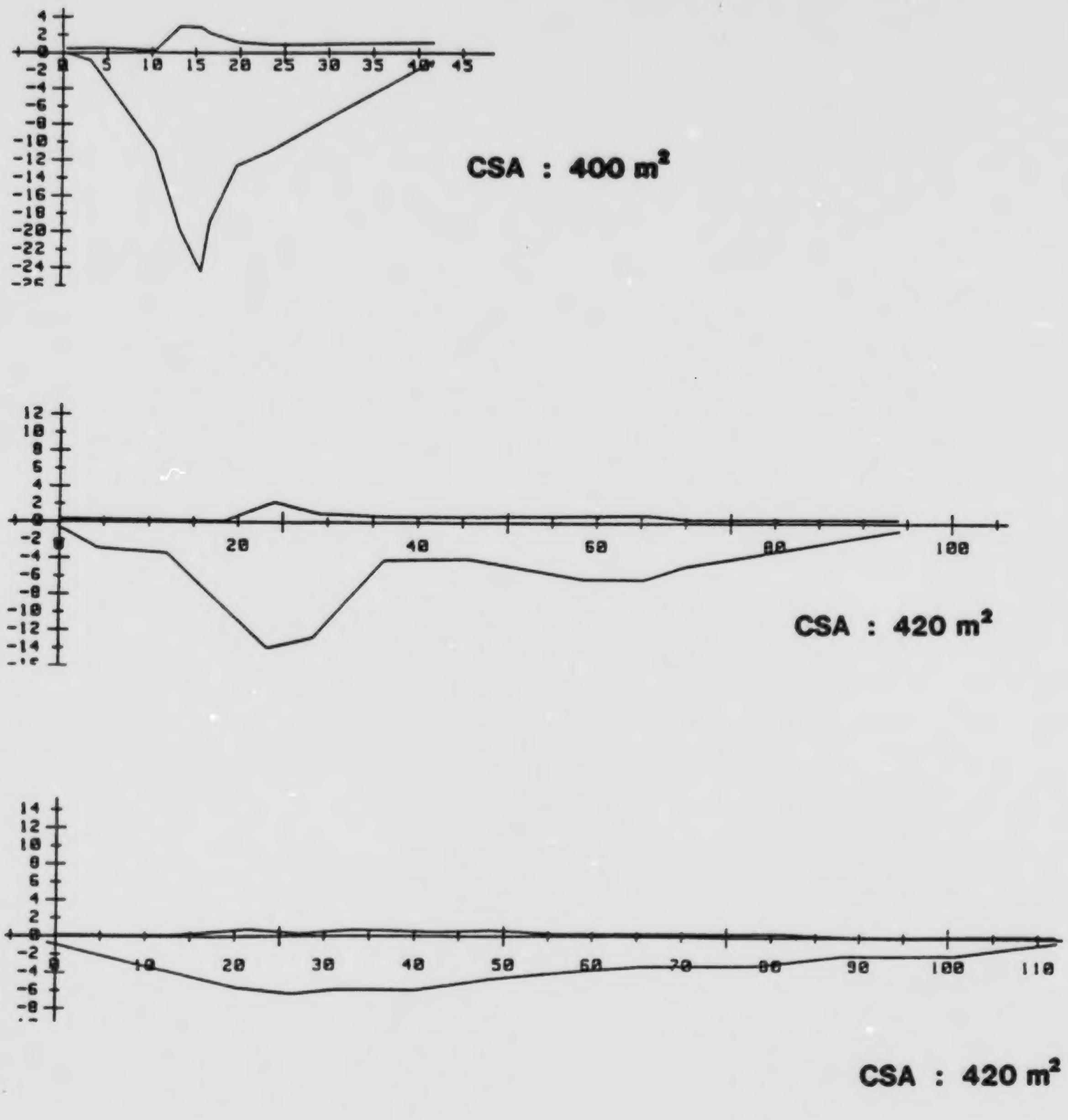

CSA : 400 m²

CSA : 420 m²

CSA : 420 m²

Figure 4.3 Range of Ridge Geometric Variations

$$CSA = 1310 * \tanh(hs) * \left(\frac{\tanh(hs)}{500 * (1 - \tanh^2(hs))}\right)^{(150* (\frac{hr}{Wr} - .02)^2)}$$

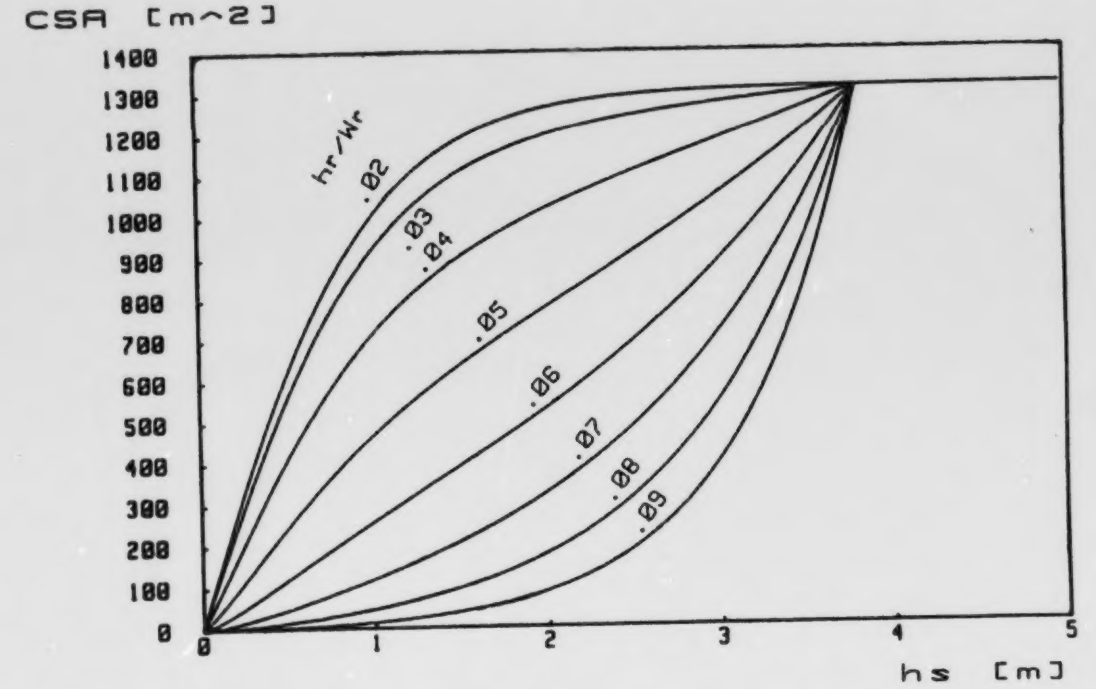

Figure 4.4 Ridge Cross Sectional Area vs. Sail Height

5.0 PENETRATION ANALYSIS

Within this section the results of full scale ridge penetration tests obtained for different ships are analyzed. The influence of individual parameters is investigated. On the basis of a detailed sensitivity analysis a frictional relation between ridge resistance and ship particulars is formulated.

5.1 Data Base

Test results of full scale penetration tests of eight different ships were used within the scope of this section. The selected ships are: Ship E, G, H, I, J, K, L and POLAR STAR. Details regarding the test site and the numbers of ridge tests for the individual ships are contained in Table 3.1.

Principal dimensions and characteristics concerning the hull form geometry and the bow form of the vessels are listed in Table 5.1. For orientation purposes Table 5.1 contains data for several other published icebreaking vessels of distinctive character. The selected ships do not have any unusual appendices. Figure 5.1 defines the symbols and terminology used.

The data base covers a wide spectrum of ship types ranging from icebreakers with extreme cylindrical bow forms to icebreaking cargo vessels.

The representative bow angles form the dominating criteria for organizing the individual vessels into three main groups:

- ships with cylindrical bow forms, i.e. Ship "K", ROBERT LEMEUR, Ship "J", KIGORIAK;
- ships with conventional and semi-conventional shapes, i.e. Ship "E", R. Class, "H", "L", "M" and POLAR STAR; and,
- icebreaking cargo ships with considerable amount of parallel midbody, i.e. Ship "I", "G" and MV ARCTIC.

As outlined in Section 4.0, Ridge Data Sources, the methods applied in obtaining ridge profiles in the POLAR SEA trials were different from the approach used during trials in the Baltic Sea. To obtain a standardized ridge geometry definition the recorded ridge sail profiles of the POLAR SEA ridges were used in combination with the principle of isostatic equilibrium to obtain complete ridge profiles. For each tested ridge the sail height (h_s), the cross sectional area (CSA), the width (W_r) and the average thickness (h_r) and the thickness of the consolidated ice layer were determined. The recorded ship performance data were used to calculate the magnitude of ship resistance as a function of penetration depth for each ship. This information was utilized to develop profiles showing resistance as a function of the ship's position within the ridge.

Parameters		R Lemeur	R CLASS	Kigoriak	POLAR STAR	M/V Arctic	Sh
Ship							
Lcwl	(m) :	82.80	85.90	84.90	107.30	196.59	
Bcwl	(m) :	19.00	19.50	17.30	25.45	22.93	
Draft	(m) :	5.50	7.20	8.50	9.70	10.93	
Displacement	(t) :	5600.00	8183.00	6549.00	13401.00	38104.00	
Lentrance	(m) :	14.00	42.95	14.50	46.22	25.80	
Lmidbody	(m) :	59.50	----	70.40	15.30	145.00	
Laft	(m) :	8.50	42.95	----	46.22	25.00	
Cm	:	0.980	0.910	0.900	0.830	0.991	0.
Cb	:	0.650	0.620	0.520	0.507	0.759	0.
Cp	:	0.660	0.750	0.580	0.609	0.764	0.
L/Disp	:	4.68	4.28	4.55	4.53	5.86	5.
B/d	:	3.45	2.71	2.04	2.62	2.10	3.
Le/Lm	:	0.24	----	0.21	3.02	0.18	0.
VALUES BELOW ARE REPRSENTITIVE OF THE TOTAL BOW							
α	:	40.00	20.00	42.00	21.00	26.00	51
β	:	65.50	51.00	45.00	37.00	34.00	70
ψ	:	29.51	46.77	33.60	56.01	62.40	19
φ	:	20.00	20.00	24.00	28.00	40.00	15
μ		0.097	0.097	0.10	0.097	0.097	0.
$\eta_{\mu\psi}$	:	0.487	0.52	0.60	0.745	1.153	0.

Table 5.1 Main Particulars and Geomet

Ship K	Ship E	Ship J	Ship H	Ship L	Ship M	Ship I	Ship G
0.91	0.932	0.850	0.945	0.877	0.912	0.900	0.990
0.52	0.604	0.560	0.580	0.519	0.519	0.756	0.730
0.57	0.605	0.660	0.616	0.590	0.627	0.839	0.742
5.11	5.44	4.21	4.50	3.91	4.40	5.28	5.62
3.33	4.57	3.03	3.33	2.52	3.76	2.26	2.56
0.28	3.47	2.56	----	----	----	0.38	0.58
51.00	28	29.00	33.00	28.50	22.40	30.00	35.00
70.00	56	56.00	46.00	51.00	46.20	39.00	29.00
19.02	37.78	38.36	40.56	44.33	50.22	49.10	50.66
15.00	20	21.00	25.00	25.00	24.60	30.00	35.00
0.10	0.097	0.10	0.097	0.097	0.097	0.097	0.097
0.38	0.500	0.52	0.615	0.62	0.64	0.761	0.904

ometric Properties of Icebreaking Vessels

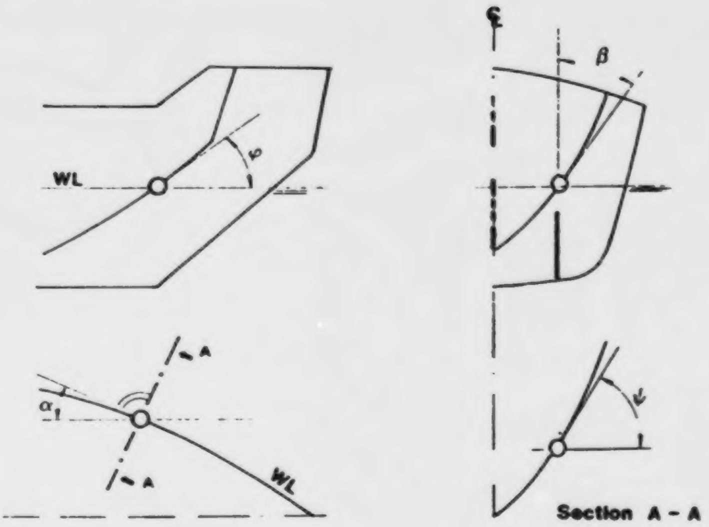
WL
φ
A
A
α_1
WL
℄
β
ψ
Section A - A

$$\psi = \arctan\left(\frac{\tan\varphi}{\sin\alpha}\right)$$

$$\eta_{\mu\psi} = \frac{\sin\varphi\cos\psi + \mu\cos\varphi}{\cos\psi\cos\varphi - \mu\sin\varphi\cos\varphi}$$

Figure 5.1 Definition on Bow Angles

5.2 Analysis of Test Data

The main objective of full scale ridge tests is to determine the resistance introduced by the ridged ice mass. This has been done in past analyses as outlined in Section 3.0 by calculating resistance values for sample points during the penetration phase and linking them to corresponding local ridge ice thickness averaged over the length of the ship in contact with the ice. The obtained data points were then subjected to a mathematical regression and a formulation for ridge resistance over ridge thickness was derived.

In view of the difficulties in determining exact ridge geometry for discrete positions within a ridge the present work considers the average performance of the tested ships over the full width of the penetrated ridges.

This is achieved by analyzing the total energy required to penetrate a ridge of a given CSA as follows:

$$E_{pen} = \int_{s=0}^{s=W_R} R\,ds \qquad (5\text{-}1)$$

where R_i is the calculated resistance at a given point during the penetration phase and s is the ship's corresponding position.

Following this approach each ridge test is summarized by a single data pair (E_{pen}, CSA). Simultaneous division by W_r yields a corresponding data pair (R_{pen}, h_r). R_{pen} is the average resistance experienced by the ship during the penetration of the ridge.

The resistance during the penetration phase comprises:

- resistance due to open water;
- resistance due to breaking of the consolidated ice layer within the ridge; and,
- resistance due to piled up ice blocks in the keel and sail area.

The open water component can be neglected due to the relatively low speed during the penetration without introduction of a high degree of inaccuracy.

In order to determine the pure ridge resistance, the resistance due to consolidation has to be eliminated.

Based on the established level ice performance of the different ships (see 6, 16, 19, 20, 21, 22, 23, 24, 25), the resistance component due to the consolidated layer was calculated for the average speed of penetration.

The pure ridge resistance is obtained by subtraction of the resistance component due to consolidation from the total average penetration resistance. The data pairs linking ridge resistance with average ridge thickness and ridge energy with cross sectional area are subjected to a mathematical regression.

The resulting linear regressions are shown in Figures 5.2 and 5.3.

Since breaching a mass of piled up ice blocks in a ridge comprises mainly the displacement of the ice mass in vertical, horizontal and transverse direction to permit the ship's passage, pure ridge resistance must be related to the size and shape of the hull. The following sensitivity analysis investigates the significance of ship size and geometry parameters on the ridge resistance.

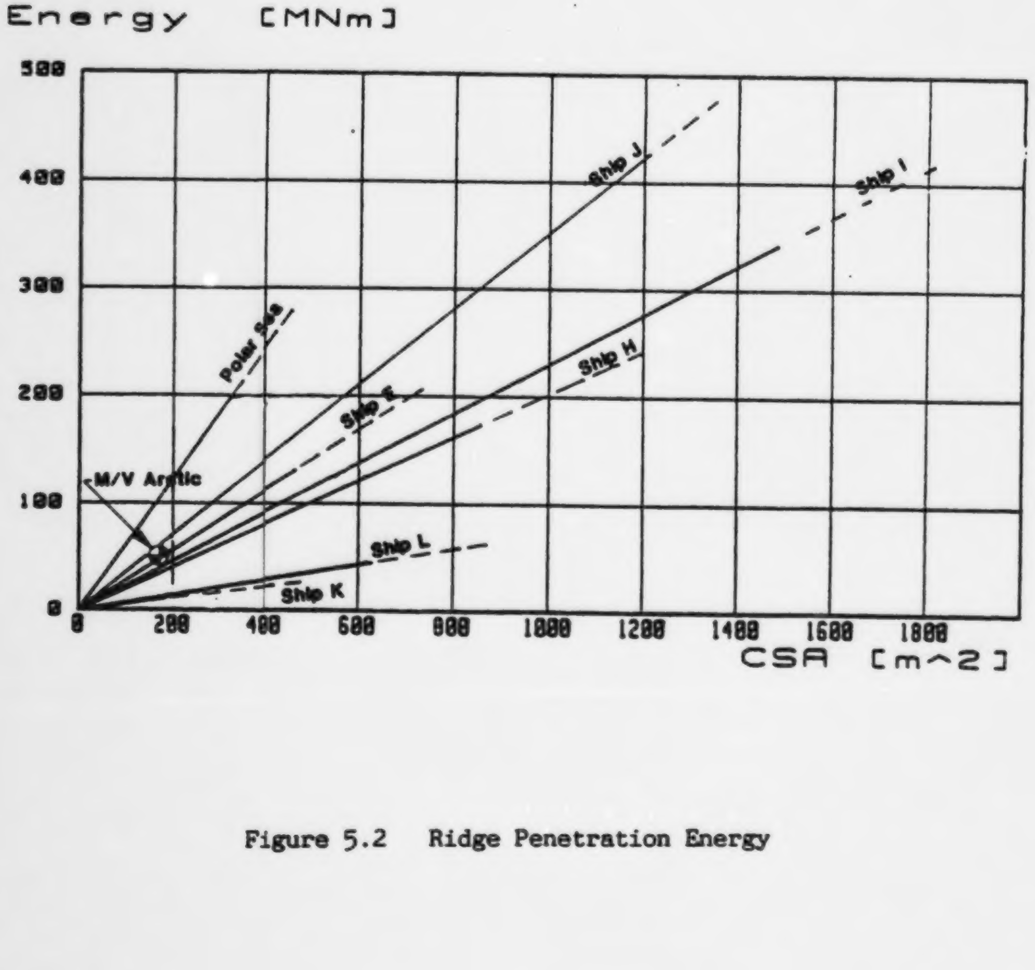

Figure 5.2 Ridge Penetration Energy

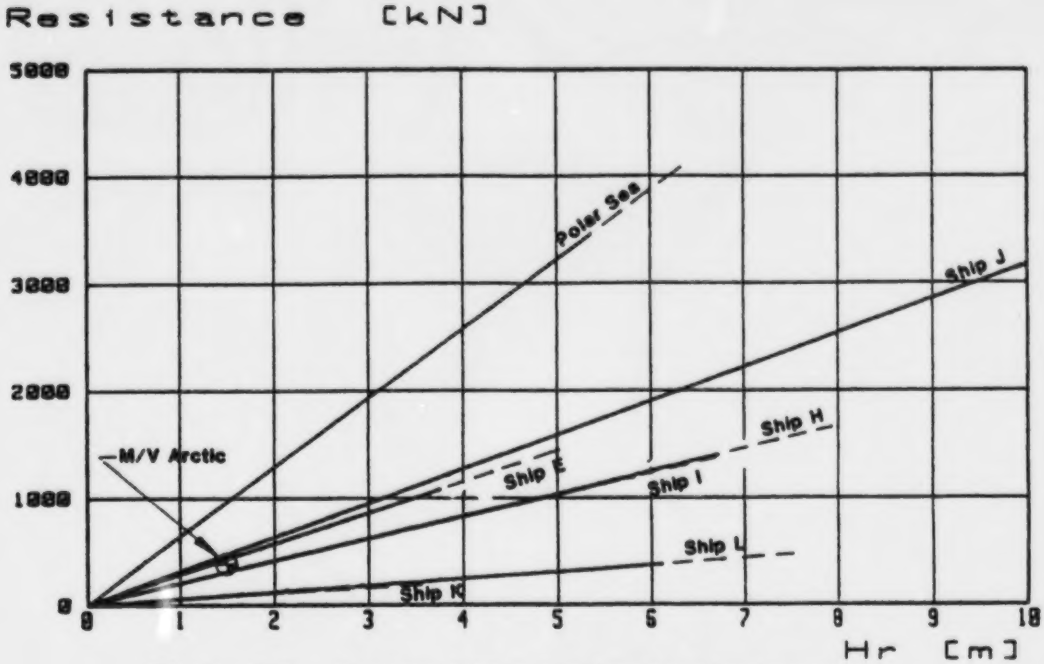

Figure 5.3 Average Ridge Penetration Resistance

5.3 Sensitivity Analysis

The form parameters used in general ship design are insufficient for the resistance prediction of ships operating in ice.

The objective of the sensitivity analysis is to determine the most significant hull form parameters and to establish their influence on ridge resistance. This approach avoids quantitative assumptions on physical parameters not measured which have an effect on ridge performance. Of influence are:

- the added mass of the ship;
- the added mass of the ridged ice mass; and,
- the thrust loss due to propeller-ice interaction during the penetration phase.

Within the scope of this work it is assumed that as a first approximation the effects of these parameters are proportional to the size of the tested ships and are therefore indirectly covered by the consideration of the most significant hull form parameters.

The sensitivity analysis comprises a comprehensive comparison of resistance values and hull form parameters. The principal procedure applied in the analysis is explained in an exemplary manner for the comparison of ship breadth and ridge resistance. The individual steps of the sensitivity analysis are also outlined schematically in Figure 5.4.

The starting point are the full scale test results reduced through a linear function (see Figure 5.2 and 5.3.). For a selected value of h_r a set of eight data pairs (R_i, B_i) is obtained where the data pairs describe the relationship between resistance predicted on the basis of the full scale trials and actual ship breadth for the individual ships and the selected ridge thickness. The (R_i, B_i) values are plotted and subjected to mathematical regressions applying the method of the least squares both for a straight line approximation and a least squares parabola.

In order to evaluate the least squares approximations the standard error of the estimate (s) and the correlation coefficient (r) are calculated. The standard error of estimate (s) has properties analogous to those of the standard deviation. Pairs of lines parallel to the regression line at vertical distances s, 2s, 3s from it will theoretically, if the number of samples is sufficiently large, include about 68%, 95%, 99.7% of the samples respectively. In other words, the smaller the absolute value of s is, the smaller the scatter of the data around the regression lines.

The correlation coefficient (r) on the other hand measures how well a given regression curve fits the sample data. The closer it is to 1 the better the correlation between curves and data. Therefore, the correlation coefficient forms a criteria to assess if the relationship between resistance and selected ship hull parameters tends to be linear or of higher order.

Ship main particulars which were used in the sensitivity analysis are listed in Table 5.2. All individual graphs are compiled in Appendix B.1. The table also shows the results from the mathematical regressions; i.e. the correlation coefficient and the standard error of estimate for both the linear and the parabolic approximation. Judging by the correlation coefficient alone the breadth of the ship squared shows the most dominating influence on the resistance. However, other hull parameters as well show correlation coefficients of 0.9 and better.

Besides the size of a vessel the bow geometry will have significant influence on the performance capabilities in ridges. The half angle of entrance of the waterlines (α), the stem angle of the buttocks with the horizontal (φ) and the angles between stations and the vertical (β) are of importance. The ship spreadsheet (Table 5.1) lists these angles for the individual ships. The angles shown are representative of the part of the forebody which is in contact with the ice mass. With reference to 26, 32, and 38 the following tendencies in relation between

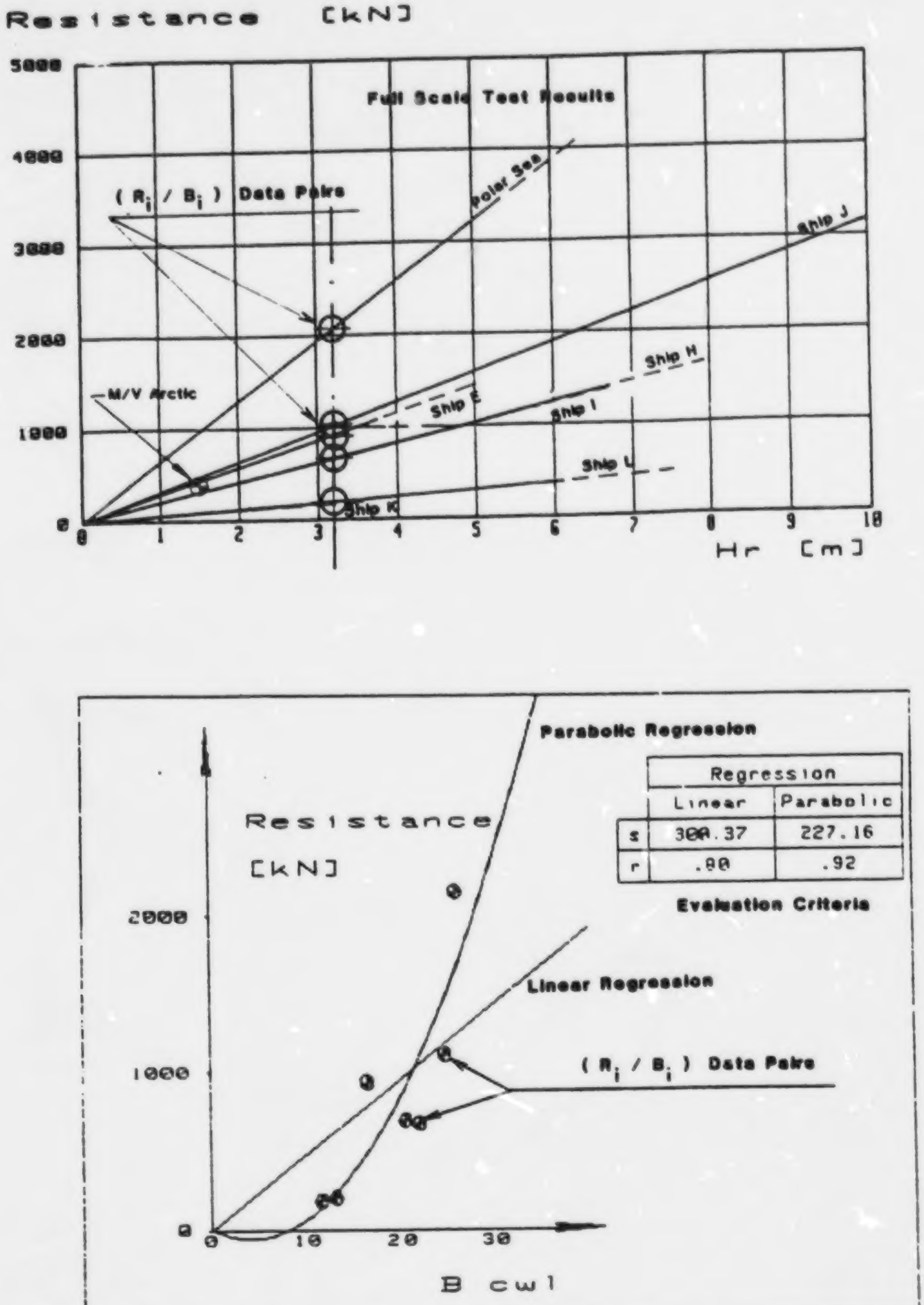

Figure 5.4 Sensitivity Analysis Schematics

Table 5.2 Significance and Sensitivity of Hull Size Parameters

Parameters	Linear Regression		Parabolic Regression	
	r	s	r	s
Bcwl	0.80	300.37	0.92	227.16
Lcwl	0.77	369.05	0.76	351.15
d	0.81	318.51	0.85	307.79
Displacement	0.78	412.37	0.89	251.80
Bcwl*d	0.89	266.05	0.92	255.77
Bcwl/d	0.68	440.07	0.69	420.12
Bcwl*(Bcwl/d)	0.78	337.20	0.82	325.59
Bcwl^2	0.88	238.08	0.94	209.39
Bcwl^2*(Bcwl/d)	0.86	258.32	0.91	234.43
(Bcwl*(Bcwl/d))^2	0.82	325.83	0.81	322.91
Am	0.87	283.11	0.89	276.02
Am*(Bcwl/d)	0.86	261.87	0.93	230.98
Am*(Bcwl/d)^2	0.84	288.87	0.88	274.25

resistance and hull angles can be expected. Resistance is proportional to:

- φ , i.e. when phi increases the resistance increases;
- $1/\alpha$, i.e. when alpha increases the resistance decreases; and,
- $1/\beta$, i.e. when beta increases the resistance decreases.

These relationships support the general trend that most efficient icebreaking is achieved when the ice fails by bending rather than by crushing or when the ridge ice mass is placed downwards rather than sideways. In summary of the above resistance is expected to be proportional to the following coefficients and combinations thereof:

$$\begin{array}{llll} \varphi, & \sin\varphi, & \tan\varphi, & 1/\cos\varphi \\ 1/\alpha, & \cos\alpha, & 1/\sin\alpha, & 1/\tan\alpha \\ 1/\beta, & \cos\beta, & 1/\sin\beta, & 1/\tan\beta \end{array}$$

Table 5.3 contains the parameters tested and the results of the sensitivity analysis of the individual hull form parameters. Individual graphs are compiled in Appendix B.2. The listed correlation coefficients and standard errors will be used to select the most significant parameters.

Table 5.3 Significance and Sensitity of Bow Geometry

Parameters	Linear Regression		Parabolic Regression	
	r	s	r	s
SIN(phi)	0.73	381.53	0.75	377.66
TAN(phi)	0.74	379.66	0.75	378.47
1/COS(PHI)	0.70	407.94	0.75	380.65
COS(alfa)	0.73	375.87	0.84	314.73
1/SIN(alfa)	0.79	312.16	0.93	210.85
1/TAN(alfa)	0.82	285.65	0.93	214.22
COS(beta)	0.75	369.93	0.77	367.51
1/SIN(beta)	0.72	388.60	0.75	378.88
1/TAN(beta)	0.77	371.00	0.76	368.70
SIN(p)/TAN(a)*COS(b)	0.87	298.72	0.89	288.45
SIN(p)/TAN(a)/SIN(b)	0.86	293.11	0.89	282.19
TAN(p)/TAN(a)*COS(b)	0.87	303.88	0.89	296.25
TAN(p)/TAN(a)/SIN(b)	0.86	298.54	0.89	290.94
1/COS(p)/SIN(a)*COS(b)	0.84	294.82	0.90	268.94
1/COS(p)/TAN(a)*COS(b)	0.86	281.90	0.91	256.32
1/COS(p)/SIN(a)/SIN(b)	0.82	295.45	0.90	257.02
1/COS(p)/TAN(a)/SIN(b)	0.85	277.83	0.92	245.21
1/COS(p)/TAN(a)/TAN(b)	0.87	295.81	0.89	286.21

The studied parameters listed in Tables 5.2 and 5.3 can be categorized into three groups of high, medium or small significance concerning their individual influence on resistance. In several cases ridge resistance is clearly linked to hull size parameters (Table 5.2) and bow geometry parameters (Table 5.3). These cases fulfill the following criteria:

- a good fit with either linear or parabolic regression, expressed by a high value of r close to 1;
- a minimum value for the standard error of estimate for the corresponding approximation;
- a wide range and distribution of parameters; and,
- agreement with physical realities.

Figures 5.5 and 5.6 show a selection of the most significant hull size and bow geometry parameters in terms of the above criteria.

The next step in the sensitivity analysis is to investigate the combined influences of size and form parameters. This is done by linking the selected parameters shown in Figures 5.5 and 5.6 and investigating their

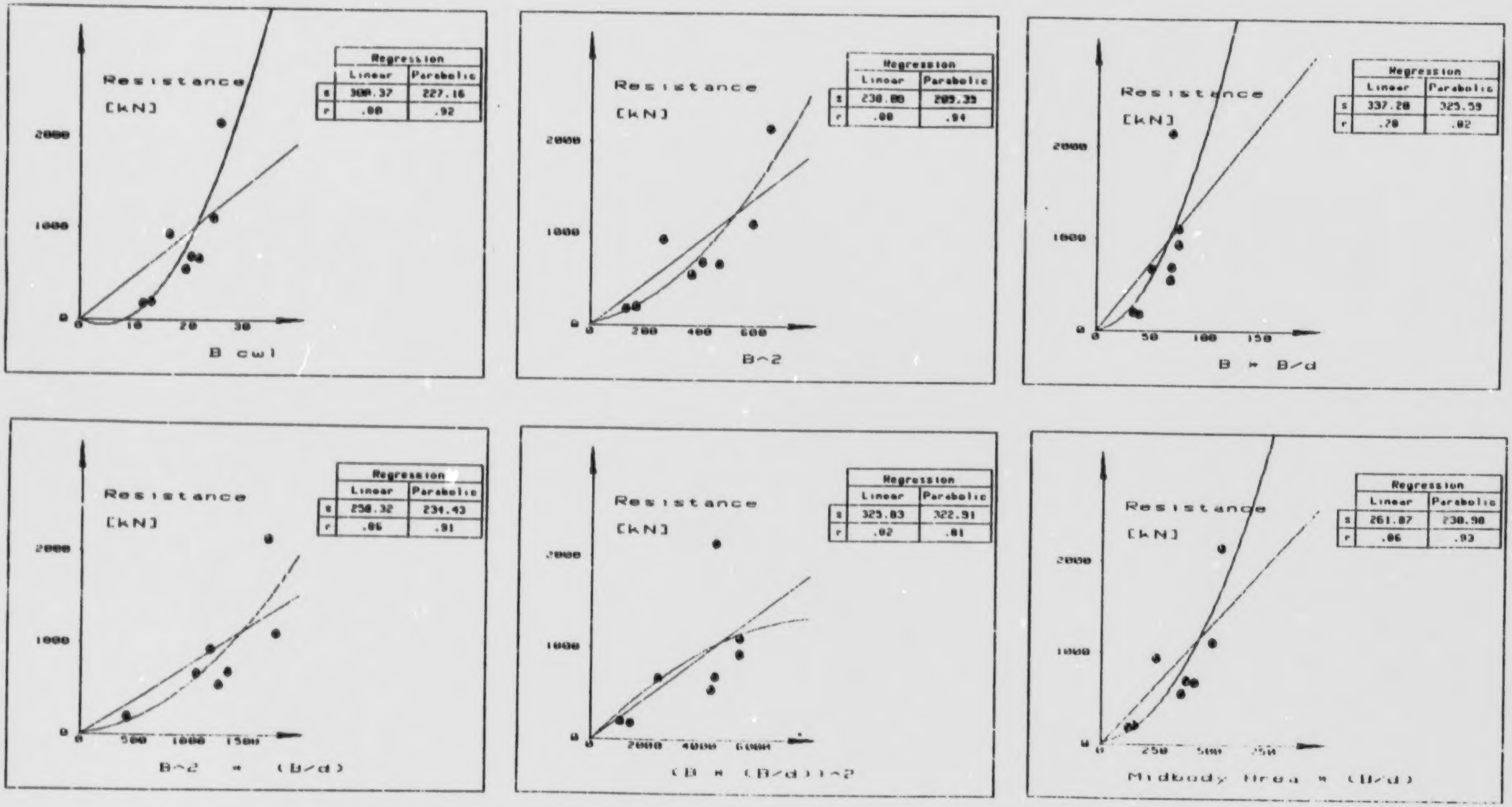

Figure 5.5 Selected Hull Size Parameter

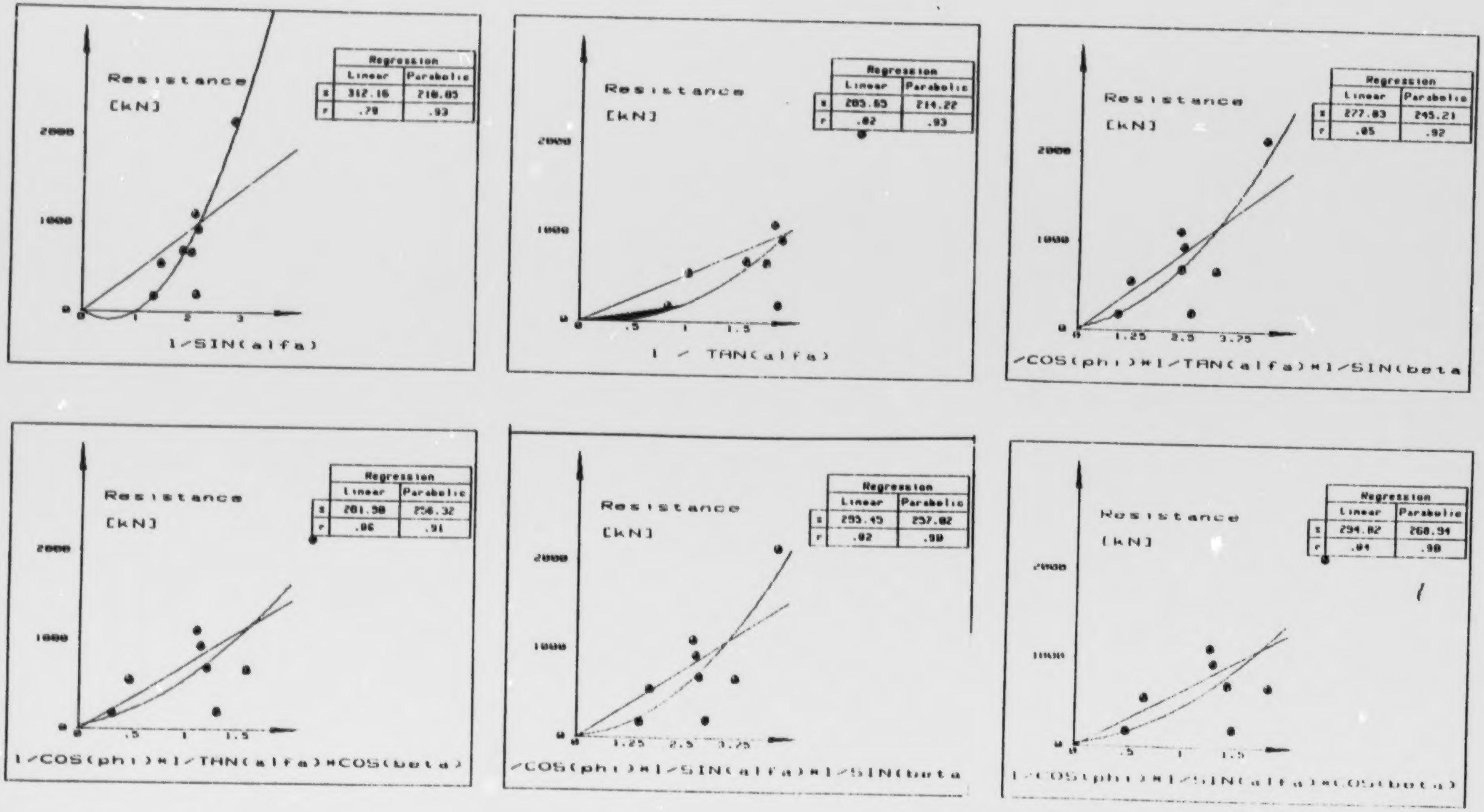

Figure 5.6 Selected Bow Geometry Parameter

combined influence on the ridge resistance. Table 5.4 lists the different alternatives and the results. Figure 5.7 shows the corresponding diagrams Appendix B.3 contains the individual graphs of this investigation.

It is apparent that all investigated combinations show significant reduction in the scatter. While the minimum standard error of estimate for the induvidual parameters lies above 230 kN the combined effects of main particulars and bow geometry reduce the scatter to approximately 100 kN. The correlation coefficient further demonstrates a good fit between the data and the mathematical approximations. This applies to both the linear regressions and the least squares parabola. On the basis of the established evaluation criteria the following function of ship main particulars and bow geometry parameters is selected:

$$B^2 \cdot (B/d) \cdot (1/\cos\varphi \cdot 1/\tan\alpha \cdot 1/\sin\beta) \qquad (5\text{-}2)$$

After considering the significance of ship main particulars and bow geometry the length of the parallel midbody still distinguishes the individual ships. While the lines of icebreaking cargo ships (Ship "E", Ship "F") show a significant amount of parallel midbody, some of the icebreaking hull forms do not have any parallel section at all. However, in accordance with (34) even ships with no parallel midbody have approximate flat bottoms and sides over part of the total length.

The reference suggests to determine the length of this so-called effective midbody in these cases as:

$$L_m = d/\tan\varphi \qquad (5\text{-}3)$$

This part of the hull will cause a resistance component which is connected with the amount of ice mass along the sides and below the ship's bottom.

Since the ridge ice mass is not subjected to any further displacement when the midbody, i.e. the widest part of the ship, enters the ridge this resistance component is of purely frictional nature. Therefore it is likely to be a function of the surface area of the midship's region in contact with ice.

An analysis of the significance and the sensitivity of parameters did not reveal any strong influence of individual parameters on ridge resistance. This indicates that the contribution of midbody to the total resistance in the penetration phase is secondary. According to (34) and (37) the midbody resistance can reach up to 20% of the total ridge resistance for ships with a considerable amount of midbody.

Since the data do not permit the isolation of a midbody component, this resistance component will be considered in the following work in the form

Table 5.4 Combination of Size and Geometry Parameters

Parameters	Linear Regression		Parabolic Regression	
	r	s	r	s
B * F(bow)1	0.90	181.97	0.98	116.08
B * F(bow)2	0.92	162.63	0.98	119.92
B * F(bow)3	0.93	190.61	0.96	179.96
B * F(bow)4	0.88	190.57	0.97	114.16
B * F(bow)5	0.91	201.31	0.95	184.77
B * F(bow)6	0.92	209.70	0.95	197.90
B^2 * F(bow)1	0.96	43.97	0.98	133.20
B^2 * F(bow)2	0.97	134.76	0.98	130.65
B^2 * F(bow)3	0.97	170.22	0.97	170.05
B^2 * F(bow)4	0.95	144.72	0.97	135.60
B^2 * F(bow)5	0.96	174.56	0.97	172.38
B^2 * F(bow)6	0.96	183.57	0.97	182.41
(B * B/d) * F(bow)1	0.87	214.45	0.97	131.96
(B * B/d) * F(bow)2	0.90	187.34	0.98	120.33
(B * B/d) * F(bow)3	0.93	154.66	0.99	97.15
(B * B/d) * F(bow)4	0.85	253.59	0.92	226.13
(B * B/d) * F(bow)5	0.90	173.60	0.99	90.52
(B * B/d) * F(bow)6	0.92	175.50	0.98	120.44
(B^2 * B/d) * F(bow)1	0.94	129.11	0.99	85.16
(B^2 * B/d) * F(bow)2	0.96	105.74	0.99	76.70
(B^2 * B/d) * F(bow)3	0.98	101.42	0.99	93.11
(B^2 * B/d) * F(bow)4	0.98	116.50	0.99	112.41
(B^2 * B/d) * F(bow)5	0.96	111.63	0.99	91.46
(B^2 * B/D) * F(bow)6	0.97	122.79	0.99	111.67
(B * B/d)^2 * F(bow)1	0.91	220.41	0.94	203.52
(B * B/d)^2 * F(bow)2	0.93	197.46	0.96	181.03
(B * B/d)^2 * F(bow)3	0.96	134.37	1.00	94.92
(B * B/d)^2 * F(bow)4	0.97	133.14	1.00	102.19
(B * B/d)^2 * F(bow)5	0.94	154.46	0.99	100.68
(B * B/d)^2 * F(bow)6	0.95	149.14	0.99	107.28
(Am * B/d) * F(bow)1	0.94	153.52	0.98	131.92
(Am * B/d) * F(bow)2	0.96	138.27	0.98	127.18
(Am * B/d) * F(bow)3	0.96	175.41	0.97	173.55
(Am * B/d) * F(bow)4	0.96	185.37	0.97	184.33
(Am * B/d) * F(bow)5	0.95	183.39	0.96	178.32
(Am * B/d) * F(bow)6	0.95	191.89	0.96	188.67

Symbols :
F(bow)1 : 1/SIN(alfa)
F(bow)2 : 1/TAN(alfa)
F(bow)3 : 1/COS(phi) * 1/TAN(alfa) * 1/SIN(beta)
F(bow)4 : 1/COS(phi) * 1/TAN(alfa) * COS(beta)
F(bow)5 : 1/COS(phi) * 1/SIN(alfa) * 1/SIN(beta)
F(bow)6 : 1/COS(phi) * 1/SIN(alfa) * COS(beta)

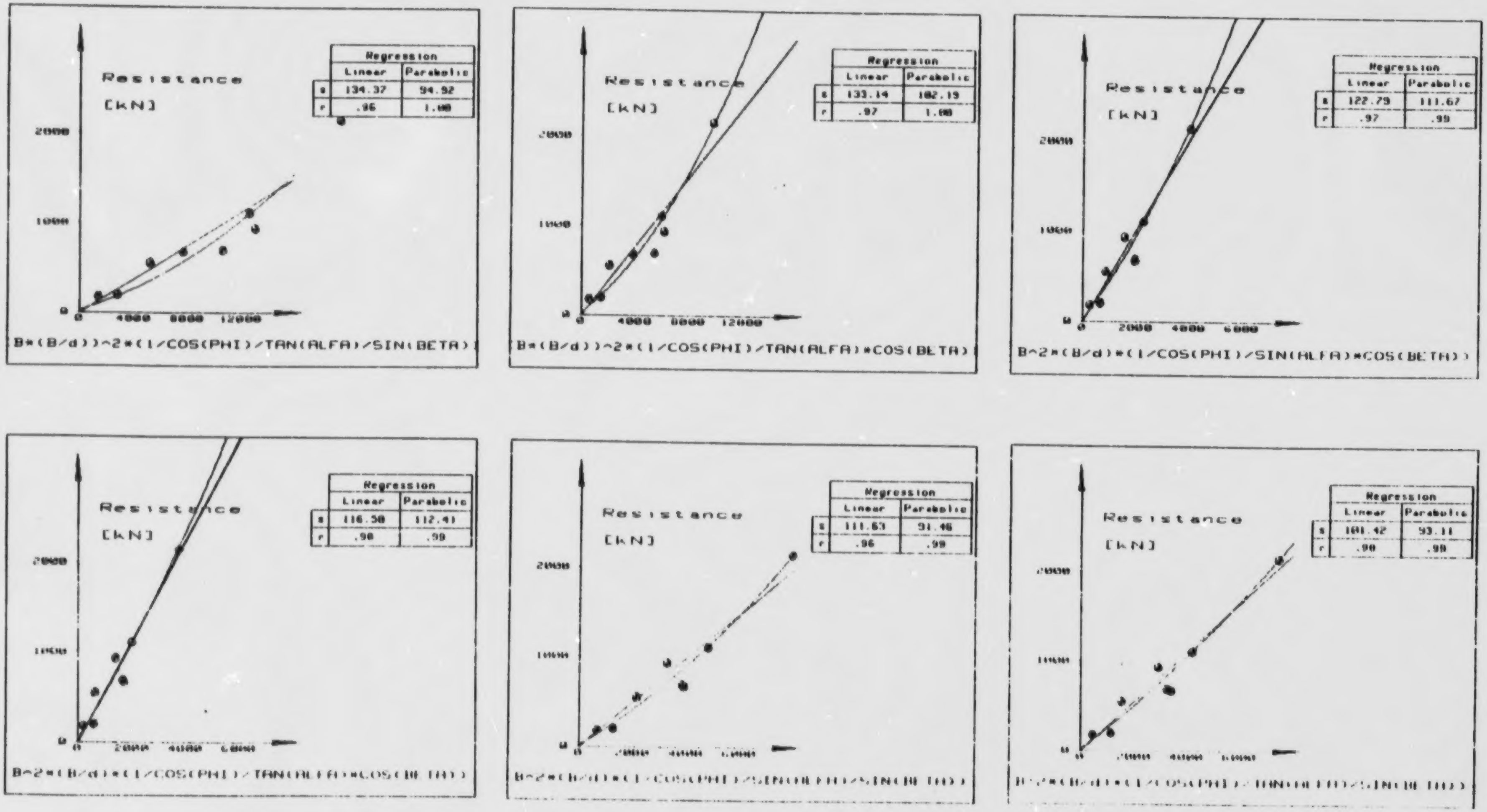

Figure 5.7 Combined Influence of Size and Bow Parameter

of a theorectically derived formula:

$$R = \mu_d \cdot L_m \cdot H_r \cdot (0.61\ B + 0.45\ d) \qquad (5\text{-}4)$$

where:

μ_d = dynamic friction coefficient
L_m = length of parallel midbody
H_r = average ridge thickness
B = breadth
d = draft

The formula is the result of a semiempirical evaluation of the various components influencing frictional resistance in ridges. The derivation of the formula is described in detail in Section 6.0.

5.4 Ridge Resistance Formula

Together with the findings of the sensitivity analysis summarized in Tables 5.2 to 5.5 and Figures 5.5 to 5.7 and the expression for the resistance component due to parallel midbody, it is now possible to formulate a preliminary relationship between ridge resistance and ship hull parameters:

$$R_r = C \cdot [F(\text{Main Particulars}) \cdot F\ (\text{Bow}) + F\ (\text{Midbody})] \cdot h_r \qquad (5\text{-}5)$$

The individual elements of the formulation are obtained from the results in Table 5.4. They are:

$F(\text{M.P.}) = B^2 \cdot (B/d)$
$F(\text{bow}) = 1/\cos\varphi \cdot 1/\tan\alpha \cdot 1/\sin/\beta$
$F(\text{midbody}) = \mu_d \cdot L_m \cdot (0.61 \cdot B + 0.45\ d)$

Applying this formula to the individual regression lines obtained directly from full scale test data the origninally wide scatter is reduced to a fraction. This is clearly demonstrated in Figure 5.8 where the original regression lines are compared to the reduced lines. 75% of the data lie within a 30% band around the mean slope. At this point in the present study the mean slope of .0886 is interpreted to quantify the combined influence of all not considered effects assumed to be proportional to the size of the individual ships.

The final formulation for ridge resistance is:

$$R_{ridge} = .0886 \cdot h_r \cdot [B^2\ B/d \cdot 1/\cos\varphi \quad 1/\tan\alpha \cdot 1/\sin\beta + \\ + \ \mu_d \cdot L_m\ (0.61B + .45d)] \qquad (5\text{-}6)$$

A discussion of the validity and limitations of the formula over a range of ship types and ridge thicknesses is enclosed in Appendix B.4.

The formula will be applied in the systematic analysis of vessel penetration when performance capabilities and power requirements for a range of ships will be established.

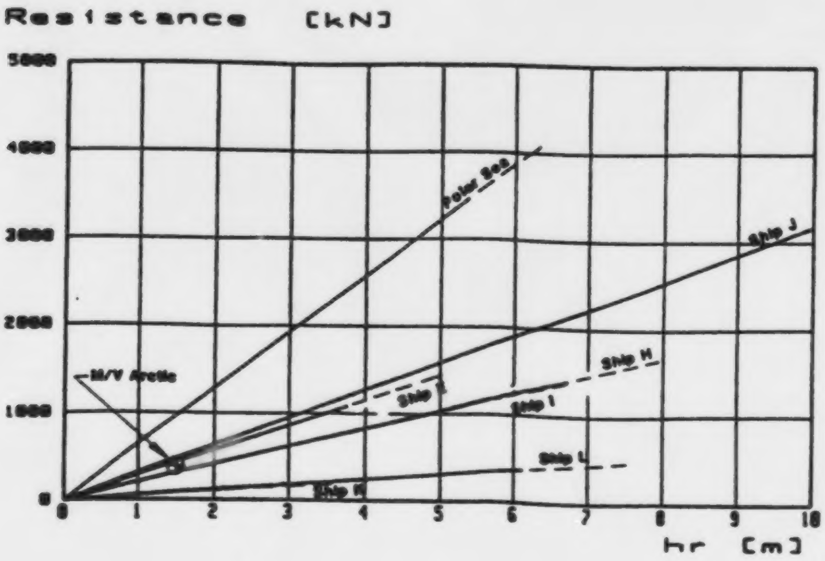

$$\text{Resistance} * \left[B^{\wedge}2 * \frac{B}{d} * \frac{1}{\text{COS}(\varphi)\text{TAN}(\alpha)\text{SIN}(\beta)} + \mu \text{Lm}(.61\ B + .45\ d) \right]^{\wedge}(-1)$$

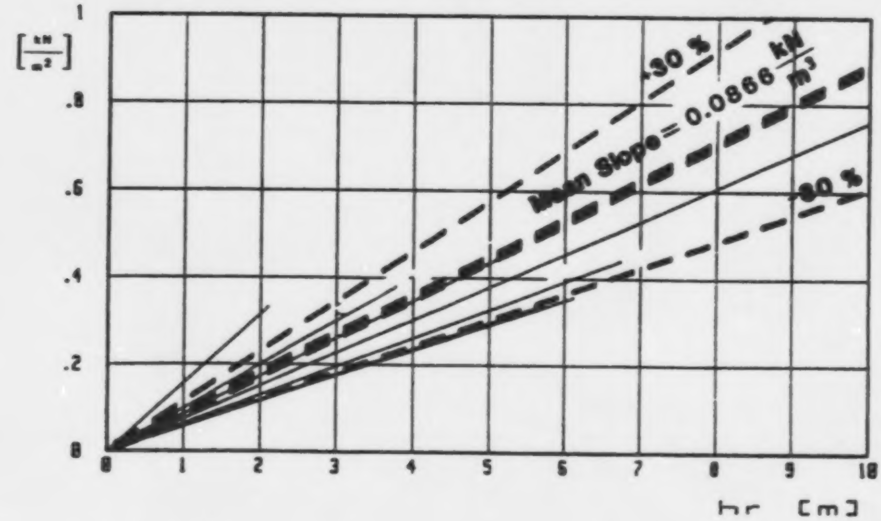

Figure 5.8 Ridge Resistance Reduced by Ship Parameters

6.0 EXTRACTION

As discussed in Section 3.6, extraction in this work refers to the moment when the ship starts to move after getting stuck in a ridge. Thus the focus is on the static forces acting on the ship before it starts moving astern.

6.1 Approach

In developing the research program, the following facts were recognized:

- the available data base is limited; and,
- existing data has considerable scatter which results from the difficulties and costs involved in properly measuring all relevant ridge characteristics. There is no documented underwater measurements on actual ridge formations around a ship after the ship has stopped in a ridge. All data is based on above and/or underwater measurements of the ridge before the ridge was displaced by the ship.

With this in mind, it was obvious that detailed theoretical derivations and complicated formulations are not justified. Such methods would have academic value, but would be of little aid to the designer of an icebreaking ship. Instead the target was set on deriving formulations which combined simplicity with reasonable accuracy, taking into account the accuracy of the present data base.

The program covered the following main blocks:

a) Analytical Development

The purpose of the analytical work was to theoretically establish, in simple form, the major dependencies between important ridge and ship parameters. This was necessary as the existing data base does not allow for an approach based on full scale test results only, as was the case in ridge penetration.

b) Calibration with Model Tests

There are still uncertainties involved in using model tests in ridges for predicting the full scale performance of a ship. However, the model test data base can be applied as long as the limitations of such tests are understood and taken into account. The benefits of model tests are the more accurate information on ridge and other parameters, and the possibility of determining not only the total resistance, but also resistance components.

c) Calibration with Ship Tests

The final calibration was made against data obtained in full scale tests.

6.2 Ice Distribution Around Ship Cross Section

The load per unit length acting perpendicularly to the midship of a vessel can in simple form be written as:

$$q_M = q_{MB} + q_{MS} \tag{6-1}$$

where:

q_{MB} = bottom component of force per unit length
q_{MS} = side component of force per unit length

The bottom component results from the buoyancy force of all ice under the bottom and is therefore directly proportional to the cross section area of the ridge under the bottom, A_B.

The side component is correspondingly the result of ice pressure at the sides of the ship and is assumed to be proportional to the ridge thickness at the side of the ship, h_b.

The definition of A_B and h_b, as well as the ridge thickness before being displaced by the ship (h_r) are presented in the following figure:

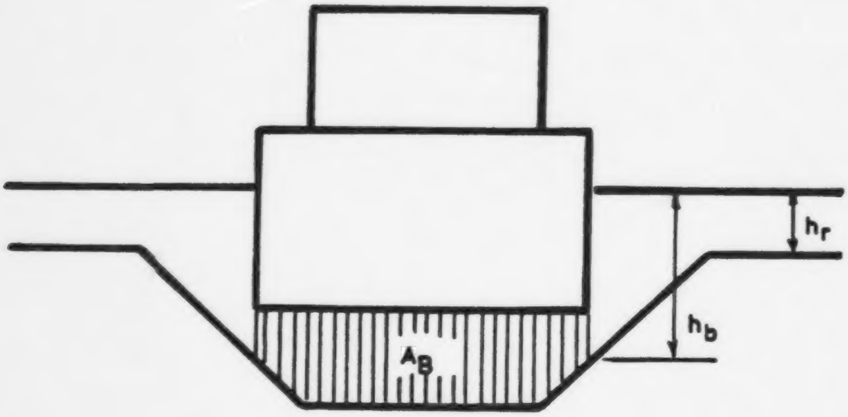

Figure 6.1 Definition of A_B and h_b

By estimating how the ice moves along the hull to its final configuration midships, h_b and A_B as a function of ship breadth (B), draft (d), bow form, and ridge thickness (h_r) can be geometrically determined. These values do not form continuous curves, but have "bends" at certain values of B/d and h_r/d.

Several formulations were developed, initially for simplified hull forms such as vertical wedge bows and landing craft bows. An iterative process including comparisons to model test data (described in Section 6.5) was undertaken resulting in the following expressions:

$$h_b = h_r + 0.65\ d \qquad (6\text{-}2)$$

$$A_B = 0.94\ B\ (h_r - 0.11\ d) \qquad (6\text{-}3)$$

These formulations were developed for ridges deeper than the ship draft. The range $h_r/d < 1$ is not significant for the intent of this work and was neglected. The final formulas also reflect simplifications derived at when accurate, but complicated formulas or parts thereof had a very shallow curvature and were replaced by straight lines. For these reasons Equation (6-2) and (6-3) only apply for reasonable ratios of ship breadth/draft ($B/d = 2 \ldots 5$) and "larger than insignificant" ridges; in practice $d/h_r < 3$. It is recognized that h_b may reach negative values outside the defined range.

Attempts were made to account for the bow shape as it obviously influences the ice flow around the hull. However, no parameters with significant correlation were found.

6.3 Derivation of Midbody Extraction Force

The longitudinal force per unit length caused by ice around the parallel midbody of a ship and preventing the stuck ship from moving can be written in the form:

$$q_1 = \mu_s\ q_M \qquad (6\text{-}4)$$

where:

μ_s = static friction coefficient
q_M = perpendicular ice load per unit length, as discussed in Section 6.2

The total parallel midbody component (F_{EP}) of the total extraction force is:

$$F_{EP} = \int^{Lp} q_1\ dL_p = \mu_s \int^{Lp} q_M\ dL_p = \mu_s \int^{Lp} (q_{MB} + q_{MS})\ dLp \qquad (6\text{-}5)$$

where:

μ_s = static friction
Lp = length of parallel midbody, measured at the waterline
q_{MB} = bottom component of q_M
q_{MS} = side component of q_M

The two components of q_M are determined as follows:

a) Bottom Component

$$q_{MB} = \mu_B \, g \, (\rho_w - \rho_i) \, A_B = C_i \, A_B \tag{6-6}$$

where:

μ_B = ridge porosity; i.e. volume of ice/total volume of ice and water
g = acceleration of gravity
ρ_w = density of water
ρ_i = density of ice
C_i = $\mu_B \, g (\rho_w - \rho_i)$
A_B = cross section area of ice under bottom Figure 6.1

By inserting the expression for A_B, Equation (6-3), the bottom component is obtained:

$$q_{MB} = C_i \cdot 0.94 \, B \, (h_r - 0.11 \, d) \tag{6-7}$$

b) Side Component

The pressure distribution along the side is assumed to be as follows:

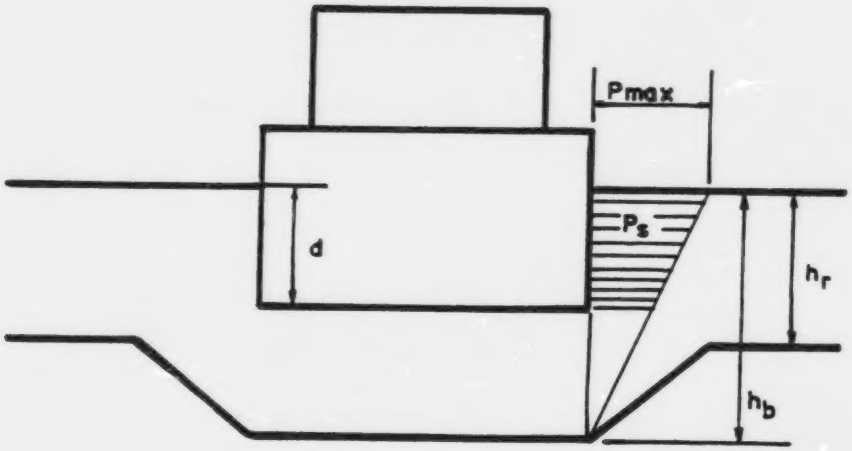

Figure 6.2 Pressure Distribution at Side of Ship

When establishing the side pressure, it is assumed that the consolidated ice in the immediate vicinity of the ship hull is broken up. If proper ice navigation is maintained, ramming will not repeatedly be made along the same track, but the channel will be made wider than the ship.

Based on Figure 6.2, the average pressure is calculated as

$$P_{max} (2 - d/h_b)/2$$

where:

$P_{max} = C_i h_b$
C_i = ridge dependent coefficient defined for Equation (6-6)

The total load per unit length on both sides of the hull is consequently:

$$q_{MS} = C_i C_\nu (2h_b - d) d \qquad (6\text{-}8)$$

where:
$C_\nu = \nu/(1 - \nu)$
ν = Poissoin's ratio for ridge mass

Substituting h_b with Equation (6-2) results in:

$$q_{MS} = C_i C_\nu d(2h_r + 0.3 d) \qquad (6\text{-}9)$$

By combining Equation (6-5), (6-7) and (6-9), and assuming that the whole midbody is covered by a uniform ridge, the total parallel midbody component of the extraction force thus becomes:

$$F_{EP} = C_i \mu_s h_r L_p [0.94 B (1 - 0.11 d/hr) + 2 C_\nu d(1 + 0.15 d/hr)] \qquad (6\text{-}10)$$

For non-uniform ridges, with varying ridge thickness, the average thickness may be used without causing any significant error.

For practical applications Equation (6-10) can be simplified. C_i and C_ν are physical constants for the ridge mass and the following values are used in this report:

$\mu_B = 0.64$
$g = 9.81 \text{ m/s}^2$
$\rho_w = 1{,}025 \text{ kg/m}^3$
$\rho_i = 910 \text{ kg/m}^3$
$\nu = 0.211$
$C_i = \mu_B g (\rho_w - \rho_i) = 722 \text{ N/m}^3$
$C_\nu = \nu/(1 - \nu) = 0.267$

By applying these values in Equation (6-10), the following expression is obtained:

$$F_{EP} = \mu_s \, Lp \, q_M \qquad (6\text{-}11)$$

where:

$q_M = h_r \, [0.68 \, B \, (1 - 0.11 \, d/h_r) + 0.39 \, d \, (1 + 0.15 \, d/h_r)]$ (kN/m)
μ_s = static friction coefficient between ship hull and ridge mass

6.4 Derivation of Midbody Resistance

By replacing the static friction coefficient μ_s with the dynamic one μ_d, Equation (6-11) can be used for calculating the midbody resistance during the penetration phase. However, in penetration the midbody only accounts for a minor part of the total ridge resistance; typically not more than 20% for a ship with long midbody. This makes the influence of the factors d/h_r insignificant. By inserting $d/h_r = 1$ the following simplified formula is derived at:

$$R_p = \mu_d \, L_p \, q_M \qquad (6\text{-}12)$$

where:

$q_M = h_r \, [0.61 \, B + 0.45 \, d]$

6.5 Calibration to Model Tests

Model tests in ridges at Wartsila's facilities are usually performed in a manner which allows the total ridge resistance to be divided into components. Segmented models are not used and it is acknowledged that the results are not fully accurate. However, the extensive data base compensates for the inaccuracy of the individual tests.

The model test data base was used to verify the order of magnitude of analytically derived formulations and to test the trends of important parameters. All comparisons were made in model scale in order to avoid possible systematic errors caused by the scaling process.

The approach was to calculate the midship resistance of each model based on Equation (6-11), using dynamic friction instead of static. In this iterative process several analytically developed expressions for q_M, were tested before the final one was selected. The calculated values were compared to measured ones and regression lines were determined for different parameters as schematically shown in Figure 6.3.

In an ideal situation the regression line would coincide with the horizontal line y = 1. A difference in average value $\overline{y}$ indicates an overall error in the tested equation; e.g. as a result of inaccurate friction or ice characteristics. A slope different from horizontal indicates shortcomings in the influence of the specific parameter in question.

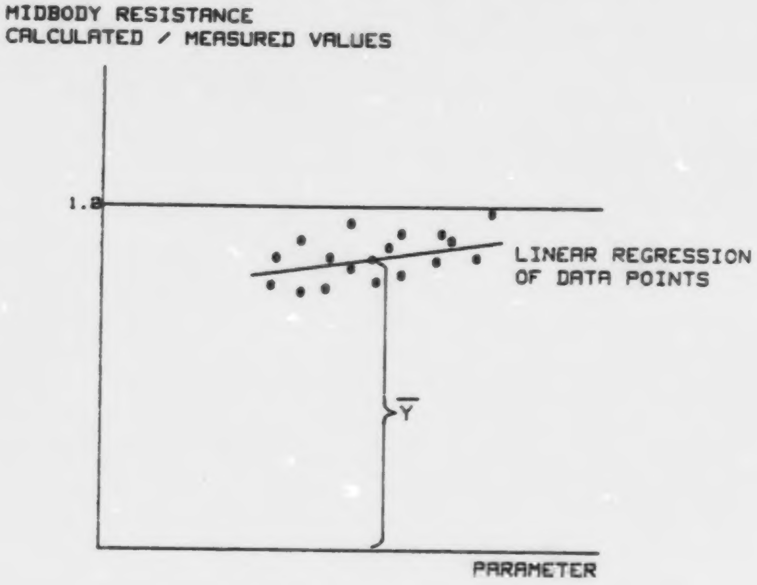

Figure 6.3 Comparison of Calculated and Measured Values (Schematic)

Figure 6.4, shows the results of comparisons for the final equation, Equation (6-11). The calculated values are on an average 16% lower than the measured ones which is well within the expected accuracy. All significant parameters except draft appear to be well described by the equation. Taking into account the small draft range of the tested models, the discrepancy in the draft influence was also accepted.

6.6 Derivation of Bow Extraction Force

The midbody component of extraction is purely dependent upon friction. However, in the bow area an active force trying to push the ship astern is introduced as well. The force equilibrium changes at each point (x, z) of the bow depending on friction, bow angles and ice pressure. The total bow extraction force can be expressed as follows:

$$F_{EB} = \int^{d}\int^{L_E} P_{xz} \cdot f(\text{bow angles, friction})\, dx\, dz \tag{6-13}$$

The total bow force can be divided into two components. Friction prevents the ship from moving astern while the ice pressure, due to the hull form, tries to push it astern. The relationship between the components and the total force is schematically shown in Figure 6.5.

In the left-hand graph the relatively high friction results in a high sticking force. With lower friction, as shown in the right-hand graph, the total force for the whole bow actually becomes negative, indicating that the pushing force is the dominant one. Although schematic, Figure 6.5 shows the sensitivity of friction to the bow form. The significance of $L_E\mu$ will be discussed at the end of this section.

In order to avoid complicated expressions which result from the numerical description of the bow form, or calculations "element-by-element", several approximations were introduced:

a) Direction of Ice Movement

At the moment the ship starts moving, the ice will move relative to the ship along a path which depends on the hull angles. Midship the ice will follow the waterlines while at the stem it follows the buttock. The path between these extreme values can be determined. However, as the area close to midship is the most critical in view of risk of getting stuck, the waterplane angle α has been used to describe the movement.

b) Bow Form-Friction Function

The trigonometric function describing the relationship between the ice pressure and longitudinal force is as follows:

$$f(\text{bow, friction}) = \frac{\mu\cos\alpha - \sin\psi\ \sin\alpha}{1 - \mu\sin\alpha\ \sin\psi\ \cos\alpha} \qquad (6\text{-}14)$$

However, this function can be approximated using the nominator only; i.e. ($\mu\cos\alpha - \sin\psi\ \sin\alpha$). The error caused by this simplification is insignificant as shown in Figure 6.6.

c) ψ - Angle

The average ψ - angle, as defined in Section 5.1 is used as representation for the whole bow.

d) Waterline Angle

Figure 6.7 graph shows representative examples of the half waterline angle between the aft end of the bow shoulder and the forward perpendicular of different types of icebreaking ships.

Despite local variations a good overall description of α_x is obtained by linear interpolation:

$$\alpha_x = \frac{x}{L_E} \alpha_s \tag{6-15}$$

where:

α_s = 1/2 angle at stem; however, disregarding abrupt roundings or other changes close to stem; see the figure on page 48.

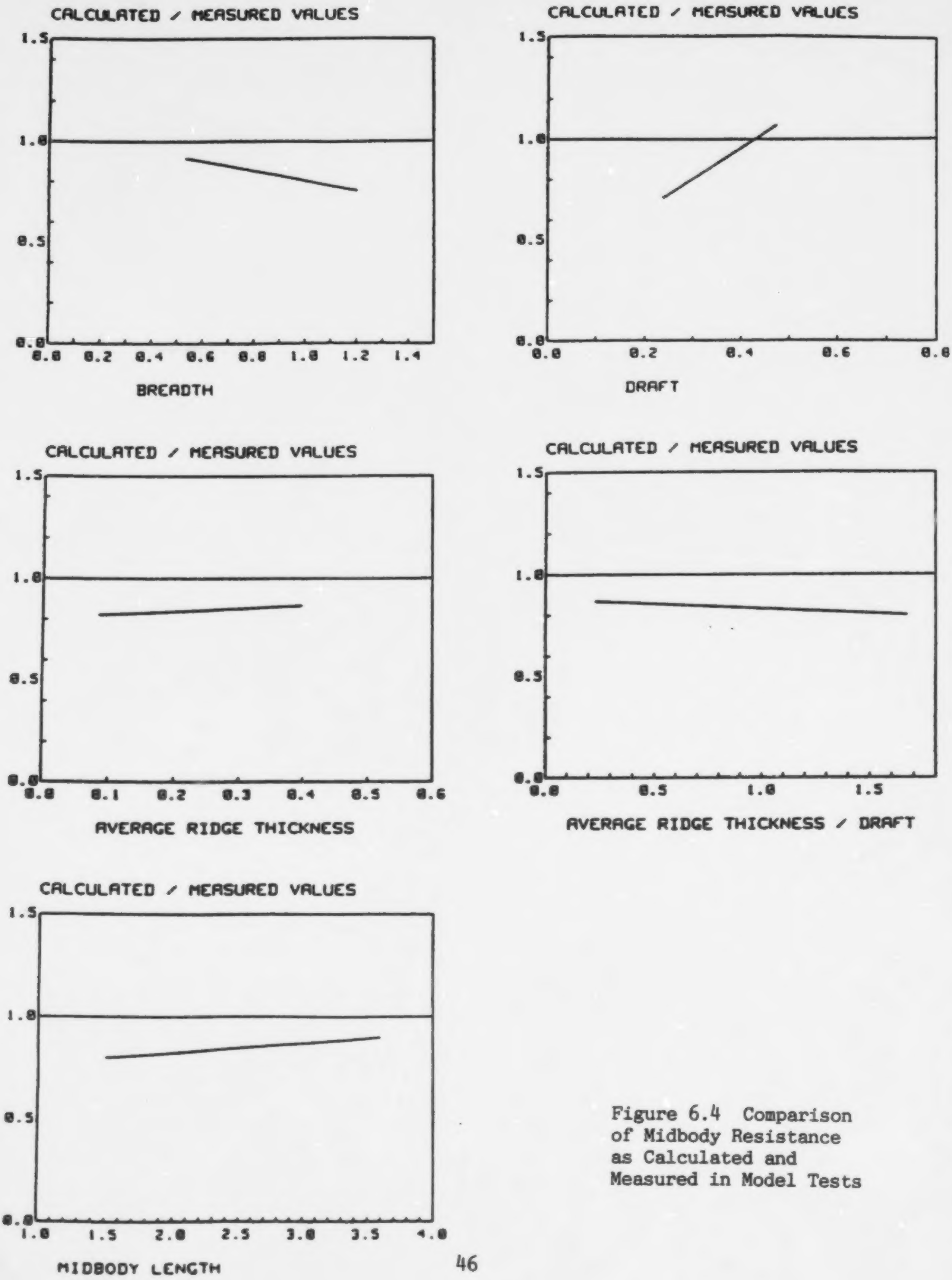

Figure 6.4 Comparison of Midbody Resistance as Calculated and Measured in Model Tests

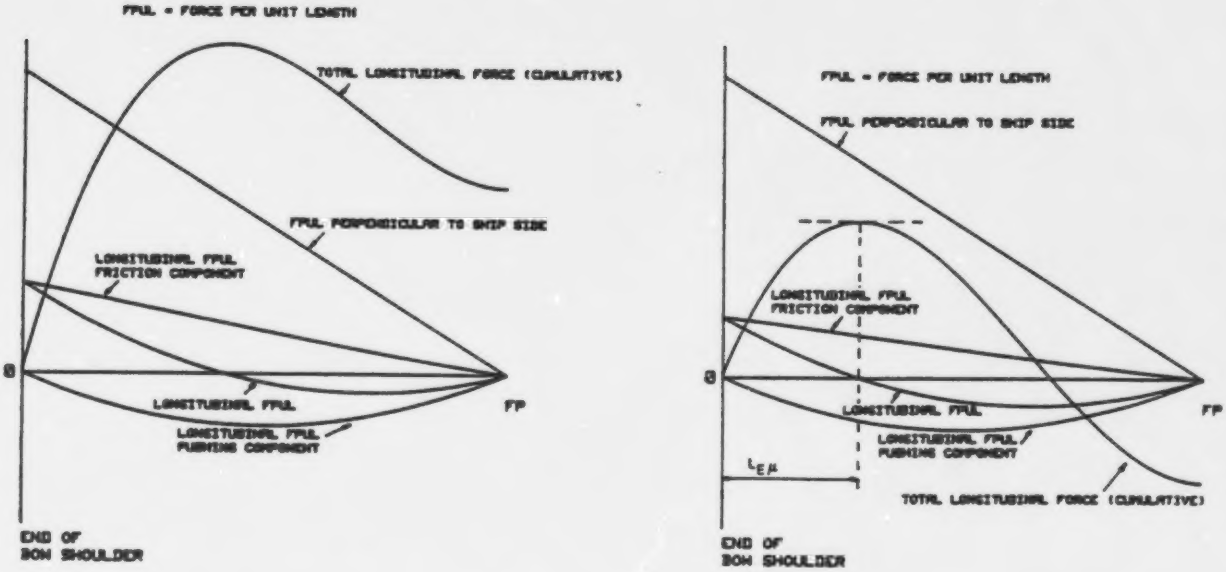
FPUL = FORCE PER UNIT LENGTH
TOTAL LONGITUDINAL FORCE (CUMULATIVE)
FPUL PERPENDICULAR TO SHIP SIDE
LONGITUDINAL FPUL FRICTION COMPONENT
0
LONGITUDINAL FPUL
FP
LONGITUDINAL FPUL PUSHING COMPONENT
END OF BOW SHOULDER
FPUL = FORCE PER UNIT LENGTH
FPUL PERPENDICULAR TO SHIP SIDE
LONGITUDINAL FPUL FRICTION COMPONENT
0
LONGITUDINAL FPUL
FP
LONGITUDINAL FPUL PUSHING COMPONENT
L_Eμ
TOTAL LONGITUDINAL FORCE (CUMULATIVE)
END OF BOW SHOULDER

Figure 6.5 Ice Forces at Bow of Ship (Schematic)

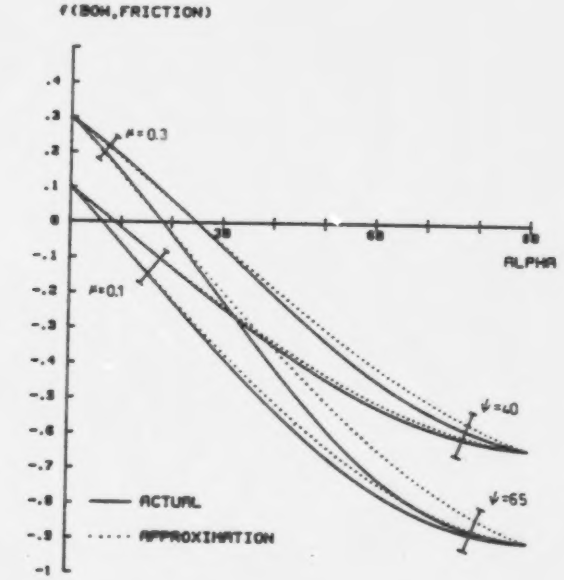

Figure 6.6 Bow Form - Friction Function, Accurate and Approximate Form

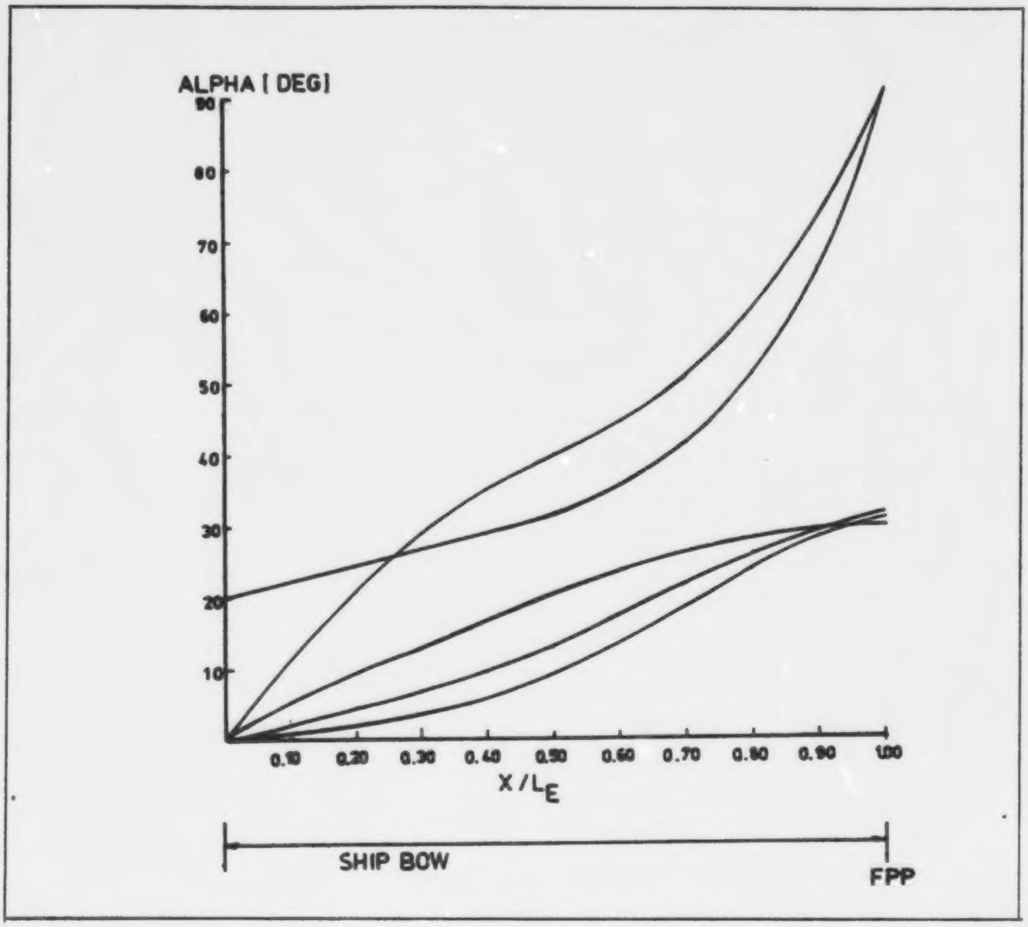

Figure 6.7 Examples of Half Waterline Angle (ALPHA) Along Bow

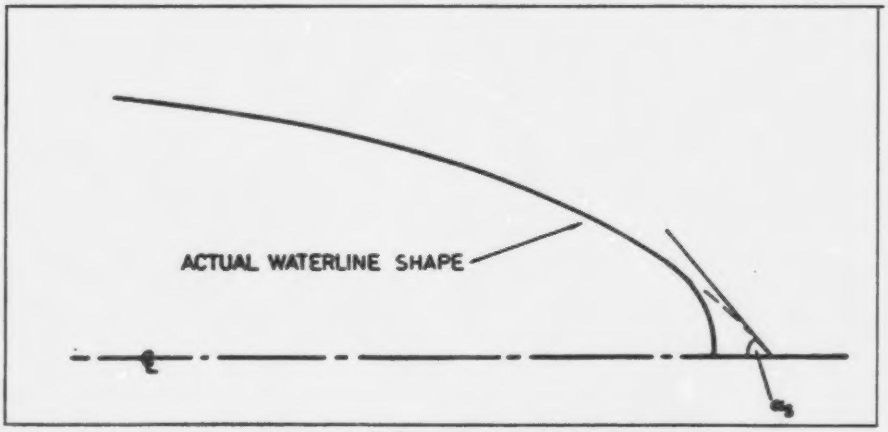
ACTUAL WATERLINE SHAPE
℄
α_s

Figure 6.8 Definition of α_s

e) Ice Pressure Distribution

The basic assumption in establishing the distribution of ice load per unit length around the bow was that in any cross section this load is directly dependent on the cross sectional area of the ship in that section. This area describes the amount of ice that has to be displaced.

Figure 6.9 presents, for several ships, the relationship between the cross section area along the bow and its location. Clearly, the cross section area can be replaced by a linear function of the location, and correspondingly the load per unit length in a point x can be expressed as:

$$q_x = q_M \, (1 - x/L_E) \qquad (6\text{-}16)$$

At x = 0, i.e. at the aft end of the shoulder, the cross section area of the midship is reached. Thus q_M as defined in Equation (6-1) and (6-11) can be used.

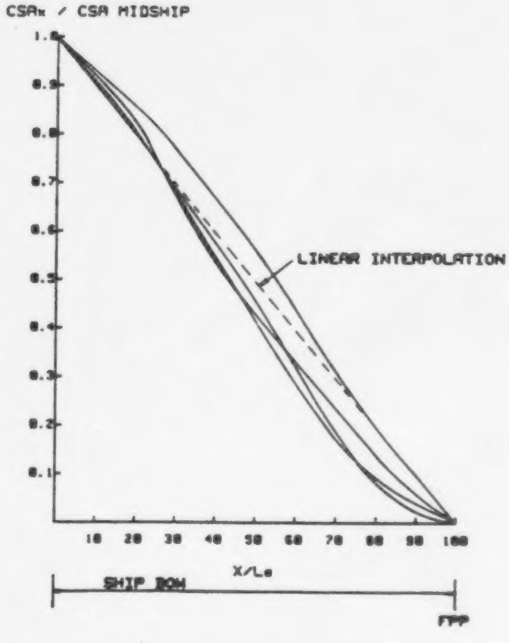

Figure 6.9 Examples of Cross Section Areas Along Bow

Based on the above approximations, Equation (6-13) can be rewritten as follows:

$$F_{EB} = \int^{L_E} [q_M (1 - x/L_E)(\mu_s \cos(\alpha_s x/L_E) - \sin \psi \sin(\alpha_s x/L_E))]dx \tag{6-17}$$

and after integration:

$$F_{EB} = q_M \left[\frac{L_E}{\alpha_s} \sin \psi \ (\sin \alpha_s / \alpha_s - 1) + \mu_s \frac{L_E}{\alpha_s^2} (1 - \cos \alpha_s) \right] \tag{6-18}$$

Note that α_s is here expressed in radians.

The value of $F_{EB}/(q_M L_E)$ calculated according to Equation (6-18) is shown in Figure 6.10 below:

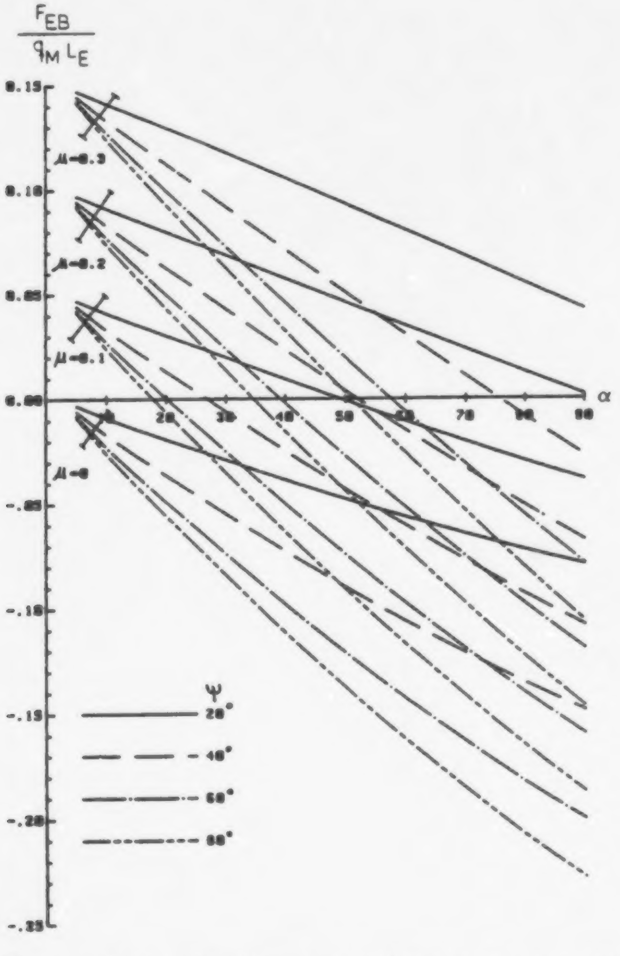

Figure 6.10 $F_{EB}/(q_M L_E)$ Calculated According to Equation (6-18)

Based on Figure 6.10, Equation (6-18) can be approximated as follows:

$$F_{EB} = \frac{q_M L_E}{2} \quad \alpha_s - (0.4 + 5 \sin \psi) \ \alpha_s/1000 \qquad (6\text{-}19)$$

with α_s in degrees

or

$$F_{EB} = C_E \, q_M \, L_E/2 \qquad (6\text{-}20)$$

where:

$C_E = \alpha_s - (0.4 + 5 \sin \psi) \ \alpha_s/1000$

with α_s in degrees

This force may be positive or negative depending on bow form and friction. A negative value means that the ship is pushed astern unless held in place by other resistance components.

In order to establish limiting conditions a more difficult situation can be found when the shoulders, with high friction forces, are covered by the ridge, but the forward parts of the bow, with high pushing forces, are free from ice. Assuming presence of ice to the point where these force components are equal, the following expression are derived at:

$$F_{EB} = \mu_s \, q_M \, L_E /2 \qquad (6\text{-}21)$$

where:

$L_{E\mu}$ = longitudinal distance at waterline from aft end of shoulder to point where friction force = pushing force, i.e. approximately when $\alpha_x = \mathrm{atan}(\mu_s/\sin \psi_x)$

The definition of $L_{E\mu}$ is further clarified in Figure 6.5.

6.7 Additional Considerations

An accurate calculation of the extraction force would include two additional elements:

a) Aftbody Extraction Force

Aft of midship or the aft of the parallel midbody, the ridge pressure on the hull rapidly decreases. Furthermore it is reduced and can actively be reduced by the suction of the propeller(s). It was therefore neglected.

b) Astern Force Due to Potential Energy

When stopping in a large ridge the bow of a ship is often lifted which results in significant trim. This creates an astern force component on the ship. It is not uncommon that a ship moves backward without any astern thrust after ramming into a ridge.

This feature is significant, however, the purpose of this study was to determine limiting situations. Consequently, a conservative approach was taken assuming that the ship is totally inside the ridge. Although lifted up by the ridge and on even keel.

6.8 Calibration to Full Scale Tests

The total extraction force, calculated as the sum of midbody force, Equation (6-11) and bow force, Equation (6-20), was compared to the results of icebreaker full scale extraction tests. The results are presented in the following figure.

A static friction coefficient value of 0.25 has been used in Figure 6.11 which corresponds to an uncoated new icebreaker hull. Taking into account the inaccuracies involved in any full scale testing in ridges, the results are quite satisfactory. Therefore, no further adjustments to the formula were made.

6.9 Final Formulations

This section summarizes the final expressions to be used for determining limiting extraction conditions.

For the whole ship embedded in a ridge, the following expression for total extraction force was obtained:

$$F_E = q_M \left(\mu_s L_P + C_E L_E/2 \right) \qquad (6\text{-}22)$$

where:

$q_M = h_r \left[0.68\ B\ (1 - 0.11\ d/h_r) + 0.39\ d\ (1 + 0.15\ d/h_r)\right]$ kN/m
valid for $d/hr < 3$
μ_s = static friction coefficient between ship hull and ridge mass
L_P = length of parallel midbody
$C_E = \mu_s - (0.4 + 5 \sin \psi)\ \alpha_s/1000$
with α_s in degrees
L_E = entrance length
B = ship breadth
d = ship draft
h_r = average ridge thickness

For a conservative situation, with no ice close to the stem pushing the ship astern, the following expression is obtained:

$$F_E = \mu_s q_M (L_P + L_E \mu/2) \qquad (6\text{-}23)$$

where L_E is the longitudinal distance between the aft end of the bow shoulder and the point where the friction force equals the pushing force as shown in Figure 6.5. This takes place approximately when
$\alpha = \mathrm{atan}\ (\mu_s/\sin\psi)$

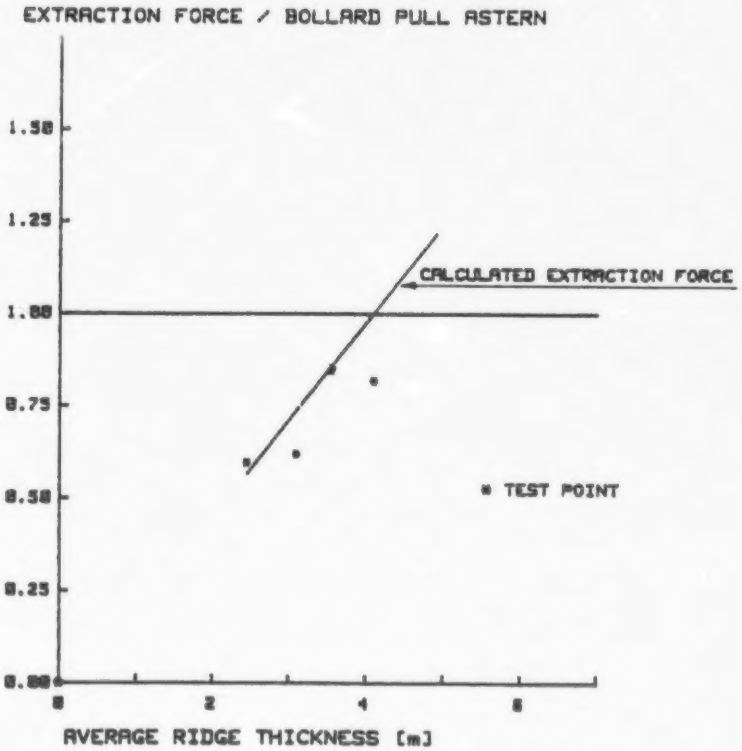

Figure 6.11 Comparison of Full Scale Test Results and Calculated Extraction Force

7.0 PARAMETRIC INVESTIGATION

The objective of this section is to establish limiting conditions for operation in first year ridges. For this purpose a parametric series of icebreaking ships were defined. The capability of these ships to penetrate ridges as well as to free themselves after getting stuck were evaluated.

7.1 Penetration

The ridge performance capabilities in the form of limiting conditions for the continuous mode of operation are determined by application of the ridge resistance formula developed in Section 5.0. The results of this section express, for the investigated ships, the limiting ridge sail height as a function of level ice thickness.

7.1.1. Assumptions

The following general assumptions affecting the performance capabilities of the tested ships were made:

Friction: - a dynamic friction coefficient of $\mu_d = 0.1$ was used.

Thrust: - a thrust/power ratio of 9 kg/hp was assumed for all ships;

- thrust was approximated as a linear function of ship speed; and,

- thrust at open water speed was assumed to be 50% of thrust in the bollard condition.

7.1.2 Systematic Analysis

The variations of power levels and bow geometric parameters for a small, medium and large sized icebreaking hull form resulted in 18 different ships to be analyzed. The range of tested main particulars, installed power levels and bow angles is summarized in Table 7.1.

Table 7.1 Ship Parameter

Block Coefficient C_b		.56		
B/d		3.3		
Displacement	[t]:	5,000	15,000	30,000
Thrust Levels in Bollard Condition	[t]:			
	Low:	40	150	300
	Medium:	95	275	550
	High:	150	400	800
Corresponding Main Particulars [m]:				
	B:	20.0	25.0	30.0
	d:	6.0	7.5	9.0
	L_{CWL}:	75.0	120.0	135.0
Bow Geometries:				
	Conventional:	$\psi = 43^\circ$		
	Medium:	$\psi = 35^\circ$		
	Extreme:	$\psi = 29^\circ$		

The variations in investigated ice conditions are listed in Table 7.2.

Table 7.2 Ice Parameters

Level Ice Thickness:	.10, .20, .30, ..., 1.70, 1.80 m
Ridge Sail Height:	.10, .20, .30, ..., 3.60, 3.70 m
Consolidation/h_{ice}:	0, 1, 2
Ridge Aspect Ratio:	h_R/W_R: .065

The individual ridges are defined through the selection of the ridge sail height h_s. In connection with the h_R/W_R ratio of .065 and Equation (4.2) presented in Section 4.0 ridge width and average thickness are determined.

The variation of level ice thickness and ridge sail height in combination with three levels of consolidation resulted in a total of 2,000 cases.

The sensitivity analysis was carried out with a computer transit simulation model developed by Wartsila Arctic Inc. The model applies Newton's Second Law of Motion to determine the combined influence of resistance forces and inertia forces on the ship's progress in defined ice conditions. The principle of the simulation model and the applied analytical methods for the determination of resistance components are explained in Appendix C.

7.1.3 Results

For each tested ship and for the investigated range of level ice thickness, the systematic analysis provided the particulars of the limiting ridge which stopped the ship. Plotting the corresponding data pairs of h_{ice} and h_s with ship size, power, bow geometry and consolidation as parameters resulted in the presentation of Figure 7.1.

The layout of this Figure enables easy determination of the ice conditions which would require a given ship to progress by ramming. Vice versa, for given ice conditions, the power requirements for a continuous mode of operation can be determined as a function of ship size.

The influence of size and power is clearly apparent. For a given displacement performance capabilities are naturally improved when installed propulsion power is increased. In the case of a 15,000 t displacement ship with a conventional bow ($\psi = 43^o$) in level ice of .70 m thickness and a consolidated thickness of 1.40 m within ridges the limiting ridge sail height for different power levels are derived from

Figure 7.1 as:

Table 7.3 Limiting h_s (h_{ice} = .70 m, ψ = 43°

shp	h_s
16,800 shp	0.60 m
30,600 shp	2.00 m
44,500 shp	2.75 m

7.1.4 Discussion of Results and Limitations

The results from the penetration analysis provide an initial tool to predict the power requirements for continuous motion in the icefield of widely spaced ridges with:

- level ice thickness;
- ridge sail height; and,
- ship particulars (in accordance with Table 7.1)

as parameters.

The h_s/h_{ice} diagrams indicate further where operational requirements demand ships with greater displacement and power. At the same time they allow identification of regions where smaller ships with relatively high installed power can compete with bigger ships with propulsion powers at the lower end of the relative scale.

In order to highlight the influence of the consolidation within the ridge cross plots for a fixed sail height of 2.0 m were developed. The results are shown in Figure 7.2. For a ship with Δ = 15000 t and ψ 45°, the following limits are established.

Table 7.4 Limiting h_{ice} (h_s = 2.00 m, ψ = 43°)

shp	hc/hice			Maximum Change Early-Late Winter
	0	1	2	
16,700	.45	.40	.35	22%
30,600		.80	.72	28%
44,500	1.55	1.32	1.05	32%

The influence of bow geometry is clearly visible in Figure 7.3. This figure was obtained by cross-plotting the results of Figure 7.1 for a consolidation of 2.0 * h_{ice}. Again, using the 15,000 t vessel as an example the following table results:

Table 7.5 Limiting h_{ice} (h_s = 2.0 m, h_c/h_{ice} = 2)

shp	29°	34°	43°	Maximum Change in Limiting h_{ice}
16,700	.75	.58	.35	53%
30,600	1.25	1.00	.72	42%
44,500	1.75	1.40	1.05	42%

Within the scope of the present work only a limited number of ships and ice parameters were investigated.

Concentration of representative ice breaker hull form (i.e. C_b = .56, B/d = 3.33) and a typical Beaufort Sea ridge geometry (h_r/W_r = .065) produces results of some practical value for Canadian Arctic applications.

To create a universal design tool a denser net of ship and ice parameters will have to be investigated. In particular the random character of ridge size and ridge spacing in nature has to be considered in more detail.

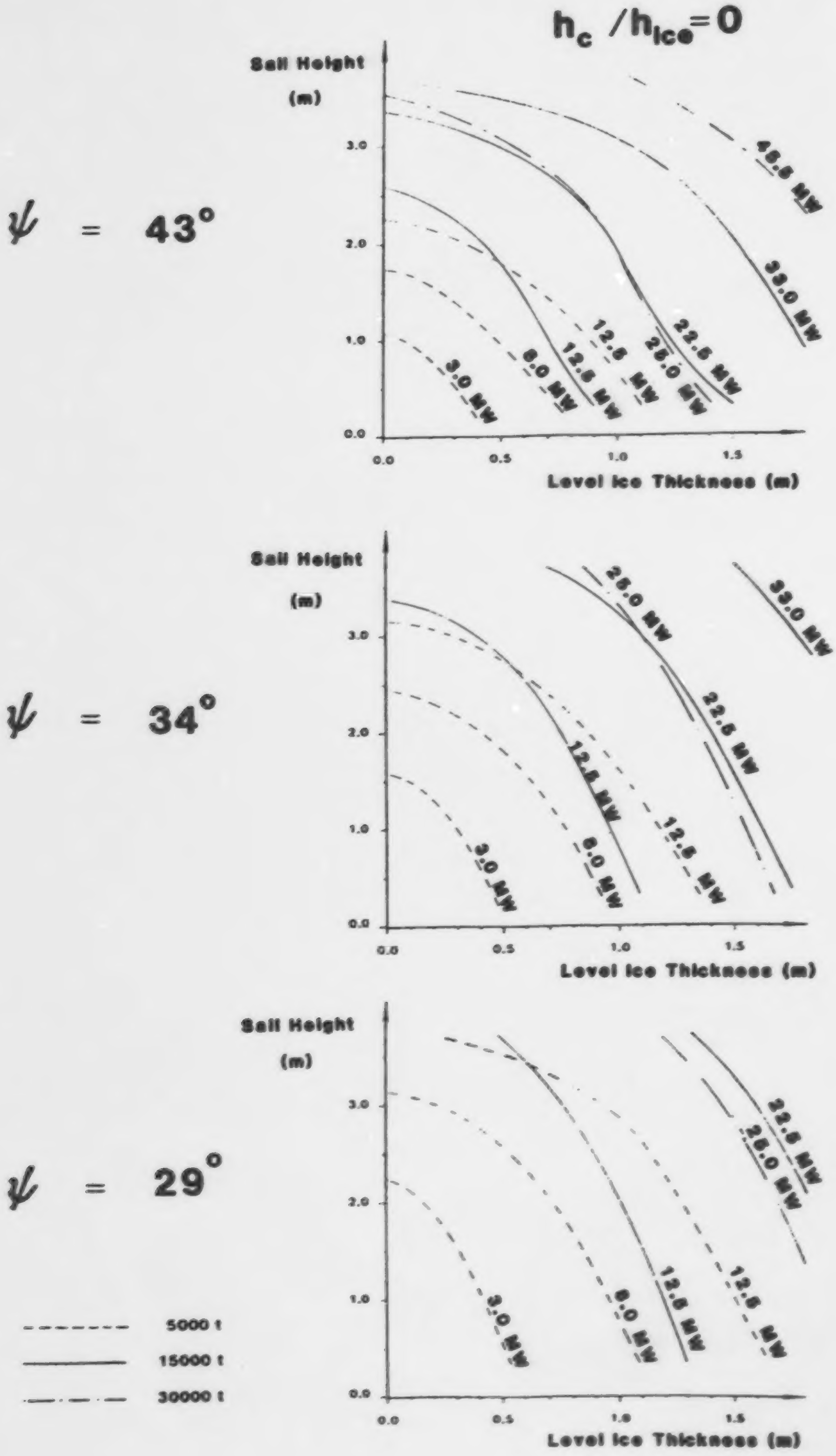

Figure 7.1 Limiting Ice Conditions

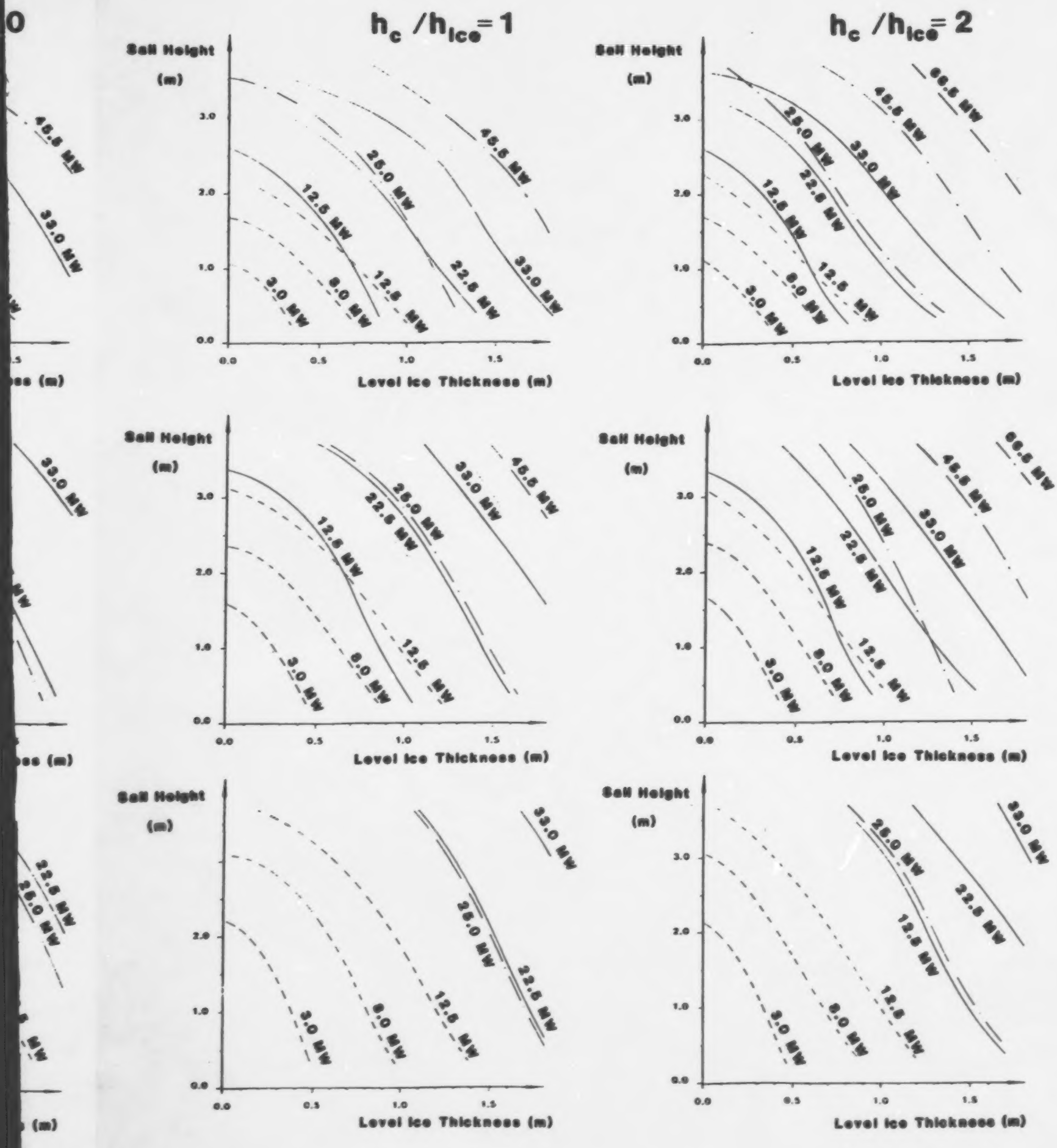

itions for Continuous Mode of Operation

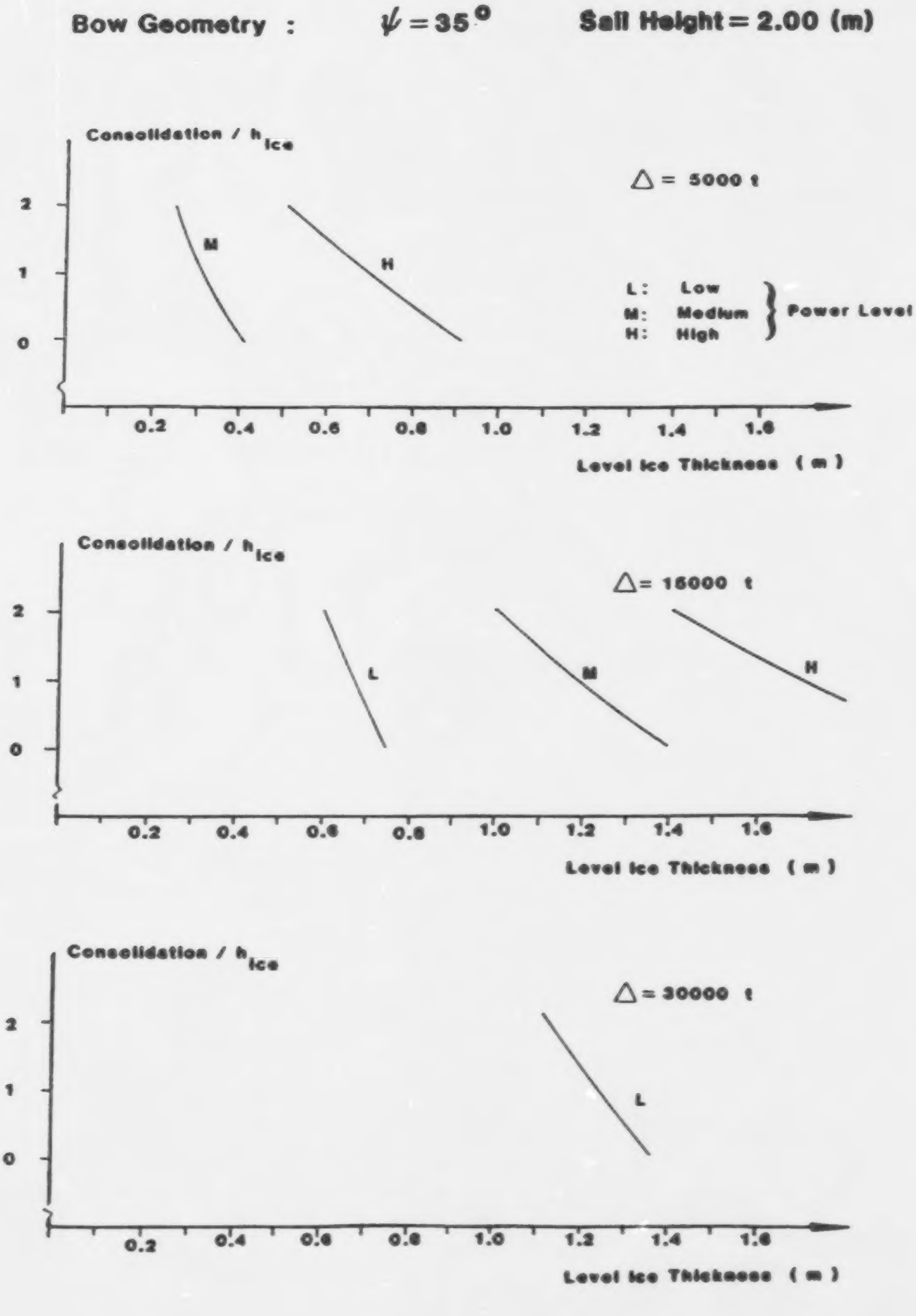

Figure 7.2 Influence of Consolidation on Performance Limits

Ridge Sail Height : 2.00 (m)

Consolidation / h_{ice} : 2.0

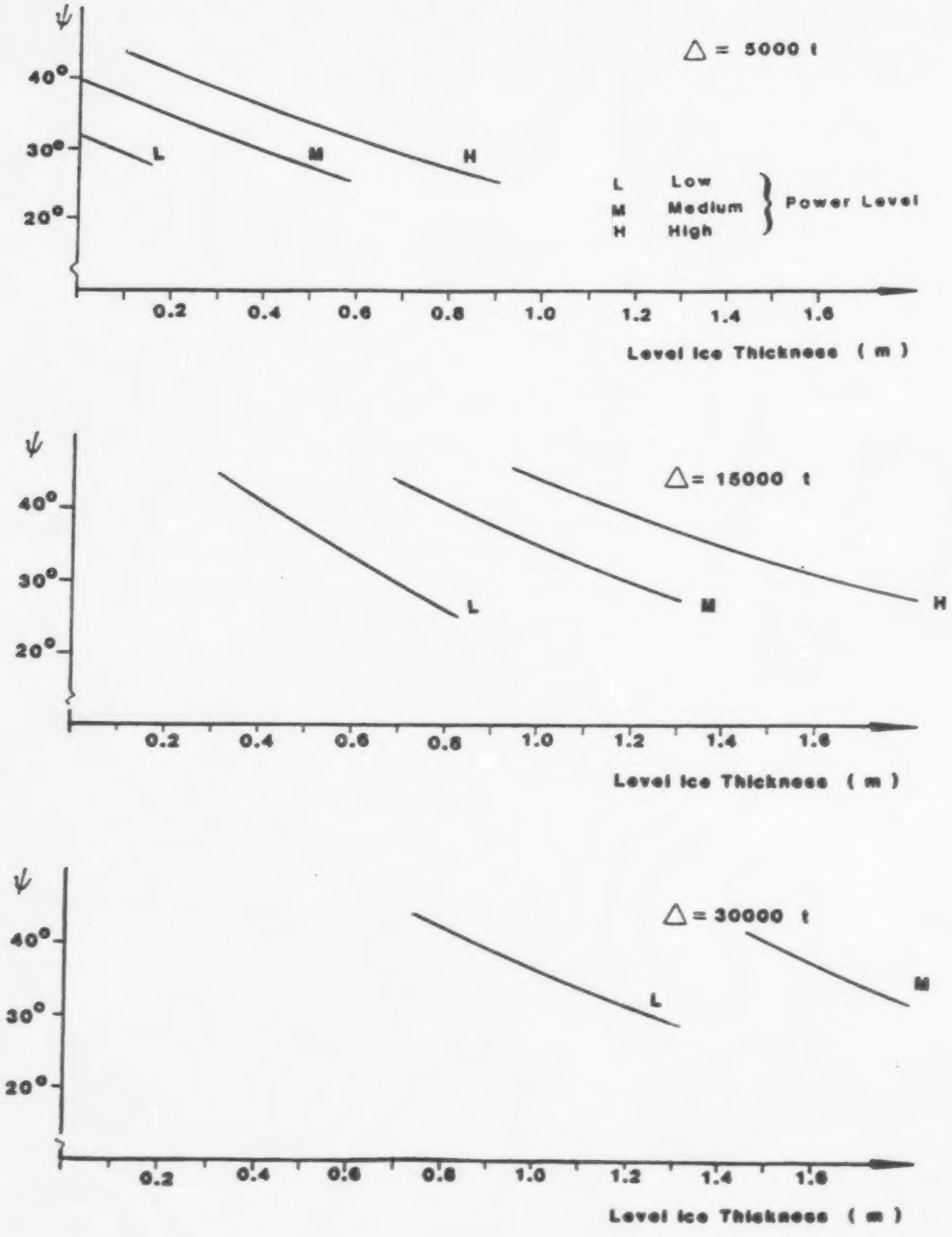

Figure 7.3 Influence of Consolidation of Performance Capabilities

7.2 Extraction

7.2.1 Approach

Due to the static nature of extraction, a more comprehensive presentation is possible compared to penetration. Limiting conditions can be established directly using Equation (6-22) and therefore computer simulations are not needed. The presentation is made for the same three vessels as used in the penetration analysis. These ships, which are presented in Table 7.1, form a systematic series for size and bow forms.

When presenting the three bow forms, "Conventional" ($\psi = 43^o$), "Medium" ($\psi = 35^o$), and "Extreme" ($\psi = 29^o$), the total length of the ship is kept constant in order to compare ships of approximately the same displacement. Consequently, a ship with a short bow, such as the extreme bow, has a longer midbody section than the ship with a longer, conventional bow.

7.2.2 Results

For all nine vessels the necessary astern thrust as function of ridge thickness was determined using Equation (6-22) and transformed into shaft power. For establishing the power vs astern thrust relationship, a CP propeller was assumed. Figure 7.4 summarizes the results of this evaluation showing the influence of ridge thickness, ship size and bow form on the required power for successful extraction.

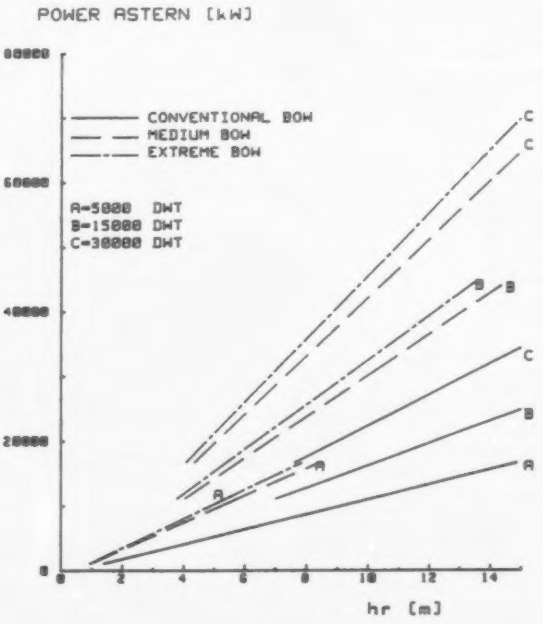

Figure 7.4 Required Extraction Power for Ships Presented in Table 7.1

It is also of interest to know how each separate ship parameter influences the required extraction power. To investigate this, a vessel with the following parameters was selected:

Ship B (15000 dwt)
h_r = 10 m
μ_s = 0.25

The required extraction power was determined for variations in ship draft, breadth, length, bow form, and friction coefficient. The influence of each of these parameters is presented in Figures 7.5 a-f.

This investigation was made for one parameter at time, keeping the others constant. However, the hull angles of the bow are interrelative and a modification of hull lines usually changes both the angles used to describe the bow in the extraction analysis. For the purpose of assessing the bow component of the extraction force, a comparison for the three actual bows defined in this Section, with simultaneous variations in all hull angles, was also made. Only the bow was taken into account, while the midbody was disregarded. The results are presented in Figure 7.6. The extreme bow is not shown as it does not get stuck in this case, i.e. the resultant force is negative.

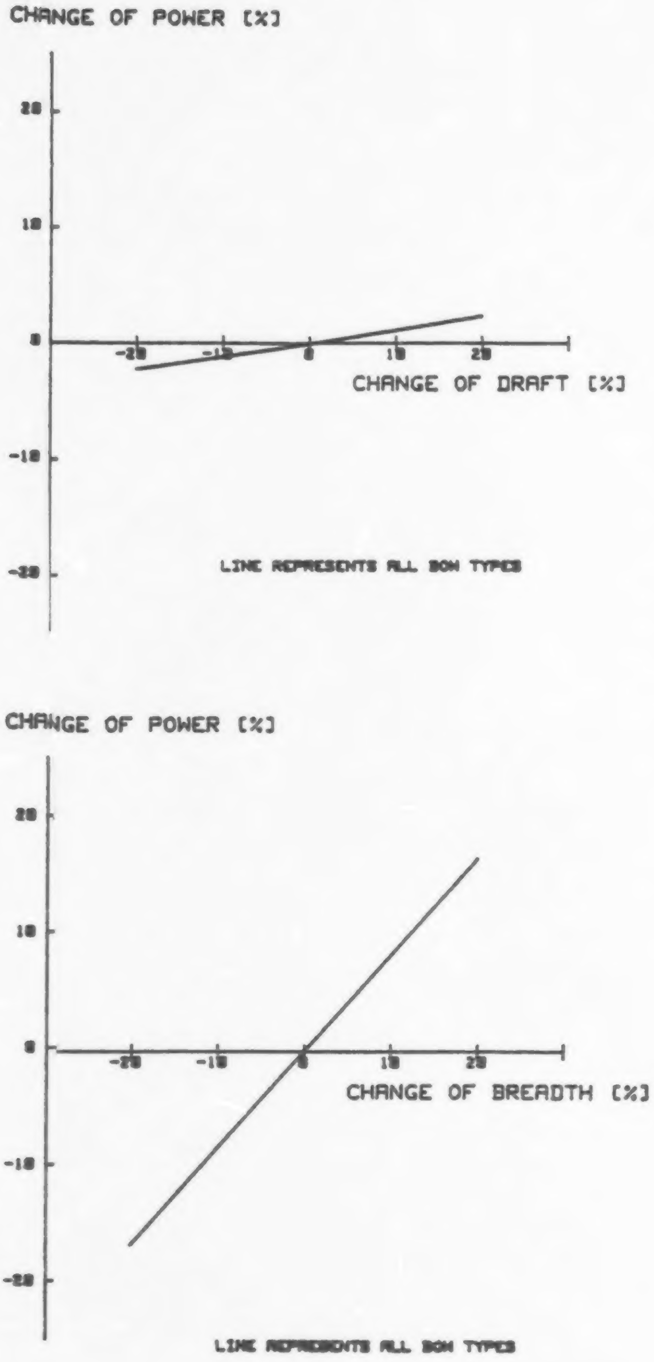

Figure 7.5 a-b Influence on Extraction Power of Parametric Draft and Breadth Variations

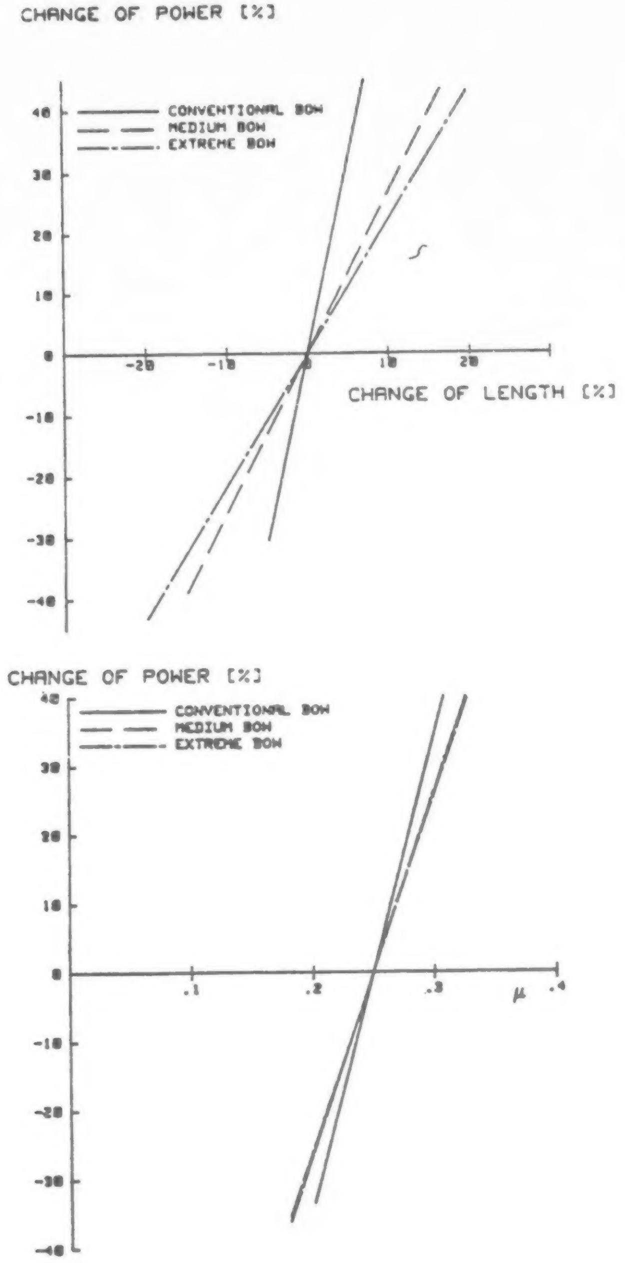

Figure 7.5 c-d Influence on Extraction Power of Parametric Ship Length and Friction Variations

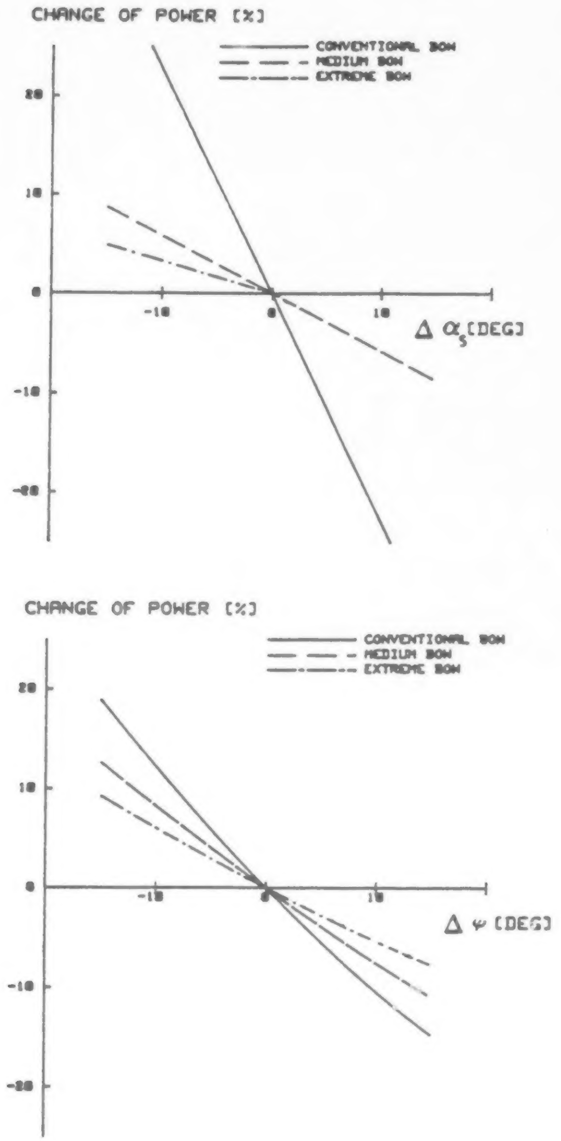

Figure 7.5 e-f Influence on Extraction Power of Parametric ψ and α_s Variations

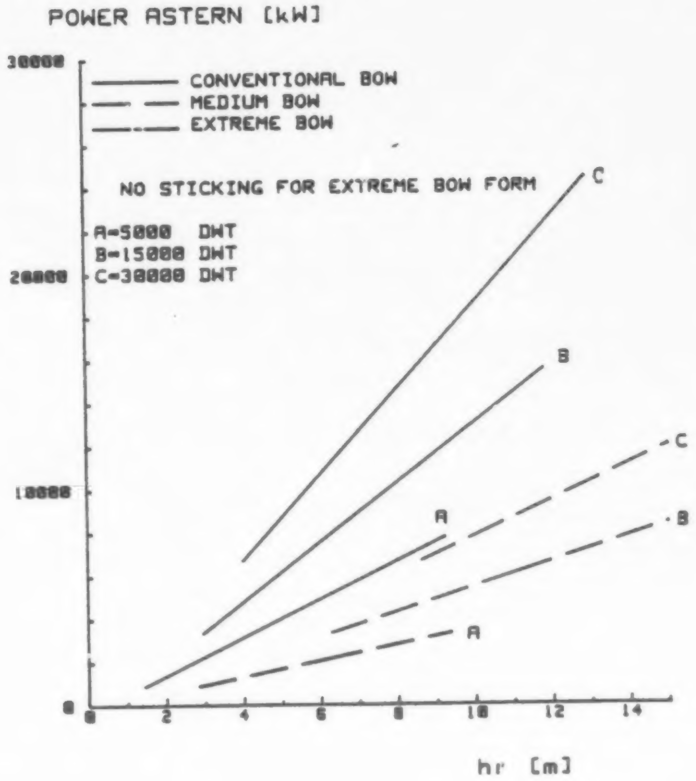

Figure 7.6 Bow Component of Extraction for "Conventional", "Medium", and "Extreme" Bows. Midbody Free of Ice.

7.2.3 Discussion of Results

As shown in Figure 7.5, the influence of ship breadth is the dominant parameter compared to the draft. In the presented case, with $B/d = 3.3$, a 10% increase in width requires an 8% increase in power. Correspondingly, a 10% increase in draft requires a 1% power increase. In the latter case the influence of possible increased propeller diameter is not accounted for.

When evaluating the influence of ship length, the increase/decrease of total length has been made as a change of midbody length, while the bow and stern are unchanged. The midbody component (side + bottom) of the extraction force is directly proportional to the midbody length. However, the influence of a variation of ship length on the total extraction force depends on the magnitude and direction of the bow force component. The ship with a conventional bow and a relatively short midbody is more sensitive to an increase/decrease of length than the ships with longer midbodies.

For a minimum bow extraction force component, a short bow with large waterline angle at the stem is beneficial as shown in Figure 7.6. However, the bow cannot be looked at in isolation. As described above, a short bow requires a longer midbody for equal displacement and the increase of midbody component may result in a higher total extraction power, as is the case for the ships presented in Figure 7.4. In general terms, short bows with large ψ and α_s angles give low extraction force components, but this influence has to be weighed against the increase of midbody length and the efficiency of the bow in other modes of ice operation.

The extraction force is quite sensitive to the friction coefficient between the ridge mass and the ship hull. Its value for full scale application is not well defined due to its variations with time and load, as well as the problems encountered in measuring it in full scale, and is therefore a source for uncertainty in any evaluation of extraction.

The midbody extraction force component is directly proportional to the friction. At the bow a change of friction causes a larger change of sticking force due to he changing relationship between friction and pushing forces along the hull.

It should be noted that all comparisons presented in this chapter are valid only for the defined ships and conclusions for ships with other combinations of dimensions, hull form and ridge thickness should not be made. However, alternative evaluations can easily be made using Equation (6-22).

8. CONCLUSIONS

The work of the preceeding sections focused on three major aspects:

- the analysis of the morphology of first year ice ridges relevant to ship transit;
- the analysis of ship ridge penetration tests; and
- the analysis of requirements related to ship extraction from ridges.

Within the scope of the investigation the most significant ship size and hull geometry parameters relevant to the performance capabilities for ships operating in first year ice ridges were identified. The following sub-sections examine closely the findings related to the above topics.

8.1 First Year Ridges

A total of 136 ridges measured during various field tests were analyzed. The investigation revealed distinct differences in the geometry of ridges found in the Baltic, Bering and Beaufort Seas. The following conclusions are apparent:

1. The ice mass within a ridge; i.e. the cross sectional area (CSA) cannot be determined sufficiently on the basis of the ridge sail height (h_s) alone.

2. The average ridge thickness (h_r) links the width of the ridge (W_r) and the CSA. The introduction of the ridge aspect ratio (h_r/Wr) provides the parameter for establishing the possible range of CSA for a given sail height.

3. The cross sectional area increases with the sail height (for h_r/Wr = constant). An upper limit for CSA is reached at CSA = 1300 m^2.

4. This upper limit is associated with a sail height of about 3.7 m. For a single ridge in the Beaufort Sea this compares to an exceedance probability of less than 1.0% (see 2). The above conclusions are reflected in Equation (4-2).

For the evaluation of the trafficability of proposed routes through ice covered waters statistical information related to ridge sail height and distribution is generally available. Through variation of h_r/Wr it is possible to establish a range for the severity of ridges to be expected in the proposed area of operation.

8.2 Ridge Penetration Analysis

A functional relation between resistance, ridge parameters and ship parameters was derived on the basis of full scale ridge penetration tests (see Equation (5-2)). Ridge resistance is expressed as a linear function of the average ridge thickness (h_r). A comprehensive sensitivity analysis identified the following ship particulars as of primary significance for the resistance:

- Breadth (B);
- Breadth/draft ratio (B/d); and
- the ships bow geometry defined through α, β and φ .

For practical design applications the following conclusions are of importance:

1. The influence of B^2 on the resistance during the penetration phase is more significant than the sectional area amidships.

2. The B/d ratio influences the resistance in a significant way. For a given sectional area amidships a relatively "deep" ship (i.e. small B/d ratio) has an advantage over a "shallow" ship.

3. The design of the bow optimized for ice operation must minimize the bow geometry term in Equation (5-2). Penetration resistance is reduced by:

   - increasing the waterplane angle;
   - increasing the flare angle; and
   - decreasing the stem angle.

   A cylindrical bow form results.

4. For considerations related to the penetration resistance the component due to parallel midbody is of secondary order.

The formula resulting from the ridge penetration analysis (Equation (5-2)) is based entirely on the unique investigation of full scale test results. The diverse ship sizes and types considered in the database warrant applicability of the prediction formula over a wide range. The following table illustrates the range of significant parameters.

Table 8.1 Tested Range of Parameters Significant for Penetration Resistance

Parameter	Investigated Range (Minimum)	(Maximum)
B [m]	11.10	25.50
B/d	2.10	4.6
"α" [deg]	20	51.0
"β" [deg]	29	70.0
"φ" [deg]	15	40.0
L_m [m]	0	76.0
L_m/L_{wl}	0	0.50
shp	4,750	60,000
Δ [t]	1,440	38,100

8.3 Ridge Extraction Analysis

In deriving the formulation for the extraction force, a three-step approach was taken due to the limited data base of full scale tests. The principal relationships between extraction force, ship parameters and ridge size were established using a theoretical approach. Alternative solutions were tested against model test results before a final selection was made. Final verification of the formula was made by comparison to full scale tests.

Parametric evaluations of the final formulation resulted in the following conclusions:

1. The required extraction power is quite sensitive to the friction between the ridge mass and the ship hull. There is a clear discrepancy between the importance of the friction and the state of the art of determining its exact value in actual full scale conditions.

2. The influence of breadth is dominant compared to the draft. Typically, a 10% breadth increase causes a 7 to 8.5% increase of extraction force while a 10% draft increase causes a 1 to 3% increase.

3. Looked at in isolation, short bows with large waterline angles are less vulnerable of getting stuck. However, for equal displacement this results in a larger midbody and often a higher total extraction force.

9. RECOMMENDATIONS

The work of the preceeding sections identified the hull size and form parameters of significant influence on ridge resistance. The parameters were combined to a format suitable for practical design applications. The formulas represent an initial step towards the improvement of power requirement predictions for ships operating in first year ridges. The primary objective of further investigations is to establish criteria applicable to regulations regarding navigation in Arctic waters of Canadian interest. The following sections focus on the areas of future research requirements.

9.1 Ridge Particulars

The present study has introduced the aspect ratio (h_r/W_r) to the well established list of ridge parameters. The significance of (h_r/W_r) for the evaluation of the severity of individual ridges was demonstrated. The available database identified the folowing predominant ratios for distinct test regions:

Area	h_r/W_r
Baltic Sea	0.02 - 0.06
Beaufort Sea	0.05 - 0.07
Bering Sea	0.08 - 0.09

The principal objective of future research into this phenomenon is to increase the scope of the data base relevant to ship transit performance and in areas of particular interest for Canadian Arctic operations.

9.2 Ridge Penetration Resistance

The present study analysed ridge penetration on the basis of the total energy required for breaching a ridge. This approach resulted in a formulation for average penetration resistance (see Equation (5-2)).

The average penetration resistance is equivalent to the resistance in a ridge of constant thickness during continuous mode of transit. The resistance/distance profiles from full scale penetration tests show distinct resistance peaks at the end of individual rams.

Performance prediction on the basis of the average penetration resistance is a reasonable valid approach in the case of ridges that are small relative to the ship size and for ridges with an evenly distributed ice mass. In ridges with distinct ice mass concentrations or of relative large size the peak resistance forces acting on the ship gain significance. In these cases the resistance peaks can stop the ship abruptly.

Further work involving dedicated full scale tests with ships of different sizes in accurately profiled ridges will allow to quantify the effects of peak resistance forces on the overall performance capabilities.

9.3 Ridge Extraction

The development of the formulation presented in Section 6 led to an initial understanding of the process involved in extraction and compared well to available model and full scale test results. However, as discussed in previous Sections, the data base on extraction forces is small and there exists a clear need for additional dedicated testing in order to verify the results. Such testing should be combined with a refinement of the present formulation.

9.4 Speed of Advance

Individual rams and extractions form single components of transiting ridged ice fields. For the evaluation of the overall performance capabilities of a ship within a defined mission profile the speed over ground is determinant. With the exception of land fast ice the ice fields are in motion due to the influence of wind and water currents. The speed of advance within an ice field is influenced by the following components:

- the speed in level ice;
- the frequency of required rams;
- the time required for extractions;
- the penetration depth per ram; and
- the spacing between adjacent ridges.

If the speed of advance within the ice field is in the same range as the ice drift speeds the ship will be drifting with the ice field.

The scope of the present work concentrated on the investigation of the influence of single ridges. In accordance with the ultimate objective to establish minimum performance criteria regarding navigation in Arctic waters the influence of the above components on the speed of advance in realistic ice fields requires further research. In particular the random character of ridge size and ridge spacing has to be considered.

10. REFERENCES

1. Voelker, R.P., DeBord, F.W., Nelka, J.J., Jacobi, J.W. and Coburn, J.L., Assessment of Ice Conditions in the South Bering Sea Based on April 1980 USCG Polar Class Frafficability Test Data, U.S. Department of Commerce, January 31, 1981, Report No. 500 C-Z.

2. Danielewicz, B.W. and Pilkington, G.R., Selected Environmental Characteristics of Beaufort Sea Ice, distributed by Pallister Resource Management Ltd., 1982.

3. Keinonen, A., Presentation of Sea Ice Ridges in General and Physical Characteristics of Baltic Ridges for Ship Resistance Calculations, Winter Navigation Research Board, Helsinki, Finland, 1978, Research Report No. 24.

4. Keinonen, A., The Shape and Size of Ice Ridges in the Baltic According to Measurements and Calculations, The Winter Navigation Research Board, Helsinki, Finland, 1979, Report 17.

5. Voelker, R.P., DeBord, F.W. Geisel, F.A. Coburn, J.L. and Dave, K.E., Winter 1981 Trafficability Tests of the USCGC "POLAR SEA", Vol. II, Environmental Data, U.S. Department of Commerce, December 14, 1981, Report 583C-3, P.B. 83-204412.

6. Voelker, R.P., Geisel, F.A., Dane, K.E., Arctic Deployment of USCGC "POLAR SEA" - Winter 1982, Volume 3, Polar Class Performance, Trafficability, Level Ice, and Pressure Ridges, 1982, 175 pp., NTIS No. PB84 129624.

7. Report on MV "ARCTIC" Experimental Voyage to Lake Melville, Labrador (February/March 1981), Melville Shipping Ltd., Transportation Development Centre, Arctic Pilot Project, Canarctic Shipping Ltd., CN Marine Inc., North Water Navigation Ltd. and the Government of Newfoundland, Vol. 1, (main report) and Vol. 2 (appendices), October 1981, TP 3646, (restricted).

8. Analysis of MV "ARCTIC" Ramming Performance in Admiralty Inlet (June 1982), Melville Shipping Ltd., (for Canarctic Shipping Company Ltd.), March 1983, TP 6748.

9. MV Arctic Ice Transiting Performance - Continuous Mode: Final Report, Albery, Pullerits, Dickson and Associates (for the Transportation Development Centre), May 1984, TP 5170, (restricted).

10. Nawwar, A.M., Goossens, L. and Steele, M., MV Arctic Ice Transiting Performance in the Ramming Mode, Final Report, Transportation Development Centre, October 1984, TP5320 E.

11. MV "ARCTIC" Dedicated Field Tests - Ship/Ice Interaction (Ramming Results and Analysis), German and Milne Inc. and VTT (for the Transportation Development Centre), January 1985, TP 6270, (restricted).

12. MV "ARCTIC" Ice Transiting Performance - Continuous Mode: Summary Report, TP 5319, (restricted).

13. MV "ARCTIC" Ice Transiting Performance in the Ramming Mode: Summary Report, TP 5321, (restricted).

14. M/T "KIISLA' Full Scale Tests 1974, Wartsila Arctic Design and Marketing, April 10, 1974, Marketing Report B10, (unpublished).

15. Full Scale Icebreaking Tests with I/B "APU" in the Gulf of Bothnia in April 1974, Wartsila Arctic Design and Marketing, December 1974, Marketing Report B11, (unpublished).

16. I/B "ALE" Full Scale Tests in Level Ice, in Clogged Channel and Ridges in the Gulf of Bothnia March 1975, Wartsila Arctic Design and Marketing, May 1975, Report B13, (unpublished).

17. I/B "URHO" and I/B "SISU". Full Scale Tests in Level Ice, in Clogged Channel and Ridges in the Gulf of Bothnia in March 1976, Wartsila Arctic Design and Marketing, May 1976, Marketing Report B17, (unpublished).

18. Ice Resistance Tests with I/B "KAPITAN KOSOLAPOV" in the Sea of Azov from February 7 to 11, 1977, Wartsila Arctic Design and Marketing, May 1977, Report B21, (unpublished).

19. Ice Performance Tests of I/B "KAPITAN CHECHKIN" in the Gulf of Finland from March 7 to 11, 1978, Wartsila Design and Marketing, Report B25, (unpublished).

20. M/T "SOTKA" Ice Resistance Tests in Level Ice, in Clogged Channel and in Ridge in the Gulf of Finland on March 20 and 21, 1977, Wartsila Arctic Design and Marketing, 1977, Report B23, (unpublished).

21. Ice Tests with M/S "WALKI" in the Gulf of Bothnia from March 27 to 28th, 1979, Wartsila Arctic Design and Marketing, June 1979, Report B36, (unpublished).

22. Ice Tests with I/B Dikson, L-438 in the Gulf of Bothnia from March 22 to 25, 1983, Wartsila Arctic Design and Marketing, July 1983, Report B67, (unpublished).

23. M/T "SOTKA", Full Scale Tests, March 1984, Wartsila Arctic Design and Marketing, May 1984, Report B73, (unpublished).

24. *Full Scale Tests with an Ice Breaking Bow in the Gulf of Finland during March 22 to April 1 1985*, Wartsila Arctic Research Centre, Report B85, (unpublished).

25. *I/B "OTSO". Full Scale Tests in Level Ice, in Clogged Channel and in Ridges in the Gulf of Bothnia in March 1986*, Wartsila Arctic Research Centre, (unpublished).

26. Enkvist, E., *On Ice Resistance Encountered by Ships Operating in the Continuous Mode of Ice Breaking*, Helsinki University of Technology, 1972, Report No. 24.

27. Gill, R.J., Aboul-Azm, A., Terry, B.F. and Russel, W.E., *A Ship Transit Model for Passage through Ice and its Application to the Labrador Area*, Sixth Ship Technology and Research Symposium, Ottawa, Ontario, June 1981.

28. Edwards, R.Y., Dunne, M.A., Confast, G., Bulat V. and Johnson, B.: *Results of the Full Scale Trials in Ice of CGCS "PIERRE RADISON"*, Sixth Ship Technology and Research Symposium, Ottawa, Ontario, June 1981.

29. Poznyak, I.T. and Ionov, B.P., *The Division of Ice Breaker Resistance into Components*, Sixth Ship Technology and Research Symposium, Ottawa, Ontario, June 1981.

30. McIntosh, C.D.R. J.A. and Welsh, J.P., *A Provisional Calculation of the Ice Breaking Resistance of the USCG "POLAR STAR"*, Sixth Ship Technology and Research Symposium, Ottawa, Ontario, June 1981.

31. Vance, G.P., Godwin, LCDR. M.J., Gracewski, LCDR. A.S., *Full Scale Icebreaking Test of USCGC "KATMAI BAY"*, Sixth Ship Technology and Research Symposium, Ottawa, Ontario, June 1981.

32. Enkvist, E., *A Survey of Experimental Indications of the Relation between the Submersion and and Breaking Components of Level Ice Resistance to Ships*, Volume 1, 7th International Conference on Port and Ocean Engineering Under Arctic Conditions, Espoo, Finland, 1983.

33. Forland, K.A., Tatinclaux, J., *Laboratory Investigation of Kinetic Friction Coefficient of Ice*, IAHR Ice Symposium 1984.

34. Keinonen, A., *An Analytical Method for Calculating the Pure Ridge Resistance Encountered by Ships in First Year Ice Ridges*, Helsinki University of Technology, Ship Hydrodynamics Laboratory, Report No. 17, Otaniemi, Finland, 1979.

35. Keinonen, A., *The Phases of Navigating through Ridges with a Ship*, Helsinki University of Technology, Ship Hydrodynamics Laboratory, 1979, Report No. 18.

36. Keinonen, A., Ship Performance and Resistance in Ice Ridges, WEGEMT, 1983.

37. Malmberg, Stig, On the Wedging of Ships in Ice, Technical University of Helsinki, Finland, November 1983 (in Swedish).

38. Mellor, M., Ship Resistance in Thick Brash Ice, Polar Record, Cold Regions Science and Technology, pp 305 - 321, Amsterdam, Holland, March 1980.

39. Makinen, E., Keinonen, A. and Laine, A., Ice Resistance Measurements in Ridges with I/B Apu in Baltic Sea, 3rd International Conference on Port and Ocean, Engineering under Arctic Conditions, 1974.

40. Keinonen, A. and Duff, J., Canmar Kigoriak - Demonstration of Arctic Capabilities, Proceedings, the 7th International Conference on Port and Ocean Engineering Under Arctic Conditions, Helsinki, Finland, April 5-9, 1983.

41. Wilckens, H. and Freitas, A., Thyssen Waas Icebreaker Concept: Model Tests and Full Scale Trials, Vol. 7 (special issue), Cold Regions Science and Technology, pp. 285-291, 1983.

42. Enkvist, E. and Mustamaki, E., Model and Full Scale Tests with an Innovative Icebreaker Bow, SNAME Annual Meeting, October 1986.

43. Model Tests for Neste Oy, Wartsila Ice Model Basin, August 1972, Report A19.

44. Model Tests in Ice and in Ridges with Model 029," VALPAS", Wartsila Ice Model Basin, Report A25, July 1973.

45. Resistance and Extraction Tests in Ridges with Model 016 During the Period May 15 - November 17, 1973, Wartsila Ice Model Basin, May 1974, Report A26.

46. Ice Resistance Tests with a Shallow Draft Type Polar Icebreaker, Model 039, Wartsila Ice Model Basin, January 1974, Report A37.

47. Ice Resistance Tests of the Gas Turbine Ferry "FINN JET" for Finn-Lines Ltd., Wartsila Ice Model Basin, December 1974, Report A40.

48. Model Tests for Determining the Ice Resistance in Level Ice, Own Channel and Ridges of an Arctic Panamax Bulk Carrier, Wartsila Ice Model Basin, June 1978, Report A53.

49. Model Tests for Determining the Ice Resistance in Level Ice, Own Channel and Ridges of an Arctic Panamax Bulk Carrier with Two Stern Alternatives, Wartsila Ice Model Basin, August 1979, Report A64, (in Swedish).

50. Model Tests for Determining the Ice Resistance in Level Ice, New Channel and Ridges of an Arctic Multipurpose Vessel, Wartsila Ice Model Basin, January 1980, Report A68, (in Swedish).

51. Model Tests for Determining the Ice Resistance in Level Ice, New Channel and Ridges of an Arctic Tanker with Two Bow Alternatives, Wartsila Ice Model Basin, Report A71, October 1980, (in Swedish).

52. Model Test in Ice with Polar Research Vessel, Wartsila Arctic Design and Marketing, September 1982, Report A83.

53. Tanker, Wartsila Arctic Research Centre, Report A91, August 1983.

54. Ice Breaking Tanker Tests in Ice, Wartsila Arctic Research Center, November 1983, Report A97.

55. Model Tests in Level Ice, Broken Channels and Ridges with MT "LUNNI" 1:20 and 1:40 and MT "KISLA" 1:20 Models, Wartsila Arctic Research Center, November 1984, Report A112.

56. Model Tests in Ice with the 1:40 Model of a Tanker, Wartsila Arctic Research Center, December 1984, Report A114.

57. Model Test of an Arctic Supply Vessel, Wartsila Arctic Research Center, 1986, Report A141, (in Finnish).

58. Popov, Yu. N., and Kashteljan, V.I., Wedging of Icebreakers in Ice, Ice Navigation Qualities of Ships, edited by Kheysin, D. Ye. and Popov, Yu. N., Translation, 1973, CRREL TL 417.

59. Tue-Fee, K.K., Full Scale Maneuvering Tests in Level Ice of "Canmar KIGORIAK" and "ROBERT LEMEUR", SNAME Arctic Section Meeting, January 1985.

60. Enkvist, E., Level Ice Resistance, WEGEMT, 1983.

61. Enkvist, E. and Mustamaki, E., Model and Full Scale Tests with an Innovative Icebreaker Bow, S.N.A.M.E. Annual Meeting, New York, N.Y., October 1986.

62. Voelker, R.P. et al., Trafficability Tests of the USCGC "POLAR SEA" - Winter 1981, Volume 8, Calculation of Pressure Ridge Pentration Forces, 1981, pp. 79, NTIS No. PB83 204479.

11. BIBLIOGRAPHY

Arctic Marine Transportation R & D Programme: List of Reports 1981-1985, Transport Canada, Ottawa, March 1986, TP 7343E.

Calabrese, S.I., Murray, S.F., Methods of Evaluating Materials for Icebreaker Hull Coatings. Selection and Use of Wear Tests for Coatings, ASTM STP 769, R.G. Bayer Ed., American Society for Testing and Materials, 1982, pp. 157-173.

Garret, R.R., Rinehart, V.W. and Voelker, R.P., Conclusions from the First Marine Transit to Point Barrow in Winter 1981 (by USCG "POLAR SEA"), Annual Offshore Technology Conference, 14th, Houston, Texas, May 1982.

Index of S.N.A.M.E. Publications, The Society of Naval Architects and Marine Engineers, New York, N.Y., 1985.

Joba, J., Guide to Marine Transportation Services in Canada, 2nd Edition, Transportation Development Centre, Montreal, Quebec, August 1985, TP 2431E.

Joba, J., Ships Navigating in Ice, A Selected Bibliography, Transportation Development Centre, Vol. 2, 1980-1984, Montreal, Quebec, July 1985, TP 3855E.

Johansson, B.M. and Revill, C.R., Future Icebreaker Design, International Polar Transportation Conference, Vancouver, B.C., May 1986.

MV Arctic, A Research Record, 1978-1984, Transport Canada, Marine Administration, Ottawa, Ontario, September 1985, TP 6791.

Makinen, E., Letti A., Rimppi, M., Influence of Friction on Ice Resistance. Search for Low Friction Surfaces, Ice Technology Symposium, Montreal, Quebec, April 1975.

Makinen, E. and Roos, R., Ice Navigation Capabilities of Lunni Class Icebreaking Tankers, Meeting of Eastern Canadian Section of SNAME, Montreal, Quebec, November 22, 1977.

Nawwar, A.M., Noble, P.G., Edwards, R.Y. and Dunne, M., Development of a Research Program for Improving Arctic Marine Transportation Technology, Volume II, Situation Reports, for Transportation Development Centre, Chapter 3 - Ship Transiting Performance, 1979, TP2004.

Pierce, T.H., Arctic Marine Technology: A Review of Ship Resistance in Ice, RINA, October 10, 1978.

Review of Transport Canada Icebreaking Trials 1967-1980, Transport Canada, Marine Administration, Ottawa, Ontario, 1985, TP 6110.

Saarikangas M., Jansson, J. and Heidleman T., Operational Experience with the New Type of Baltic Icebreaker "OTSO", Polar Tech 86, Helsinki, Finland, 1986.

Sanderson, D., Smith, G: Ships Navigating in Ice, A Selected Bibliography, Transportation Development Centre, Montreal, Quebec, October 1982, TP 3855E.

Stubbs, J.T. and Makinen, E., Arctic Marine Technology State-of-the-art and Prospects for the 1990's, International Polar Transportation Conference, Vancouver, B.C., May 1986.

TDC Publications, Transportation Development Centre, Montreal, Quebec, December 1982, TP 2602.

Tunik, A., Continuous Motion of a Ship in Ridged Ice, Ice Tech 84, International Conference on Icebreaking and Related Technologies, 3rd, Calgary, Alberta, May 1984.

Voelker, R.P., DeBord, F.W., Brennan, L.C.D.R. T. Parker, C.W., Evaluation Commerical Arctic Marine Transportation with Polar Class Ice Breakers, Sixth Ship Technology and Research Symposium, Ottawa, Ontario, June 1981.

Voelker, R.P., DeBord, F.W. and Dane, K.E., Operational Assesment of Commerical Ice Breaking Ships in Western Alaskan Waters Based on USCG Polar Class Trafficability Test Data, Vol. I and II, July 20, 1979, Report No. 500C-1.

APPENDIX A

Principles of Isostatic Equilibrium Calculations

APPENDIX A

Calculations of Ridge Underwater Profiles

In order to rationalize the data base of ridges to common units, ridge topside profiles were digitized and analyzed using the following computer program. The computer equipment used was a 9836C Hewlett Packard computer and 9111A Digitizer. The program which calculates the underside profile originates from Keinonen's work (see 4) and forms a subroutine of a large program written for this Report.

Formula for Isostatic Equilibrium:

$$\frac{H_B}{H_A} = \frac{\mu_A \times \rho_I}{\mu_B \times (\rho_W - \rho_I)}$$

where:

H_B = height of bottom profile point
H_A = height of sail profile point
μ_A = coefficient of permeability for sail
μ_B = coefficient of permeability for keel
ρ_W = density of water
ρ_I = density of ice

The final profile for the underwater part of the ridge is determined using the following procedure:

1. The area of the ridge section below the water level is calculated with the h_b values.

2. The profile curve below the water level is smoothed with the weighed mean values.

3. The area of the ridge section below the water level is calculated with the h_{2b} values.

4. The final h_b values are now

$$h_{3b} = \frac{A_{R1}}{A_{R2}} \times h_{2b}$$

For this Report the following values were used:

$\rho_W = 1023$ kg/m^3

$\rho_I = 900$ kg/m^3

$\rho_{Snow} = 250$ kg/m^3

Porosity of Ridge Sail = 30%

```
8940  SUB Createkeel
8950  !
8960    COM /W/ X1(*),Y1(*),Ptt(*)
8970  COM /Ridge/ A(8.50),A$[50],C(2.6),D(2.100)
8980  ! MASS BALANCE PROFILE OF A RIDGE BY AK760622.PART 1
8990  ! UPDATED AND TRANSFORMED TO HP9836C BY RW860916
9000  !
9010  DIM B(2.6).B$[5]
9020  MAT A= (0)
9030  MAT B= (0)
9040  MAT C= (0)
9050  MAT D= (0)
9060  C(1.1)=1023     !   Specific Weight of Baltic Sea Water
9070  C(1.2)=900      !   Specific Weight of Baltic Sea Ice
9080  C(1.3)=250      !   Speciofic Weight of Snow
9090  C(1.5)=.70      !   Density of Ridge Sail
9100  C(1.6)=7.76     !   ?
9110  N=Ptt(1)-1
9120  A(6.3)=N
9130  DIM Rg(5).Rgg(5)
9140  INPUT "NUMBER OF DISTINCT SAILS".Nusail
9150  FOR Spt=0 TO Nusail-1
9160  PRINT "ENTER RANGE FOR SAIL";Spt;".START FINISH"
9170  INPUT Rg(Spt).Rgg(Spt)
9180  NEXT Spt
9190  FOR I=1 TO N
9200    A(1.I)=X1(1,I)
9210    IF Nusail=1 THEN
9220    IF X1(1.I)>Rg(0) AND X1(1.I)<Rgg(0) THEN
9230    A(2.I)=Y1(1.I)*C(1.5)
9240    GOTO 9400
9250    END IF
9260    END IF
9270    !
9280    IF Nusail=2 THEN
9290    IF X1(1.I)>Rg(0) AND X1(1.I)<Rgg(0) THEN 9340
9300    IF X1(1,I)>Rg(1) AND X1(1.I)<Rgg(1) THEN 9340
9310    GOTO 9390
9311    END IF
9320    !
9321    IF Nusail=3 THEN
9322    IF X1(1.I)>Rg(0) AND X1(1.I)<Rgg(0) THEN 9340
9323    IF X1(1,I)>Rg(1) AND X1(1.I)<Rgg(1) THEN 9340
9324    IF X1(1.I)>Rg(2) AND X1(1.I)<Rgg(2) THEN 9340
9325    GOTO 9390
9326    END IF
9328    !

9329    !
9330    GOTO 9390
9331    !
```

```
9950    B(1,3)=B(1,1)*(1+C(2,6)/C(2,5))
9960    B(1,4)=B(1,3)/A(1,N)
9970  !
9980  ! Profile Below
9990  !
10000   IF H1<>0 THEN Vier_vier
10010   A(6,1)=(2*A(5,1)+A(5,2))/2
10020   GOTO Vier_fuenf
10030 Vier_vier:!
10040   A(6,1)=H1
10050 Vier_fuenf:!
10060   IF H2<>0 THEN Vier_acht
10070   A(6,N)=(2*A(5,N)+A(5,N-1))/2
10080   GOTO Vier_neun
10090 Vier_acht:!
10100   A(6,N)=H2
10110 Vier_neun:!
10120 !
10130   FOR I=1 TO N
10140     D1=D1+A(6,I)
10150     D2=D2+A(6,I)^2
10160   NEXT I
10170 !
10180   B(1,2)=SQR((D2-D1^2/N)/(N-1))
10190 !
10200   FOR I=2 TO N-1
10210     A(6,I)=(A(5,I-1)+1.5*A(5,I)+A(5,I+1))/3.5
10220   NEXT I
10230 !
10240 !
10250   Are1=0
10260   Are2=0
10270   FOR I=1 TO N-1
10280     Dare1=(A(1,I+1)-A(1,I))*.5*(A(5,I+1)+A(5,I))
10290     Dare2=(A(1,I+1)-A(1,I))*.5*(A(6,I+1)+A(6,I))
10300     Are1=Are1+Dare1
10310     Are2=Are2+Dare2
10320   NEXT I
10330 !
10340   FOR I=1 TO N
10350     A(7,I)=Are1/Are2*A(6,I)
10360   NEXT I
10370 !
10380   FOR I=0 TO 50
10390           X1(2,I)=A(1,I)
10400           Y1(2,I)=A(7,I)*(-1)
10410           NEXT I
10420 SUBEND
```

```
9340     A(2,I)=Y1(1,I)*C(1,5)
9350     GOTO 9400
9360     !
9370     !
9380     !
9390     A(2,I)=Y1(1,I)
9400     A(3,I)=0
9410   NEXT I
9420   FOR J=1 TO 5
9430     IF C(2,J)>0 THEN GOTO Vier_neun
9440     C(2,J)=C(1,J)
9450 Vier_neun: !
9460   NEXT J
9470   MAT O= (0)
9480   !
9490 Sieben_zehn: !
9500   ! begin of isostatic balance calculations !
9510   CALL Ballance
9520 !GOTO Corrections
9530   !
9540   SUBEND
9550   SUB Ballance
9560     COM /W/ X1(*),Y1(*),Ptt(*)
9570   ! Mass Balance Profile of a Ridge
9580   !
9590     COM /Ridge/ A(*),A$,C(*),O(*)
9600     DIM B(2,6),P$[6],F$[100]
9610     INPUT "H1",H1
9620     INPUT "H2",H2
9630     I1=0
9640     N=A(6,3)
9650     MAT B= (0)
9660   !
9670     FOR I=1 TO N
9680       IF A(2,I)>9 THEN Zwei
9690       A(4,I)=A(2,I)+(C(2,3)/C(2,2))*A(3,I)
9700       GOTO Zwei_vier
9710 Zwei: !
9720       A(8,I)=1
9730       A(4,I)=(A(2,I)-10)*C(2,5)
9740       A(4,I)=A(4,I)+(C(2,3)/C(2,2))*A(3,I)
9750       A(2,I)=A(2,I)-10
9760 Zwei_vier: !
9770     NEXT I
9780   !GENERAL rIDGE dATA
9790   !
9800     B(1,1)=.5*(A(4,1)*(A(1,2)-A(1,1))+A(4,N)*(A(1,N)-A(1,N-1)))
9810     FOR I=2 TO N-1
9820       B(1,1)=B(1,1)+.5*A(4,I)*(A(1,I+1)-A(1,I-1))
9830     NEXT I
9840   !
9850     FOR I=1 TO N
9860       B(1,5)=B(1,5)+A(2,I)/N
9870     NEXT I
9880     D1=0
9890     D2=0
9900     C(2,6)=C(2,2)/(C(2,1)-C(2,2))
9910     FOR I=1 TO N
9920       A(5,I)=C(2,6)*A(4,I)/C(2,5)
9930     NEXT I
9940   !
```

APPENDIX B.1

Significance and Sensitivity of Hull Main Particulars

Parameters	Linear Regression		Parabolic Regression	
	r	s	r	s
Bcwl	0.80	300.37	0.92	227.16
Lcwl	0.77	369.05	0.76	351.15
d	0.81	318.51	0.85	307.79
Displacement	0.78	412.37	0.89	251.80
Bcwl*d	0.89	266.05	0.92	255.77
Bcwl/d	0.68	440.07	0.69	420.12
Bcwl*(Bcwl/d)	0.78	337.20	0.82	325.59
Bcwl^2	0.88	238.08	0.94	209.39
Bcwl^2*(Bcwl/d)	0.86	258.32	0.91	234.43
(Bcwl*(Bcwl/d))^2	0.82	325.83	0.81	322.91
Am	0.87	283.11	0.89	276.02
Am*(Bcwl/d)	0.86	261.87	0.93	230.98
Am*(Bcwl/d)^2	0.84	288.87	0.88	274.25

Significance and Sensitivity of Hull Size Parameters

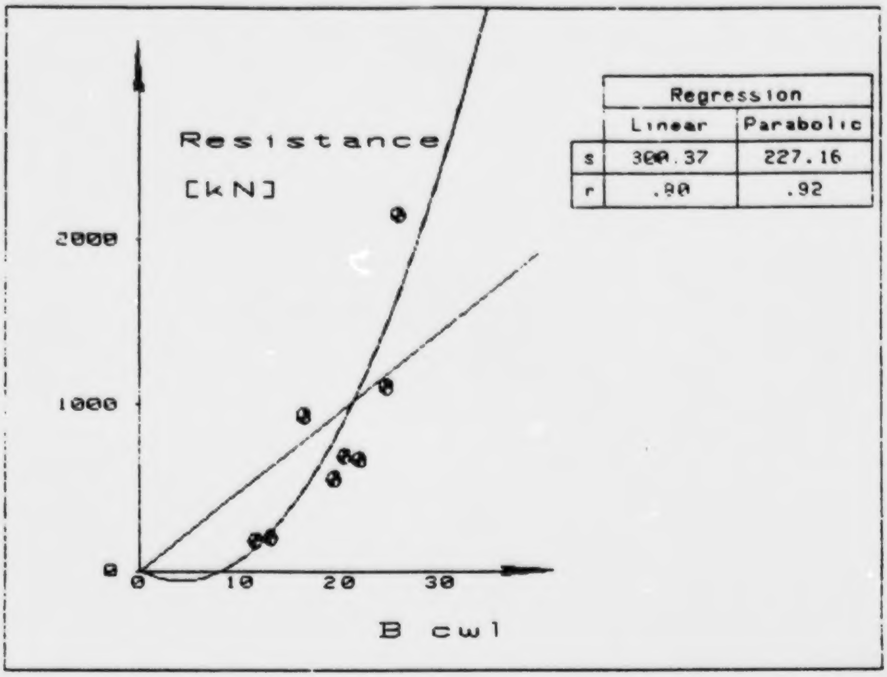

	Regression	
	Linear	Parabolic
s	300.37	227.16
r	.80	.92

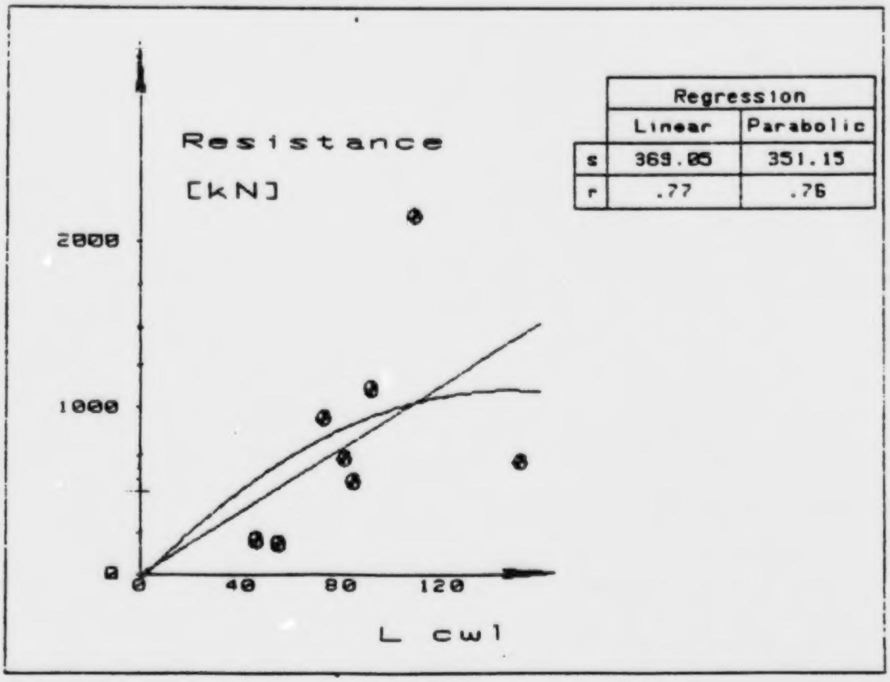

	Regression	
	Linear	Parabolic
s	369.05	351.15
r	.77	.76

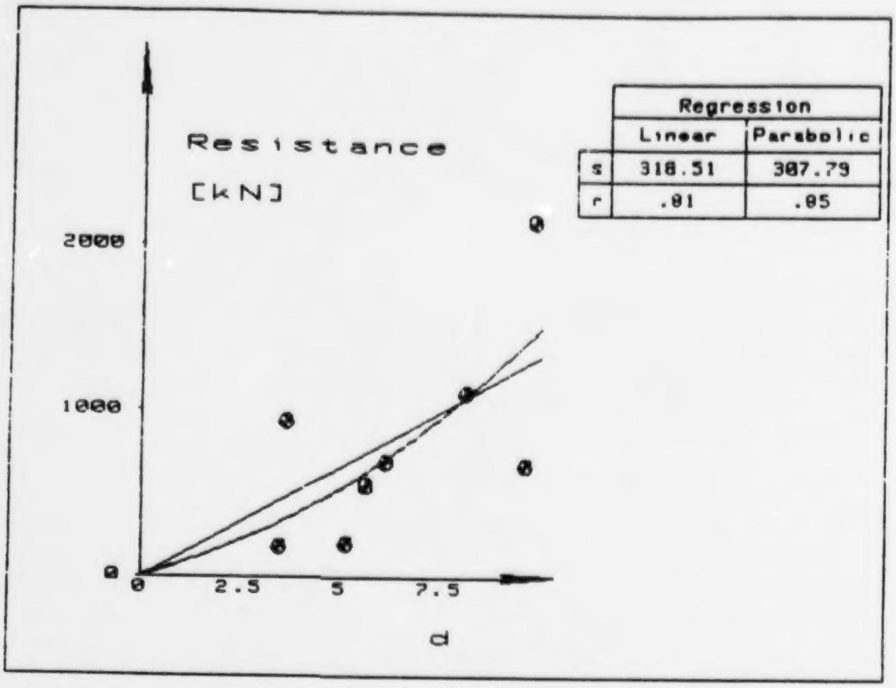

	Regression	
	Linear	Parabolic
s	318.51	307.79
r	.81	.85

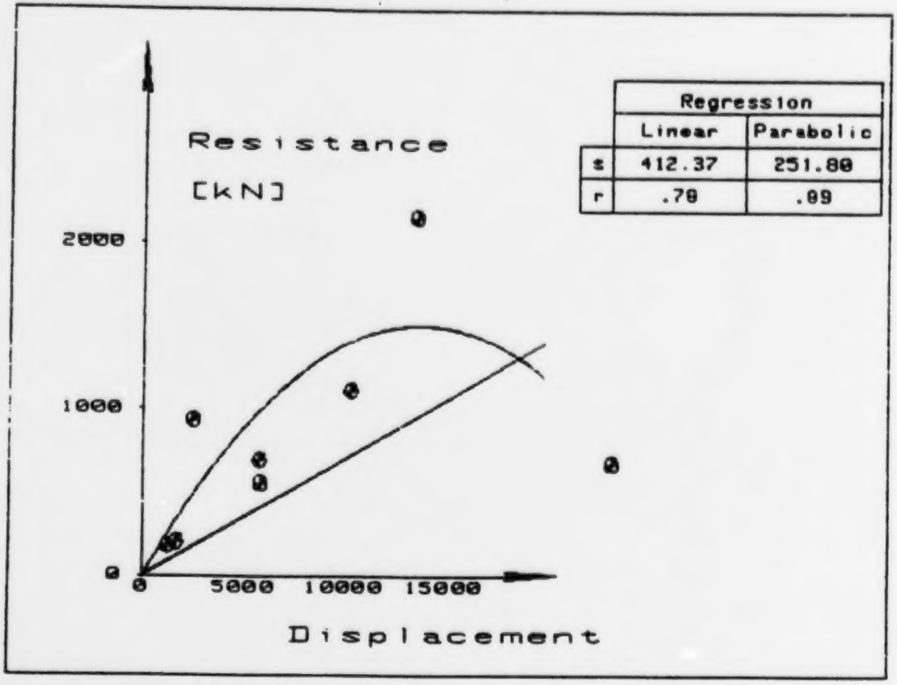

	Regression	
	Linear	Parabolic
s	412.37	251.80
r	.78	.89

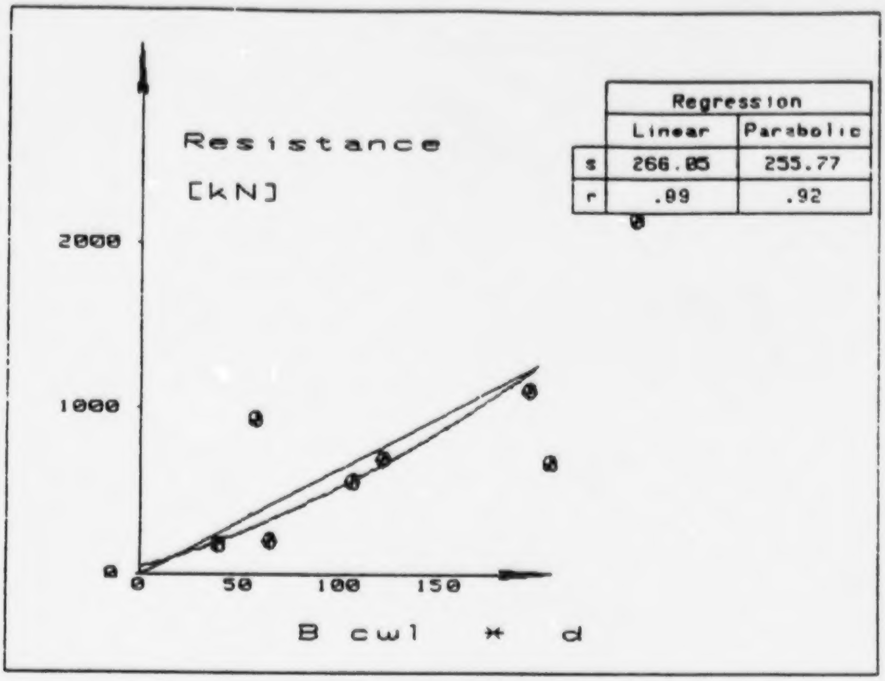
Regression
Linear
Parabolic
s
266.85
255.77
r
.89
.92
Resistance
[kN]
2000
1000
0
0
50
100
150
B cwl * d

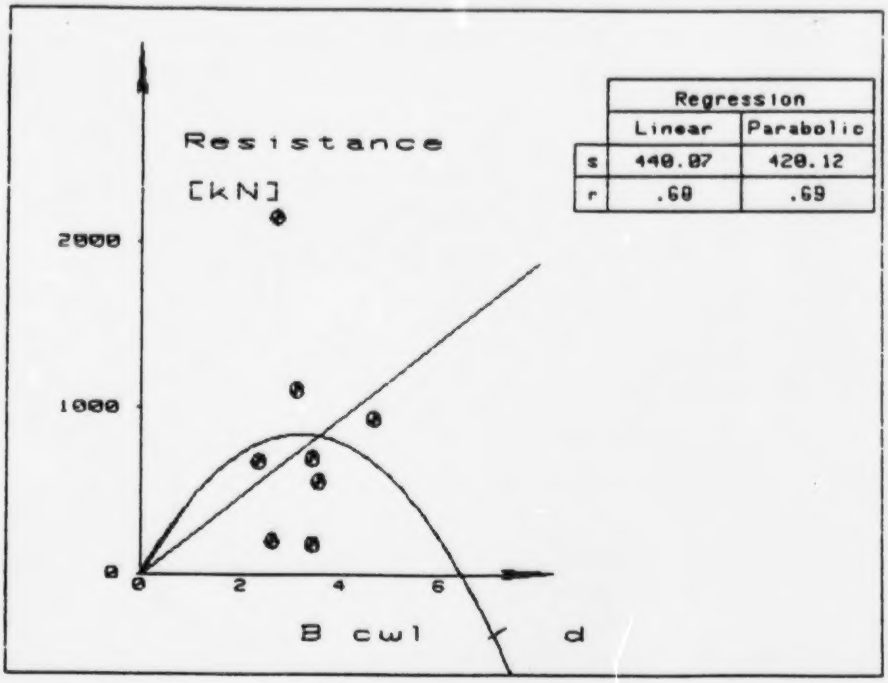
Regression
Linear
Parabolic
s
440.87
420.12
r
.68
.69
Resistance
[kN]
2000
1000
0
0
2
4
6
B cwl / d

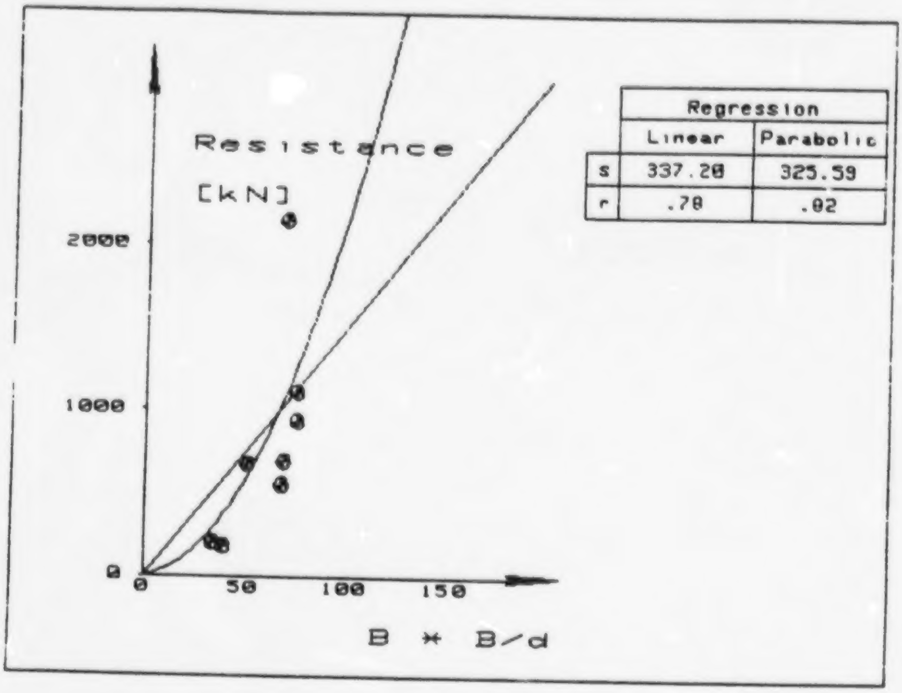

	Regression	
	Linear	Parabolic
s	337.20	325.59
r	.70	.82

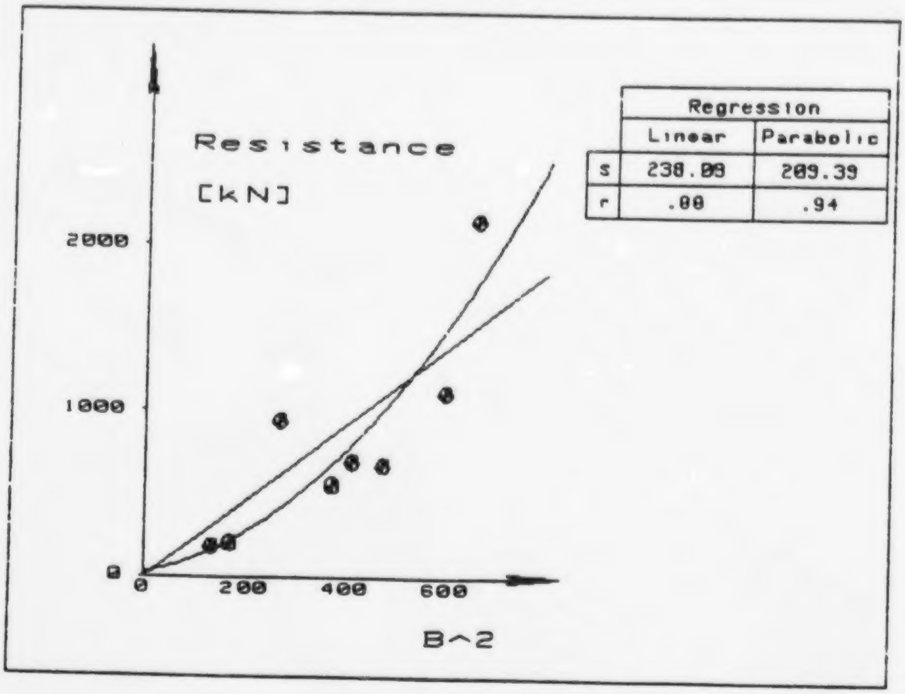

	Regression	
	Linear	Parabolic
s	230.00	209.39
r	.80	.94

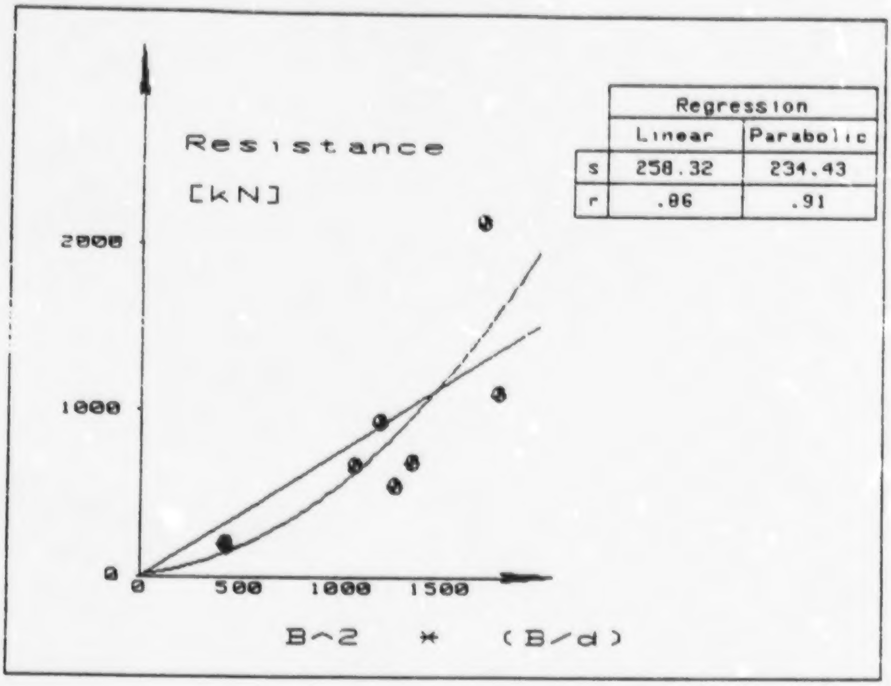
Resistance
[kN]
2000
1000
0
0
500
1000
1500
B^2 * (B/d)
Regression
Linear
Parabolic
s
258.32
234.43
r
.86
.91

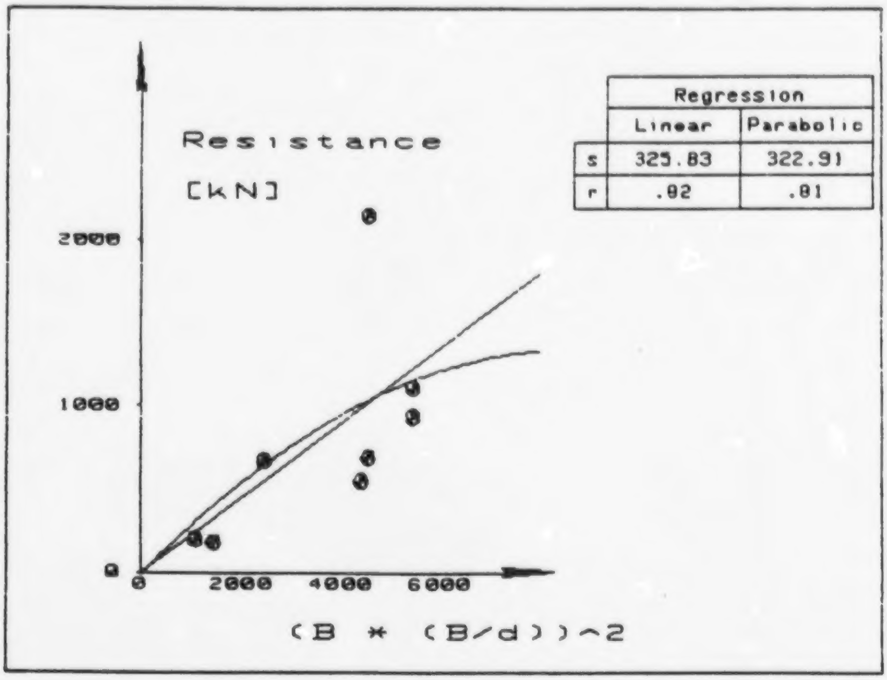
Resistance
[kN]
2000
1000
0
0
2000
4000
6000
(B * (B/d))^2
Regression
Linear
Parabolic
s
325.83
322.91
r
.82
.81

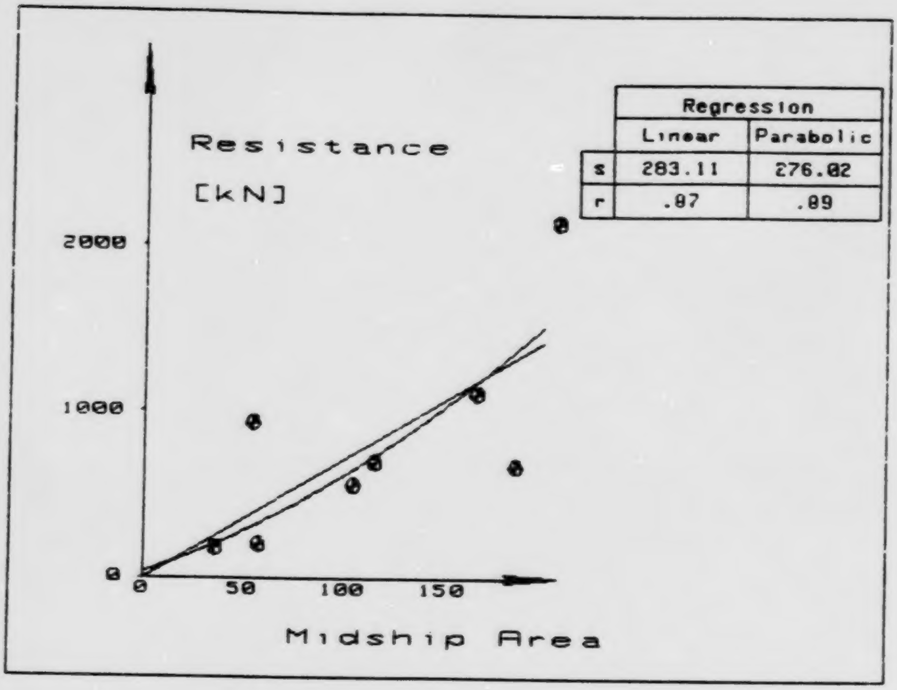

	Regression	
	Linear	Parabolic
s	283.11	276.02
r	.87	.89

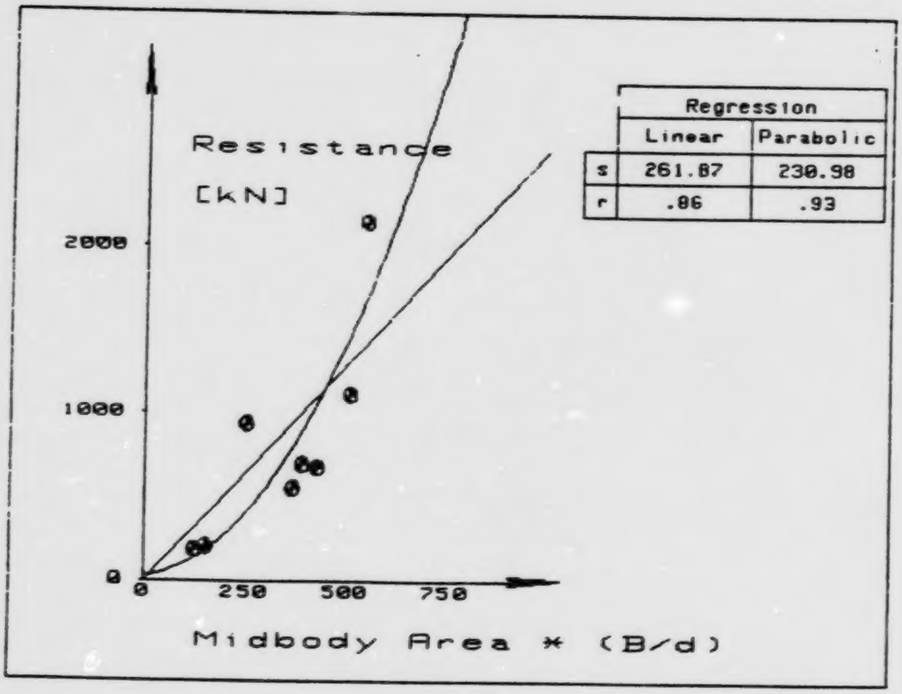

	Regression	
	Linear	Parabolic
s	261.87	230.98
r	.86	.93

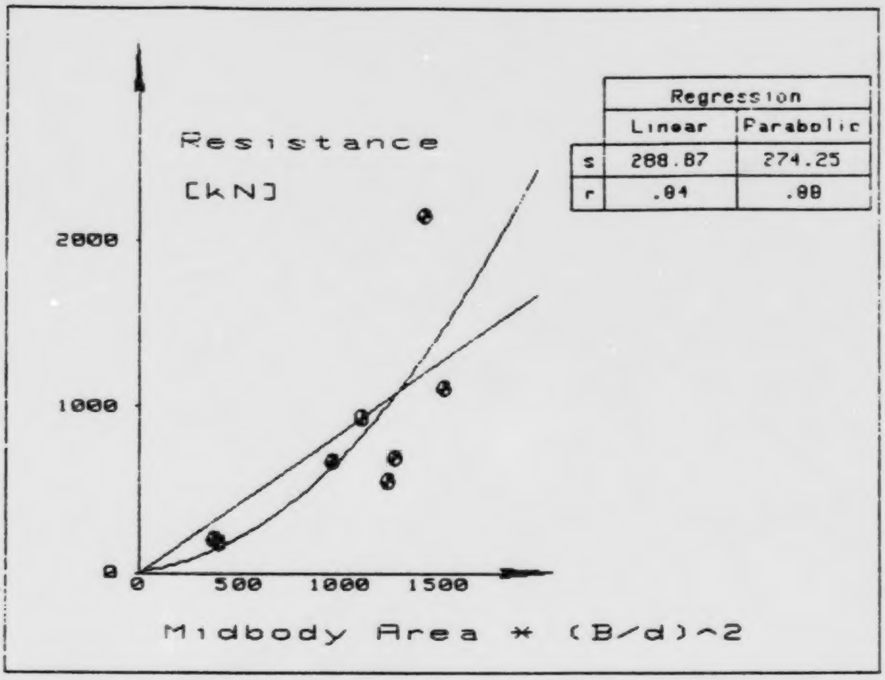

	Regression	
	Linear	Parabolic
s	288.87	274.25
r	.84	.88

APPENDIX B.2

Significance and Sensitivity of Bow Geometry Parameters and Combinations Thereof

Parameters	Linear Regression		Parabolic Regression	
	r	s	r	s
SIN(phi)	0.73	381.53	0.75	377.66
TAN(phi)	0.74	379.66	0.75	378.47
1/COS(PHI)	0.70	407.94	0.75	380.65
COS(alfa)	0.73	375.87	0.84	314.73
1/SIN(alfa)	0.79	312.16	0.93	210.85
1/TAN(alfa)	0.82	285.65	0.93	214.22
COS(beta)	0.75	369.93	0.77	367.51
1/SIN(beta)	0.72	388.60	0.75	378.88
1/TAN(beta)	0.77	371.00	0.76	368.70
SIN(p)/TAN(a)*COS(b)	0.87	298.72	0.89	288.45
SIN(p)/TAN(a)/SIN(b)	0.86	293.11	0.89	282.19
TAN(p)/TAN(a)*COS(b)	0.87	303.88	0.89	296.25
TAN(p)/TAN(a)/SIN(b)	0.86	298.54	0.89	290.94
1/COS(p)/SIN(a)*COS(b)	0.84	294.82	0.90	268.94
1/COS(p)/TAN(a)*COS(b)	0.86	281.90	0.91	256.32
1/COS(p)/SIN(a)/SIN(b)	0.82	295.45	0.90	257.02
1/COS(p)/TAN(a)/SIN(b)	0.85	277.83	0.92	245.21
1/COS(p)/TAN(a)/TAN(b)	0.87	295.81	0.89	286.21

Table 5.3
Significance and Sensitivity of Bow Geometry

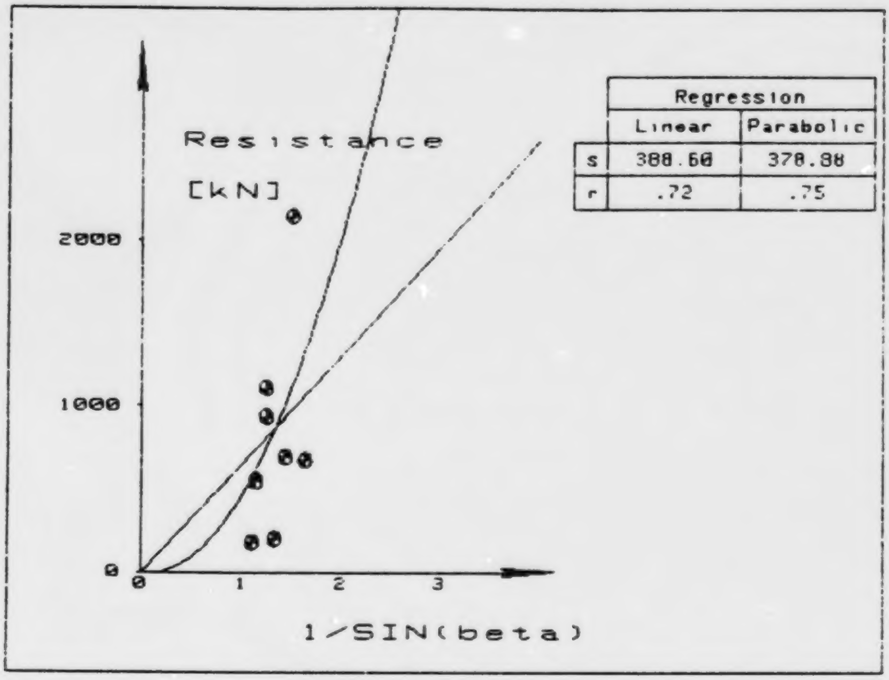

	Regression	
	Linear	Parabolic
s	388.60	378.80
r	.72	.75

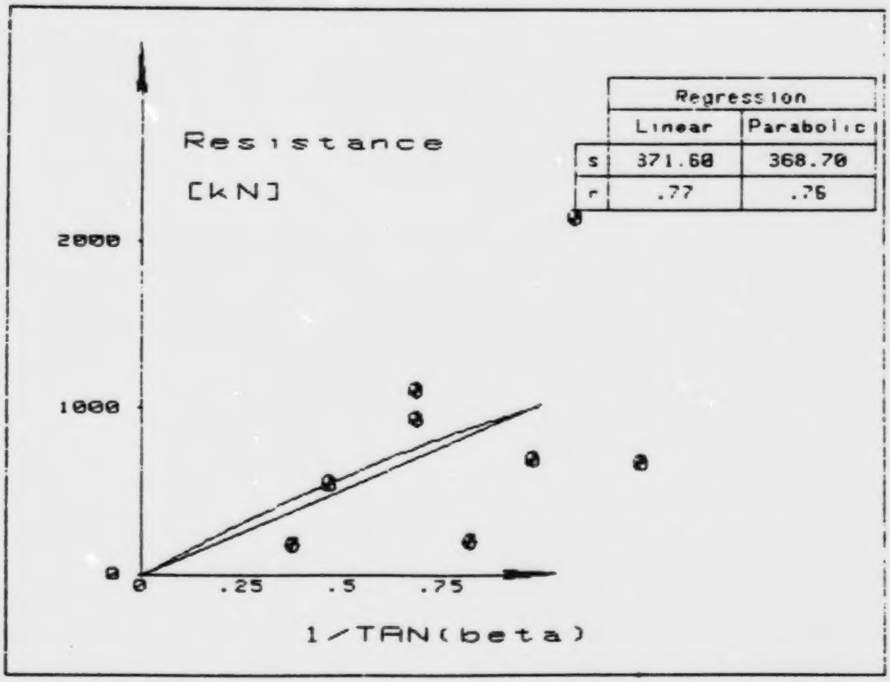

	Regression	
	Linear	Parabolic
s	371.60	368.70
r	.77	.76

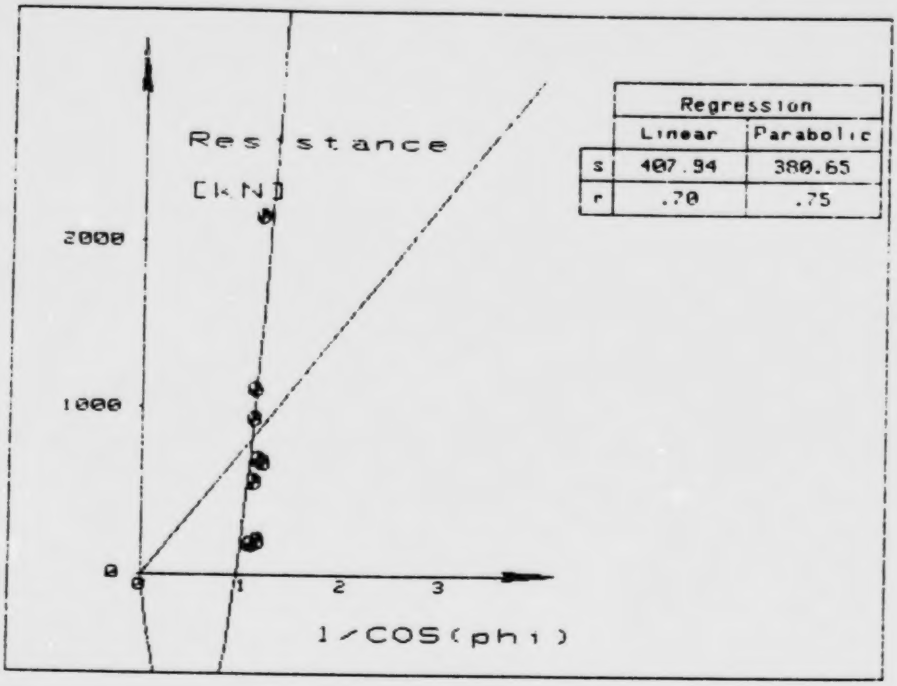

	Regression	
	Linear	Parabolic
s	407.94	380.65
r	.70	.75

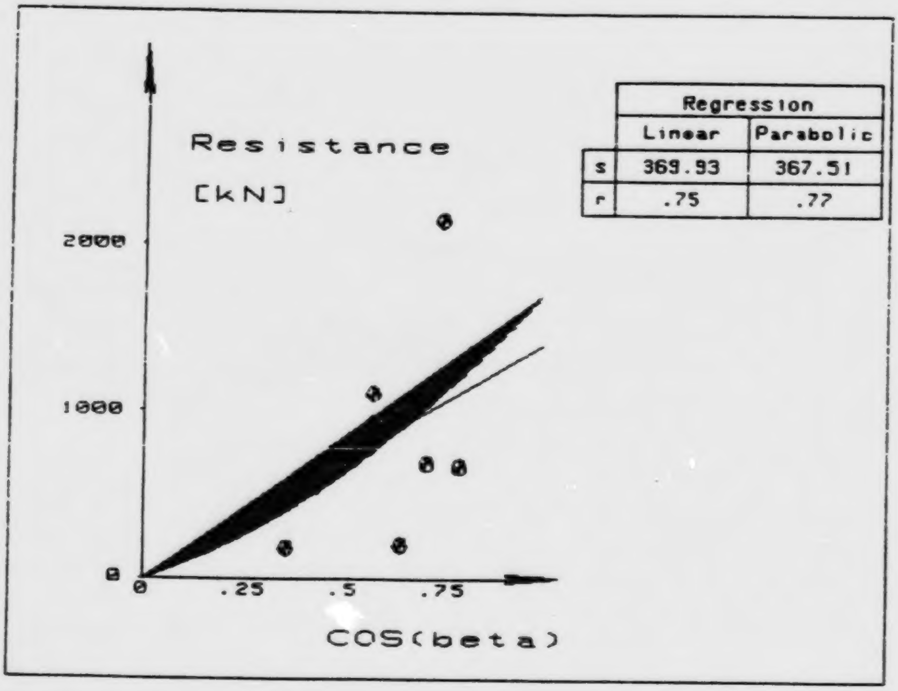

	Regression	
	Linear	Parabolic
s	369.93	367.51
r	.75	.77

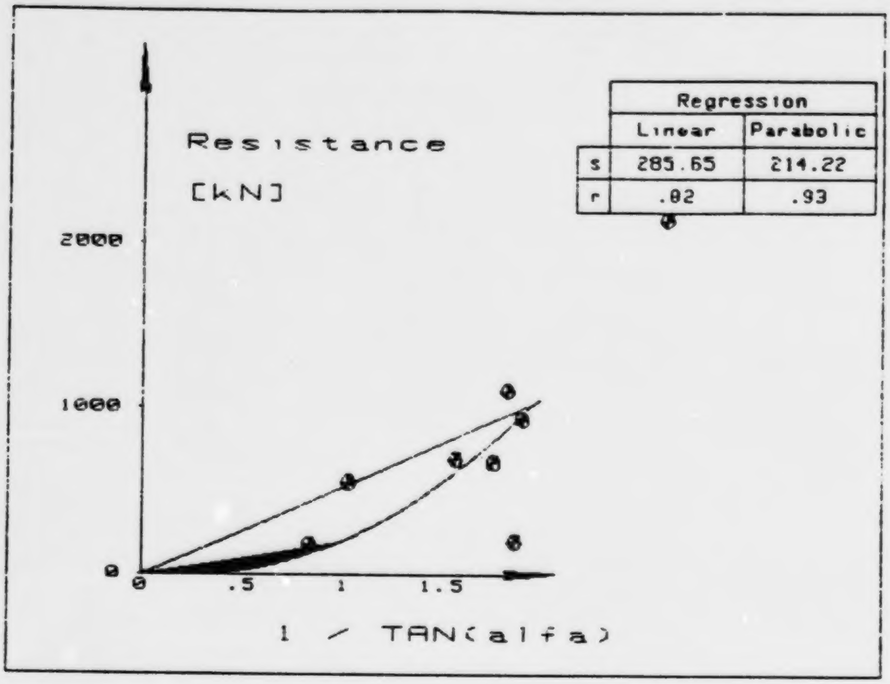

	Regression	
	Linear	Parabolic
s	285.65	214.22
r	.82	.93

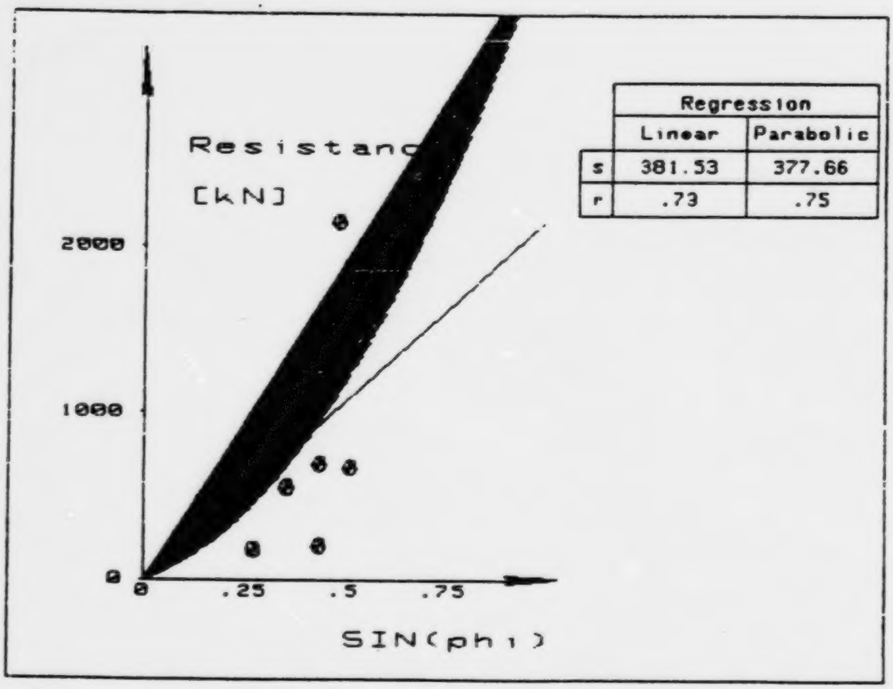

	Regression	
	Linear	Parabolic
s	381.53	377.66
r	.73	.75

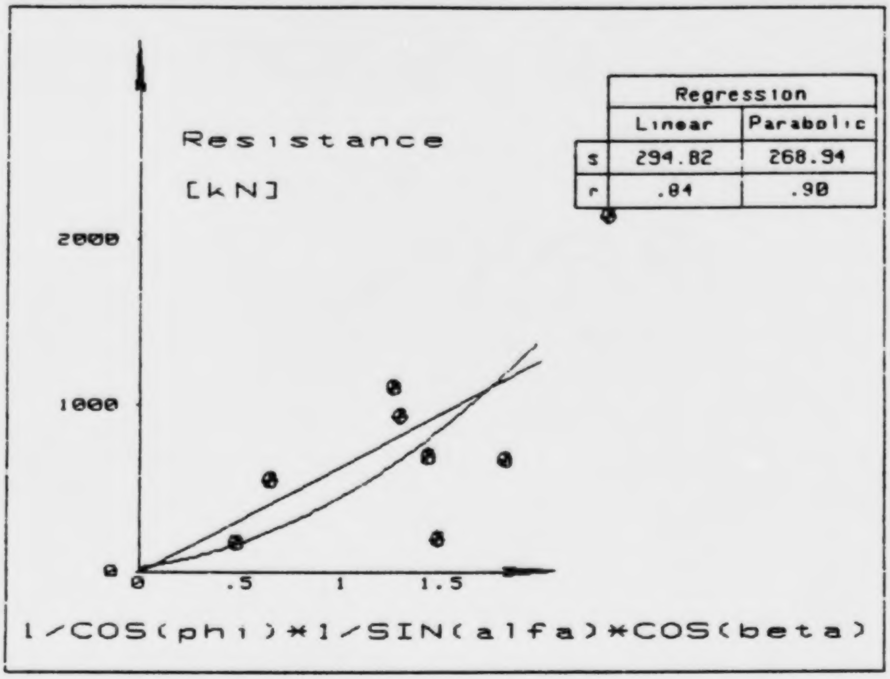
Resistance
[kN]
Regression
Linear
Parabolic
s
294.82
268.94
r
.84
.90
2000
1000
0
0
.5
1
1.5
1/COS(phi)*1/SIN(alfa)*COS(beta)

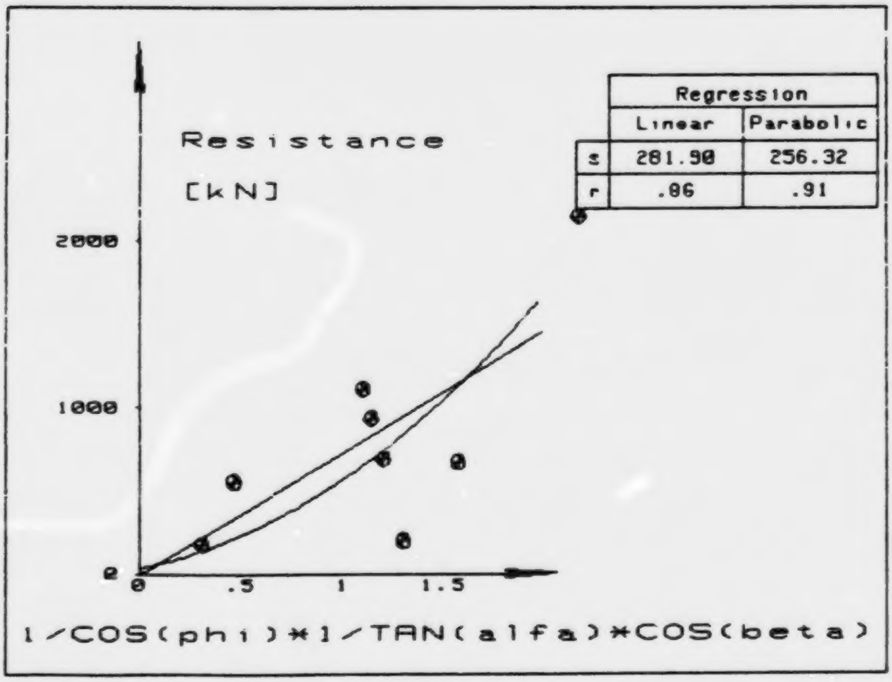
Resistance
[kN]
Regression
Linear
Parabolic
s
281.90
256.32
r
.86
.91
2000
1000
0
0
.5
1
1.5
1/COS(phi)*1/TAN(alfa)*COS(beta)

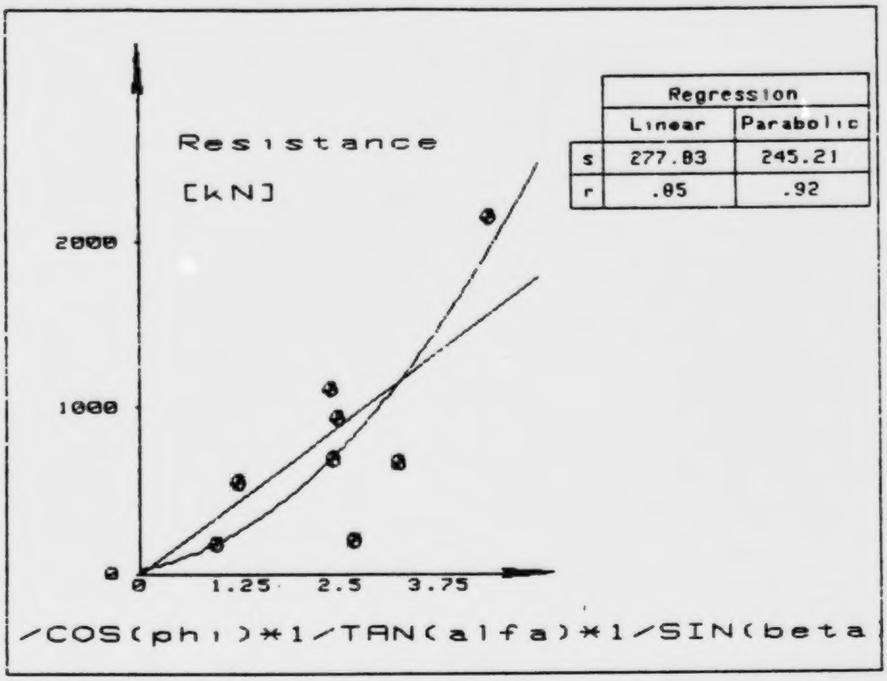

	Regression	
	Linear	Parabolic
s	277.83	245.21
r	.85	.92

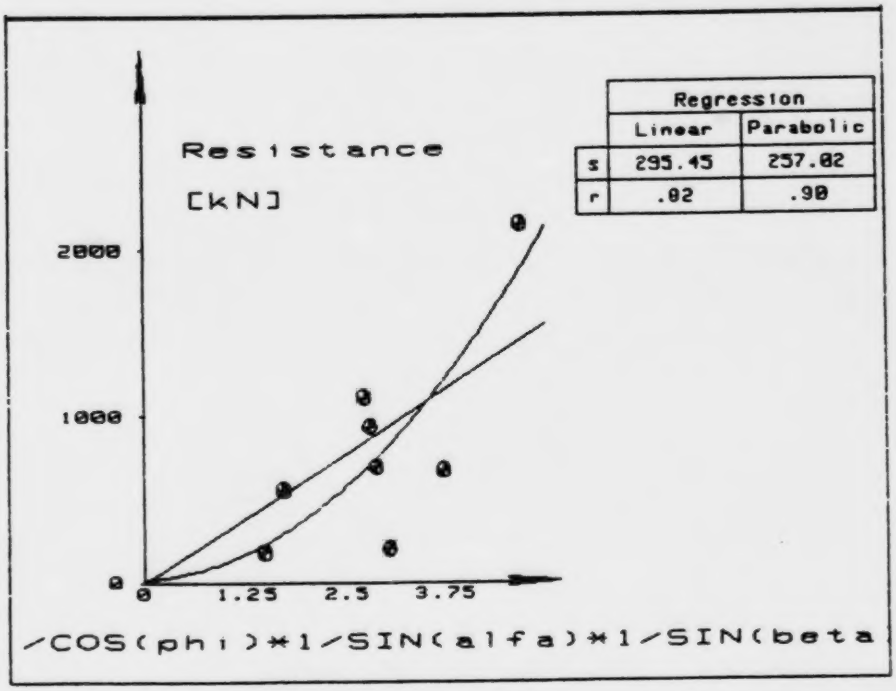

	Regression	
	Linear	Parabolic
s	295.45	257.82
r	.82	.90

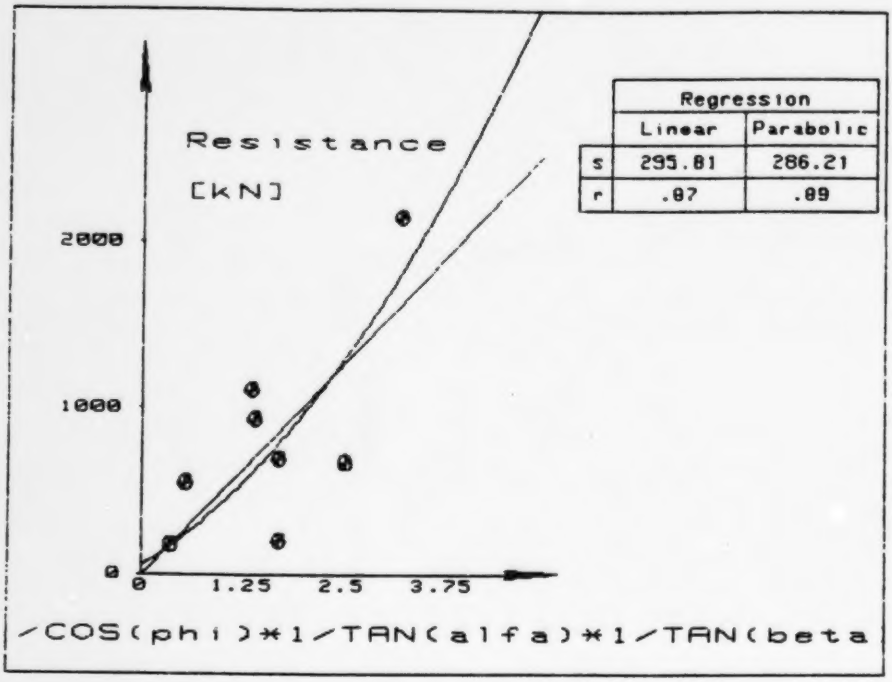

	Regression	
	Linear	Parabolic
s	295.81	286.21
r	.87	.89

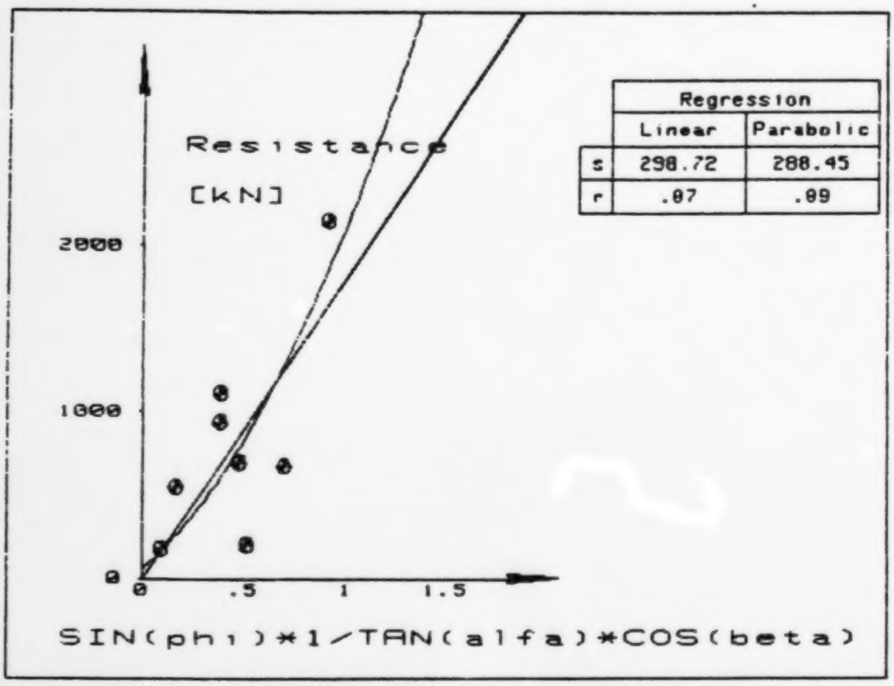

	Regression	
	Linear	Parabolic
s	298.72	288.45
r	.87	.89

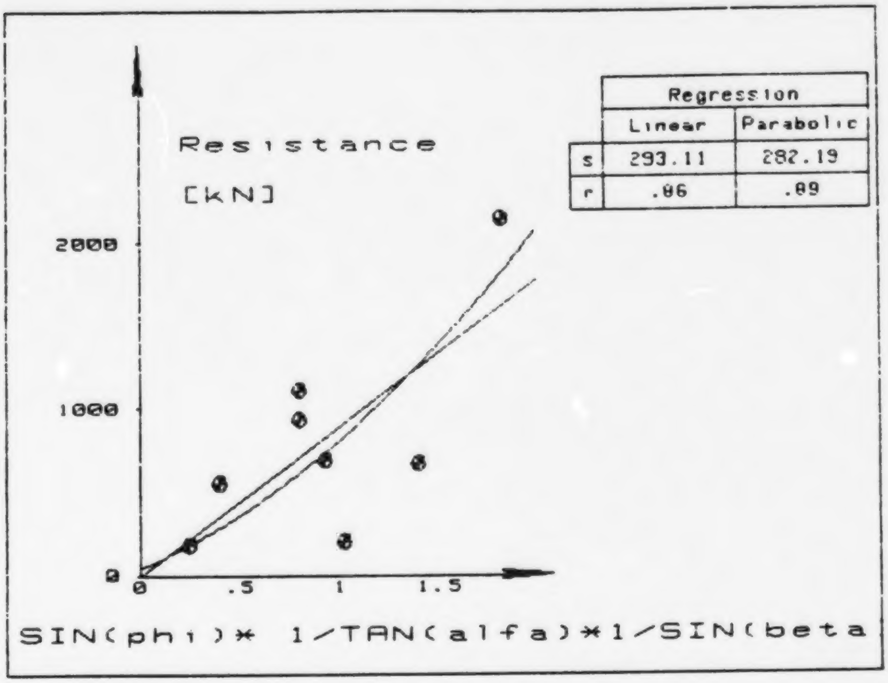

	Regression	
	Linear	Parabolic
s	293.11	282.19
r	.86	.89

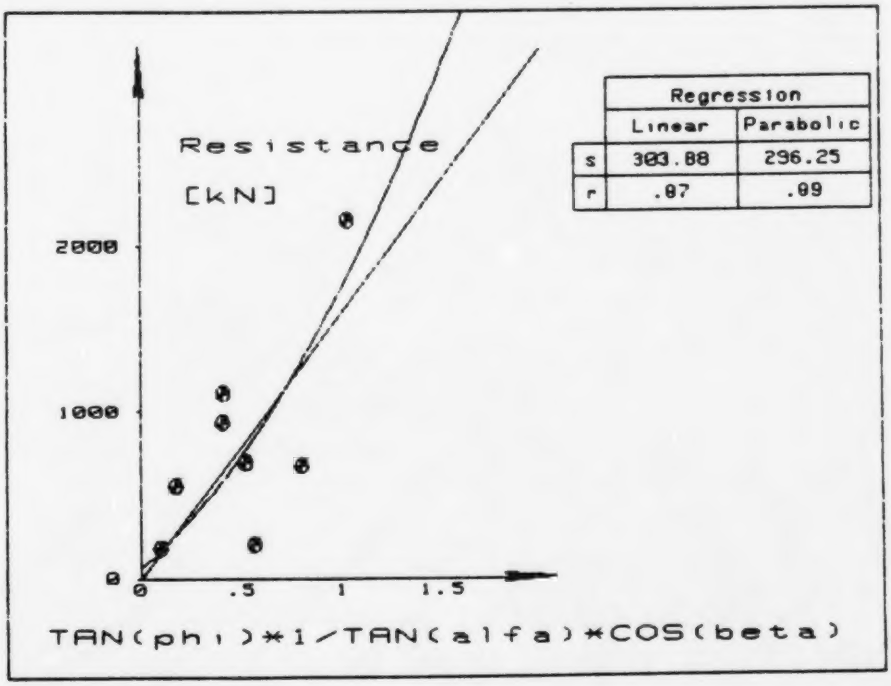

	Regression	
	Linear	Parabolic
s	303.88	296.25
r	.87	.89

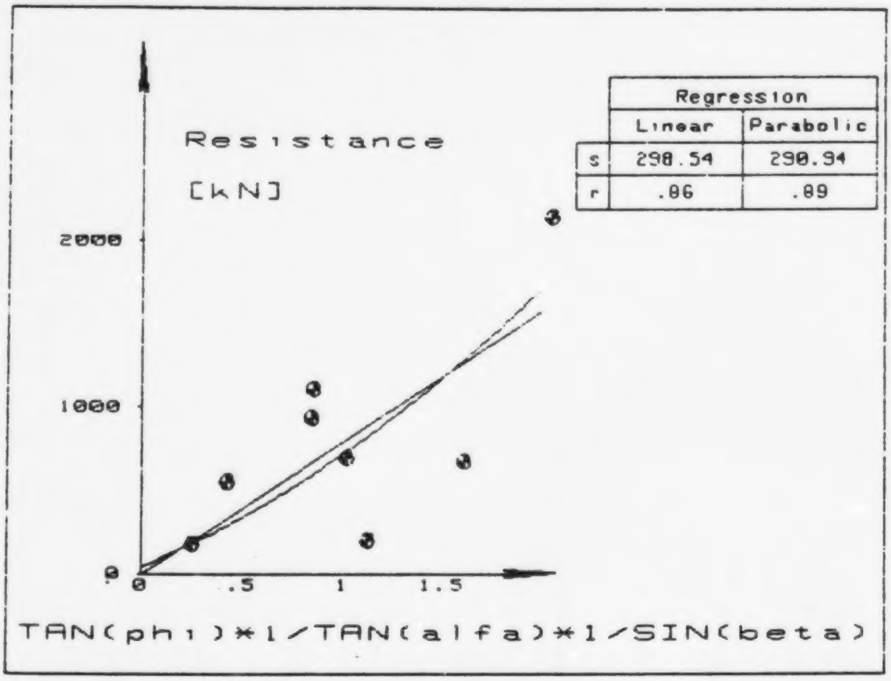
Resistance
[kN]
2000
1000
0
0
.5
1
1.5
TAN(phi)*1/TAN(alfa)*1/SIN(beta)
Regression
Linear
Parabolic
s
298.54
290.94
r
.86
.89

APPENDIX B.3

Significance and Sensitivity of Combined Hull Main Particulars and Bow Geometry Parameters

Parameters	Linear Regression		Parabolic Regression	
	r	s	r	s
B * F(bow)1	0.90	181.97	0.98	116.08
B * F(bow)2	0.92	162.63	0.98	119.92
B * F(bow)3	0.93	190.61	0.96	179.96
B * F(bow)4	0.88	190.57	0.97	114.16
B * F(bow)5	0.91	201.31	0.95	184.77
B * F(bow)6	0.92	209.70	0.95	197.90
B^2 * F(bow)1	0.96	143.97	0.98	133.20
B^2 * F(bow)2	0.97	134.76	0.98	130.65
B^2 * F(bow)3	0.97	170.22	0.97	170.05
B^2 * F(bow)4	0.95	144.72	0.97	135.60
B^2 * F(bow)5	0.96	174.56	0.97	172.38
B^2 * F(bow)6	0.96	183.57	0.97	182.41
(B * B/d) * F(bow)1	0.87	214.45	0.97	131.96
(B * B/d) * F(bow)2	0.90	187.34	0.98	120.33
(B * B/d) * F(bow)3	0.93	154.66	0.99	97.15
(B * B/d) * F(bow)4	0.85	253.59	0.92	226.13
(B * B/d) * F(bow)5	0.90	173.60	0.99	90.52
(B * B/d) * F(bow)6	0.92	175.50	0.98	120.44
(B^2 * B/d) * F(bow)1	0.94	129.11	0.99	85.16
(B^2 * B/d) * F(bow)2	0.96	105.74	0.99	76.70
(B^2 * B/d) * F(bow)3	0.98	101.42	0.99	93.11
(B^2 * B/d) * F(bow)4	0.98	116.50	0.99	112.41
(B^2 * B/d) * F(bow)5	0.96	111.63	0.99	91.46
(B^2 * B/D) * F(bow)6	0.97	122.79	0.99	111.67
(B * B/d)^2 * F(bow)1	0.91	220.41	0.94	203.52
(B * B/d)^2 * F(bow)2	0.93	197.46	0.96	181.03
(B * B/d)^2 * F(bow)3	0.96	134.37	1.00	94.92
(B * B/d)^2 * F(bow)4	0.97	133.14	1.00	102.19
(B * B/d)^2 * F(bow)5	0.94	154.46	0.99	100.68
(B * B/d)^2 * F(bow)6	0.95	149.14	0.99	107.28
(Am * B/d) * F(bow)1	0.94	153.52	0.98	131.92
(Am * B/d) * F(bow)2	0.96	138.27	0.98	127.18
(Am * B/d) * F(bow)3	0.96	175.41	0.97	173.55
(Am * B/d) * F(bow)4	0.96	185.37	0.97	184.33
(Am * B/d) * F(bow)5	0.95	183.39	0.96	178.32
(Am * B/d) * F(bow)6	0.95	191.89	0.96	188.67

Table 5.5
Combination of Size and Geometry Parameters

Symbols :
F(bow)1 : 1/SIN(alfa)
F(bow)2 : 1/TAN(alfa)
F(bow)3 : 1/COS(phi) * 1/TAN(alfa) * 1/SIN(beta)
F(bow)4 : 1/COS(phi) * 1/TAN(alfa) * COS(beta)
F(bow)5 : 1/COS(phi) * 1/SIN(alfa) * 1/SIN(beta)
F(bow)6 : 1/COS(phi) * 1/SIN(alfa) * COS(beta)

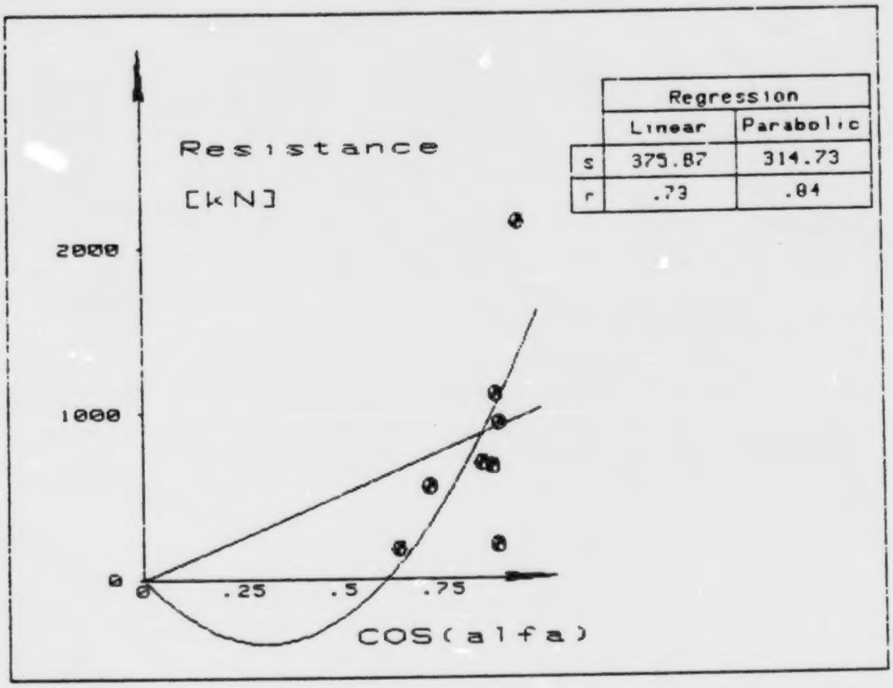

	Regression	
	Linear	Parabolic
s	375.87	314.73
r	.73	.84

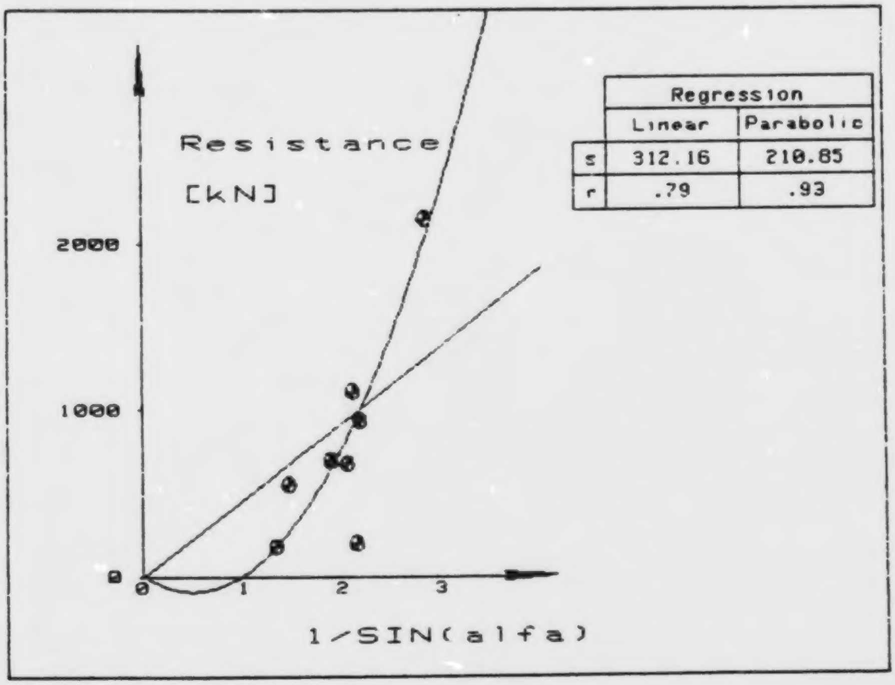

	Regression	
	Linear	Parabolic
s	312.16	210.85
r	.79	.93

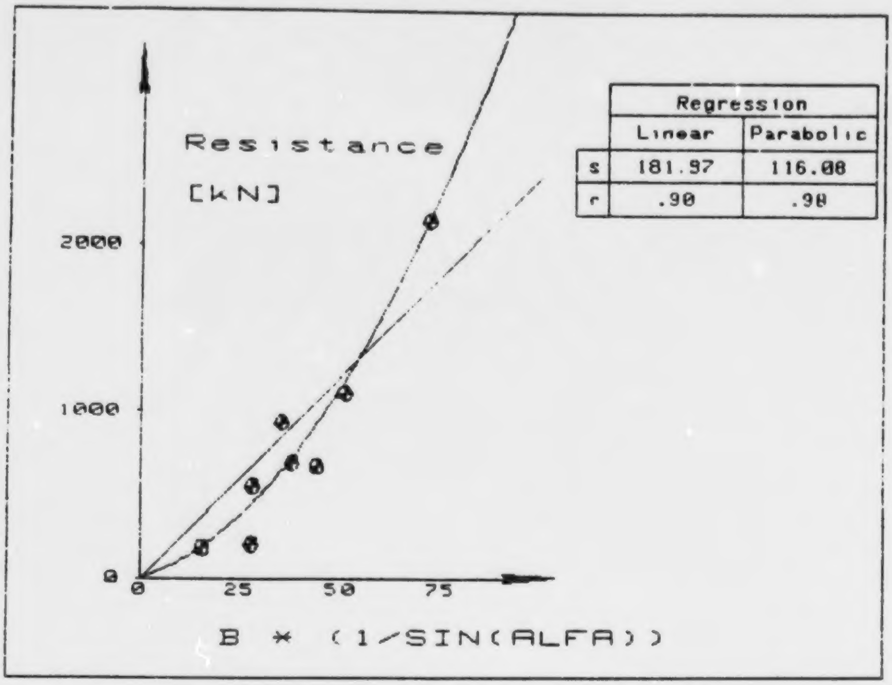

	Regression	
	Linear	Parabolic
s	181.97	116.08
r	.90	.98

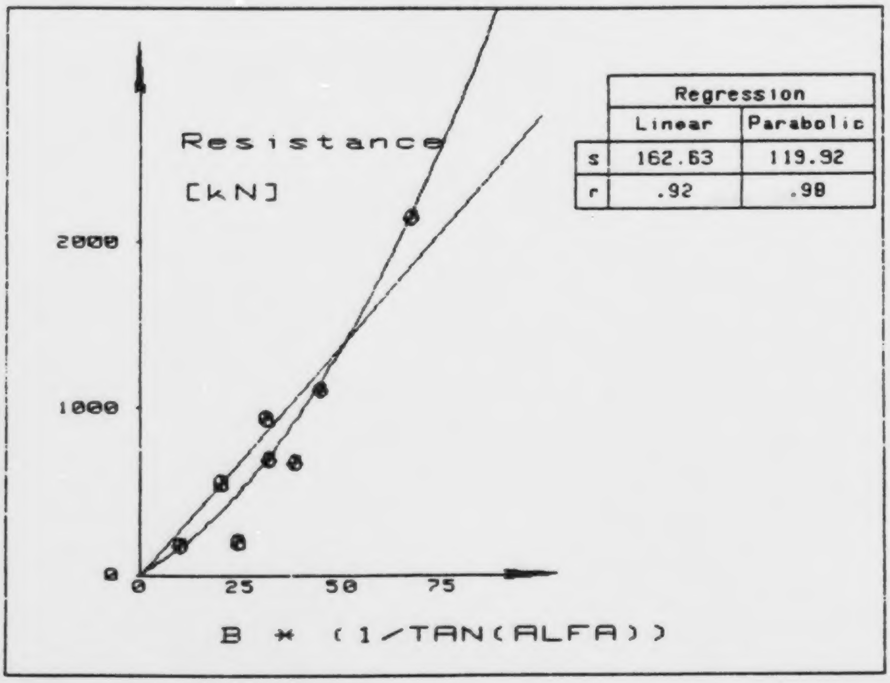

	Regression	
	Linear	Parabolic
s	162.63	119.92
r	.92	.98

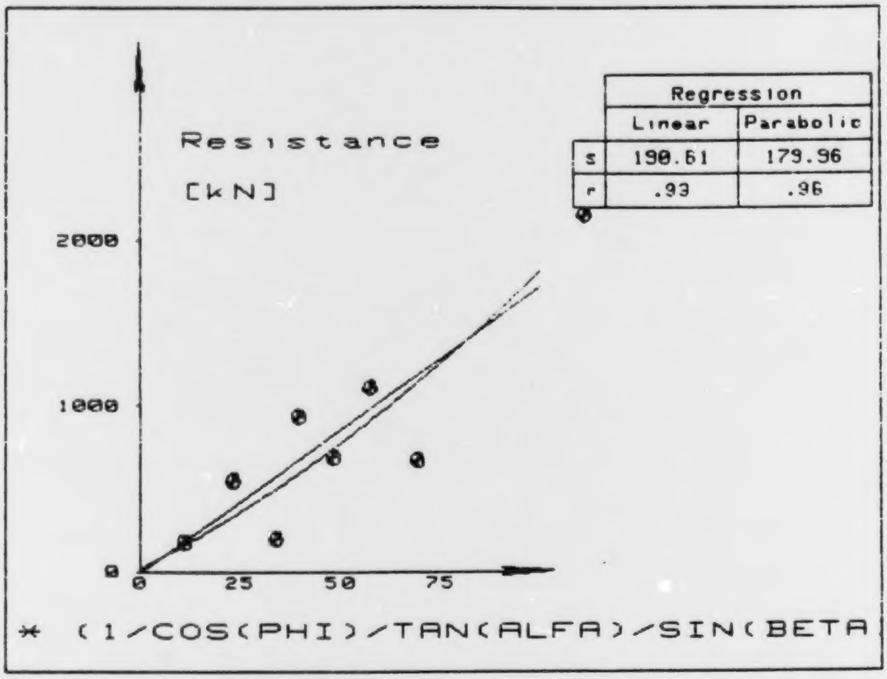

	Regression	
	Linear	Parabolic
s	190.61	179.96
r	.93	.96

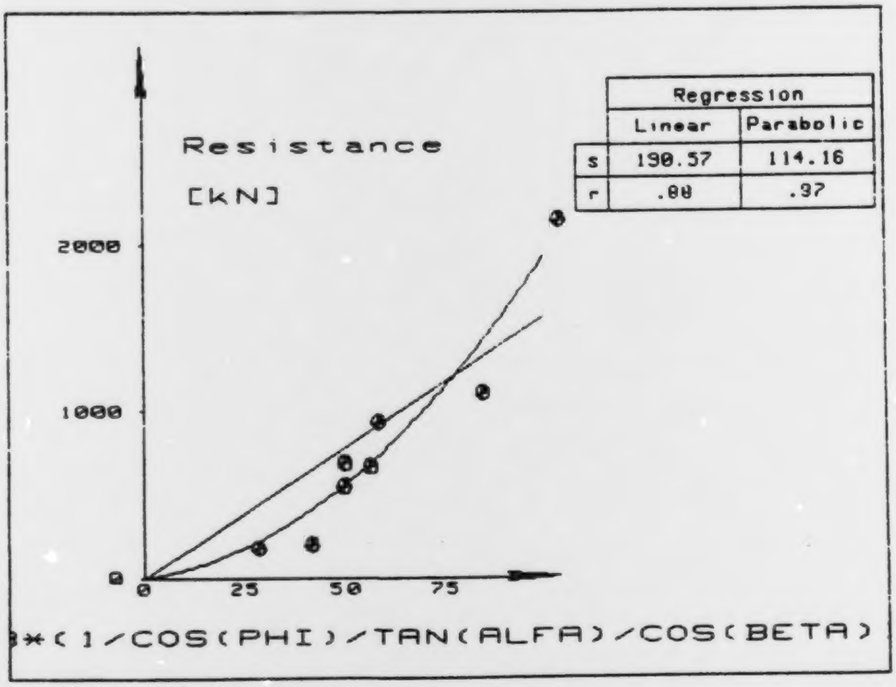

	Regression	
	Linear	Parabolic
s	190.57	114.16
r	.80	.97

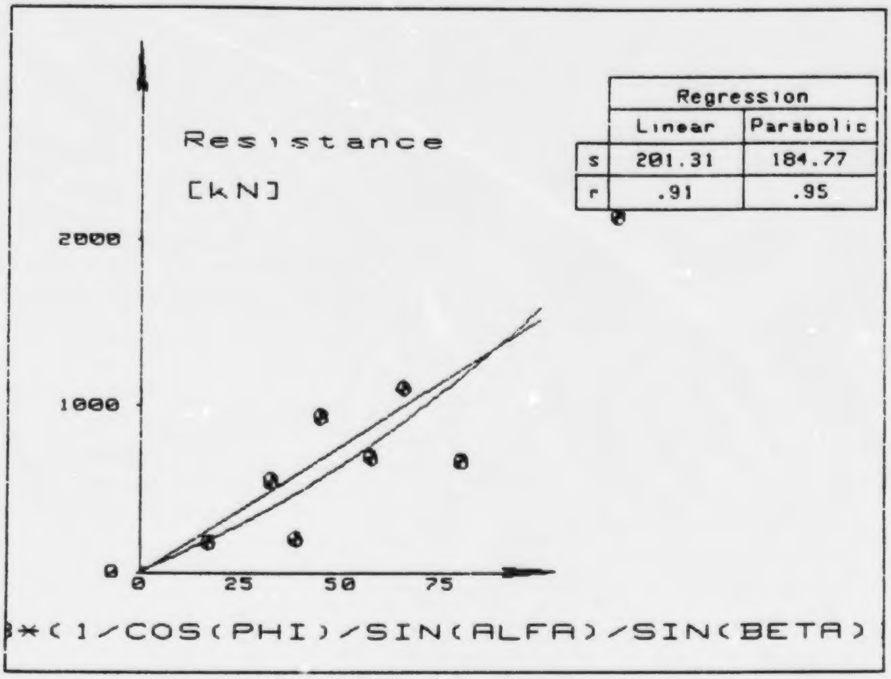

	Regression	
	Linear	Parabolic
s	201.31	184.77
r	.91	.95

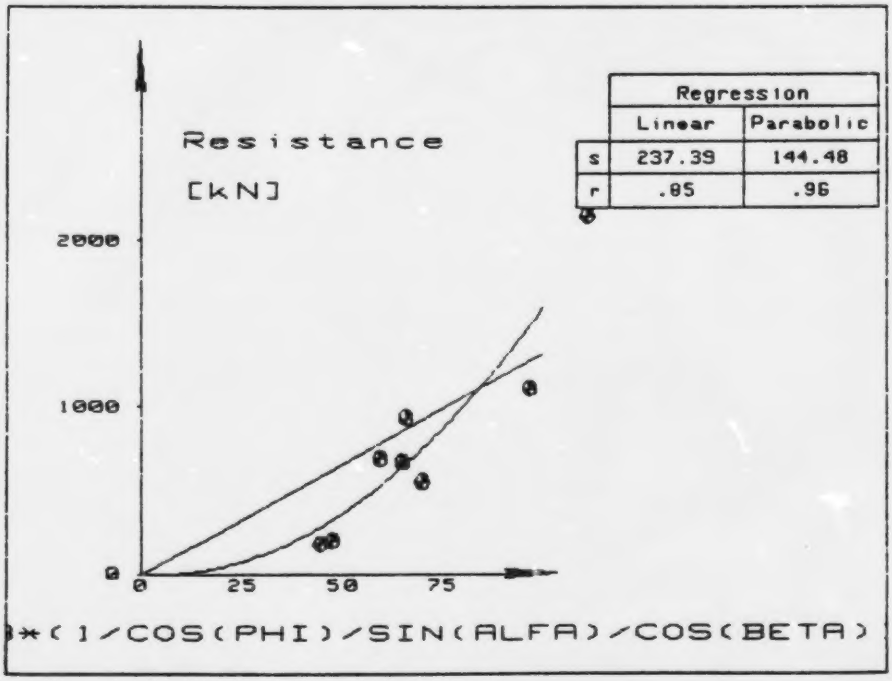

	Regression	
	Linear	Parabolic
s	237.39	144.48
r	.85	.96

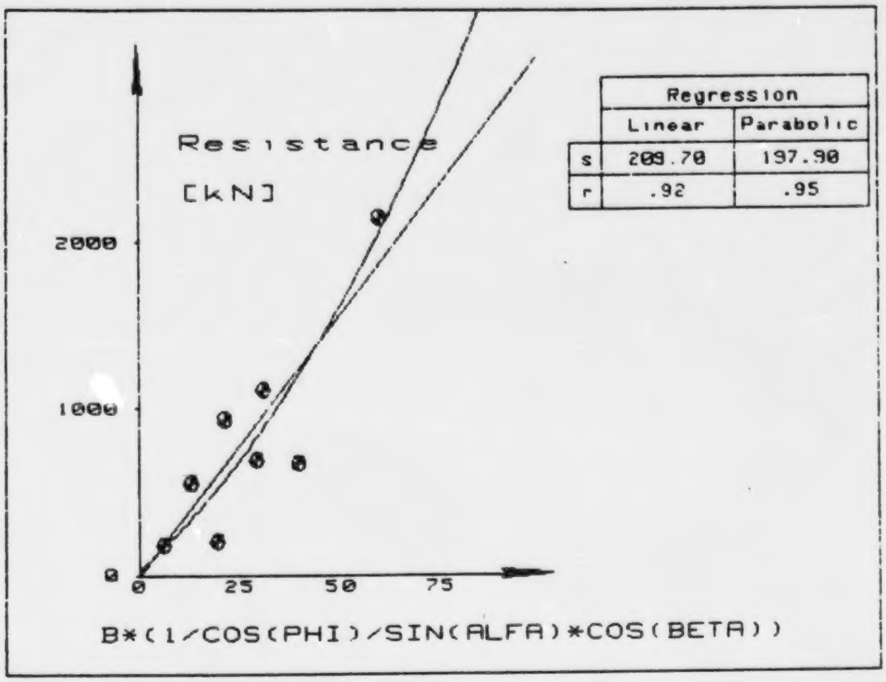

	Regression	
	Linear	Parabolic
s	209.70	197.90
r	.92	.95

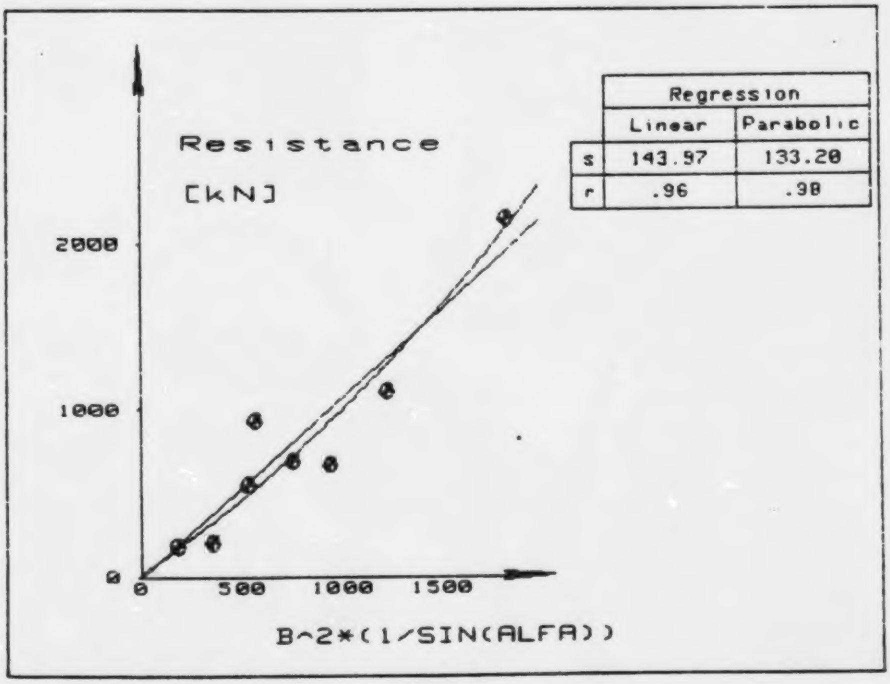

	Regression	
	Linear	Parabolic
s	143.97	133.20
r	.96	.98

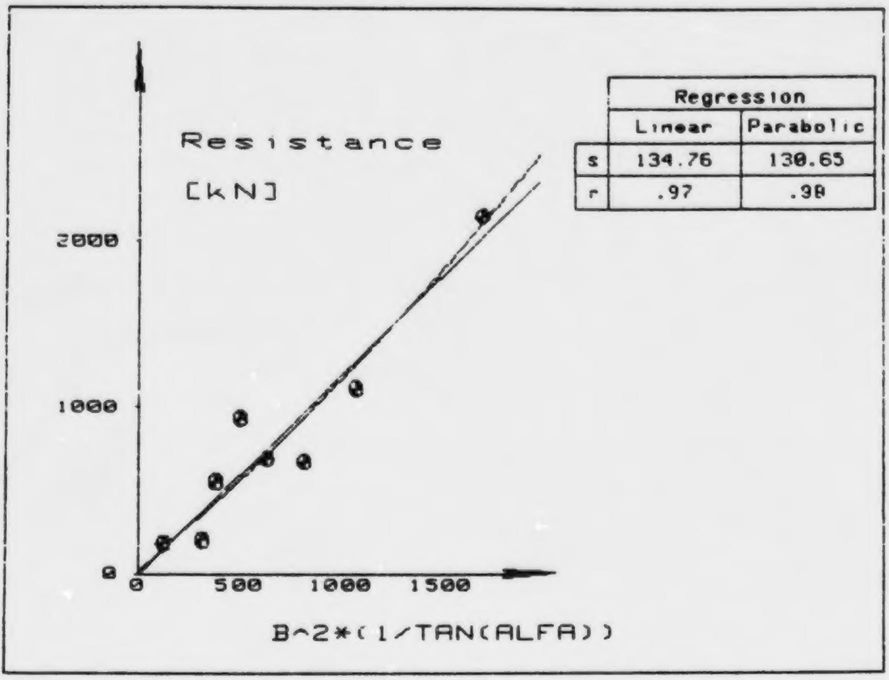

	Regression	
	Linear	Parabolic
s	134.76	130.65
r	.97	.98

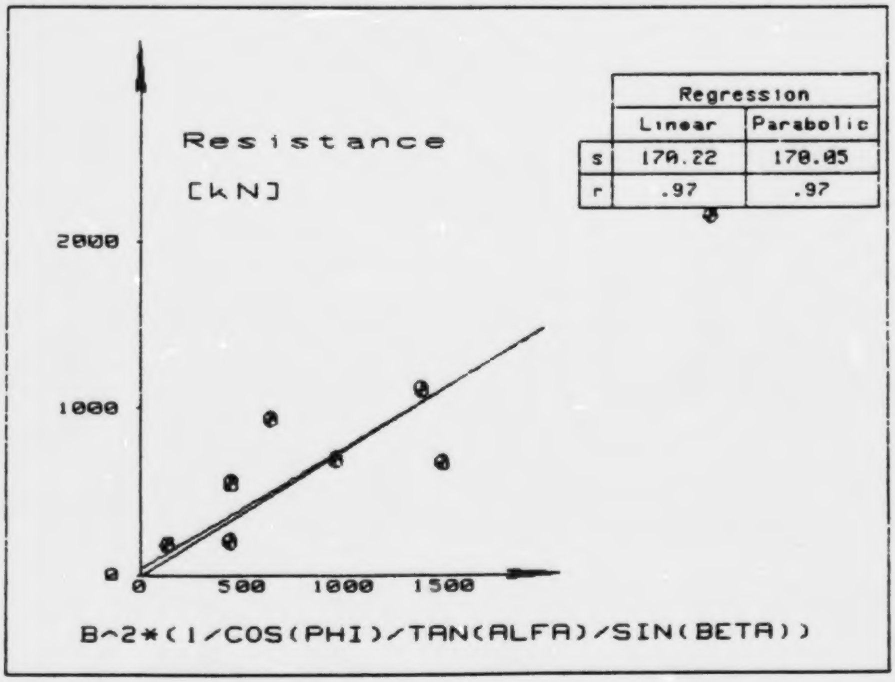

	Regression	
	Linear	Parabolic
s	170.22	170.05
r	.97	.97

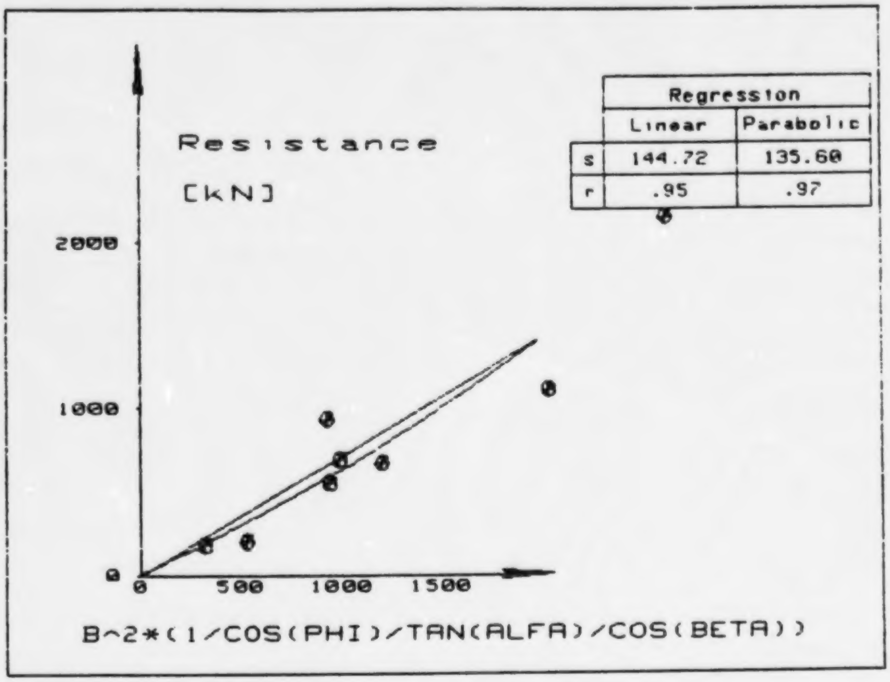

	Regression	
	Linear	Parabolic
s	144.72	135.60
r	.95	.97

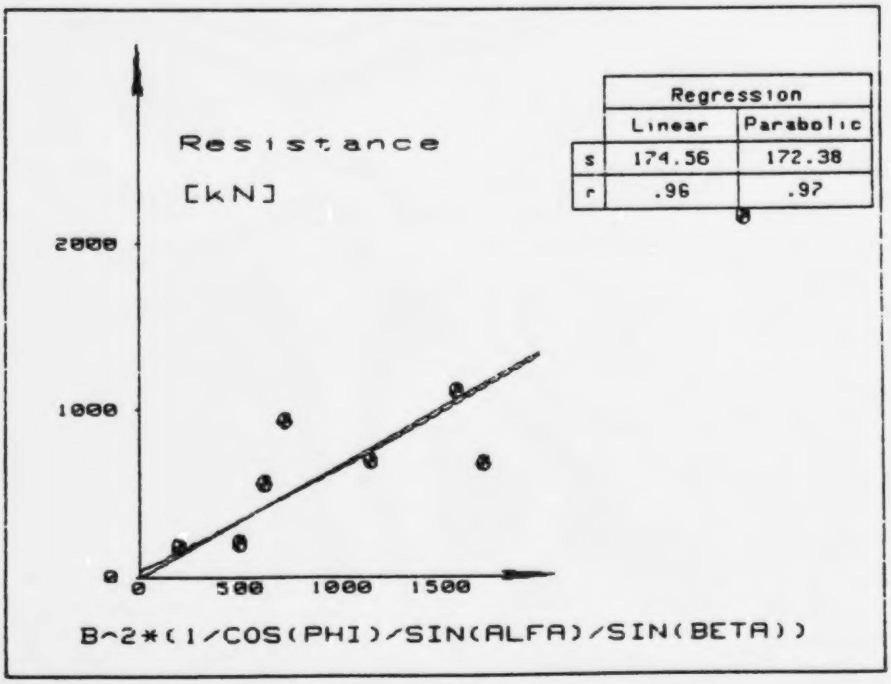

	Regression	
	Linear	Parabolic
s	174.56	172.38
r	.96	.97

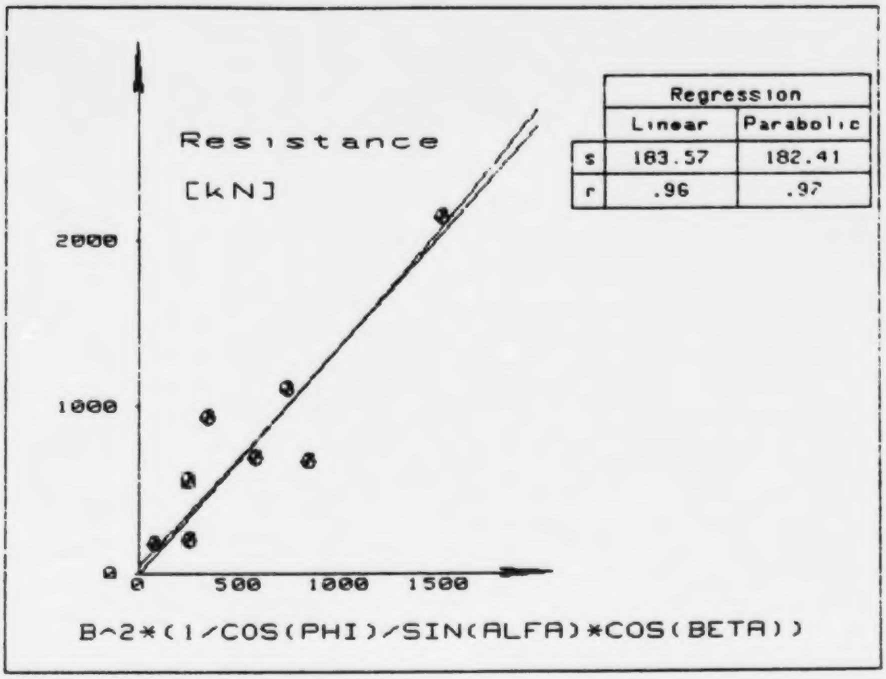

	Regression	
	Linear	Parabolic
s	183.57	182.41
r	.96	.97

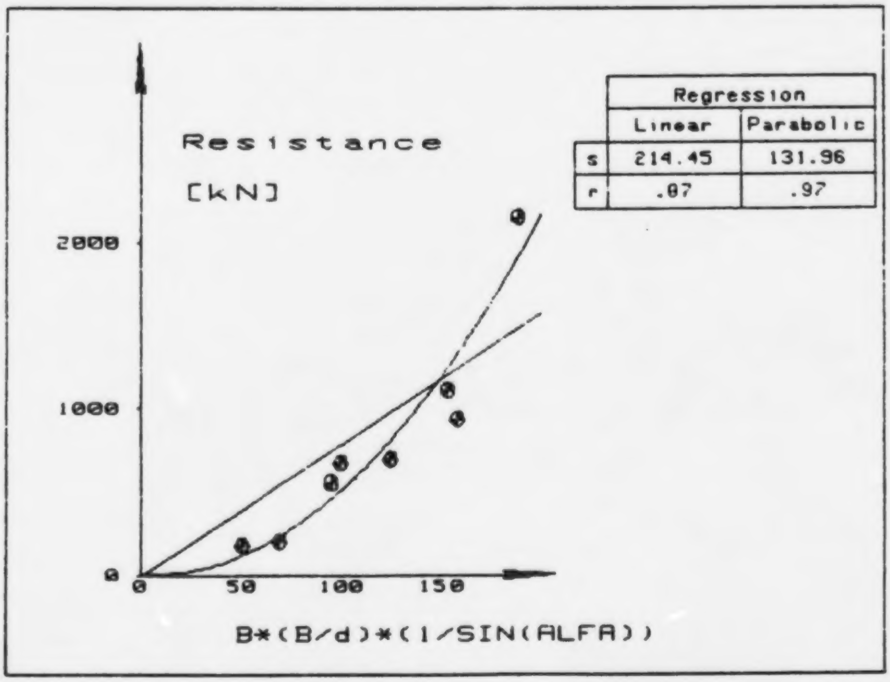

	Regression	
	Linear	Parabolic
s	214.45	131.96
r	.87	.97

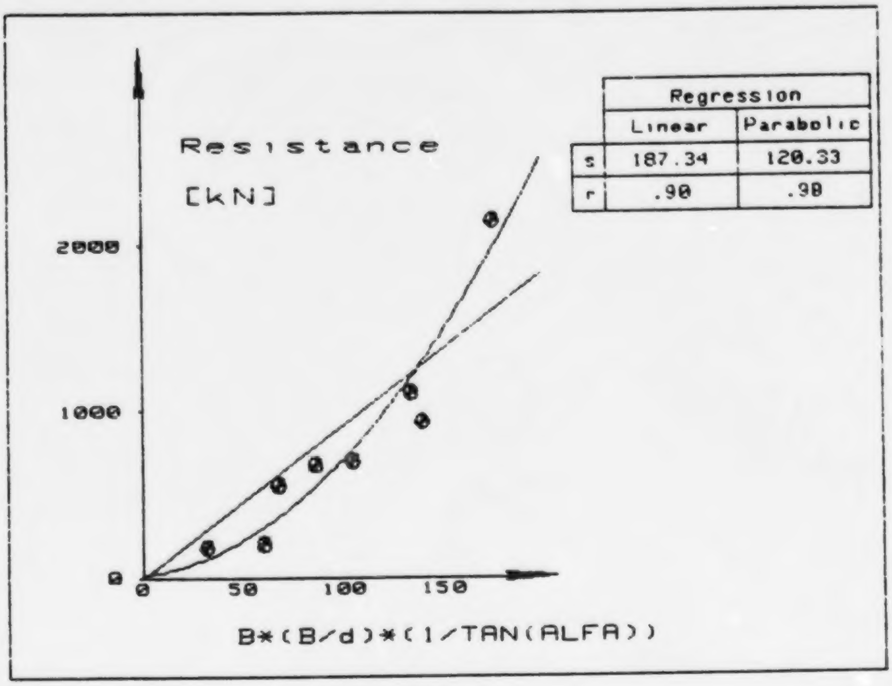

	Regression	
	Linear	Parabolic
s	187.34	120.33
r	.90	.98

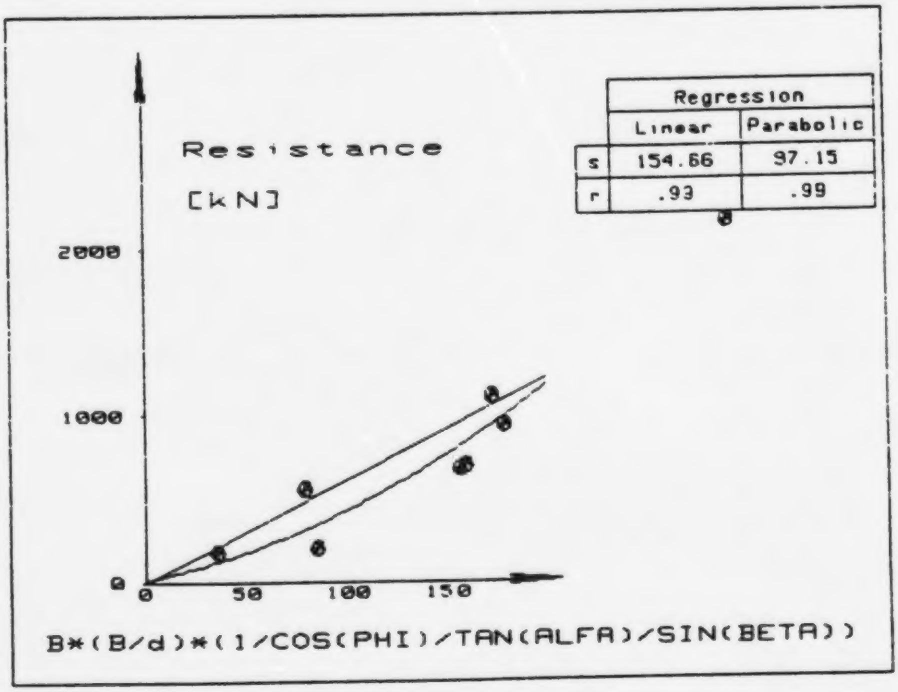

	Regression	
	Linear	Parabolic
s	154.66	97.15
r	.93	.99

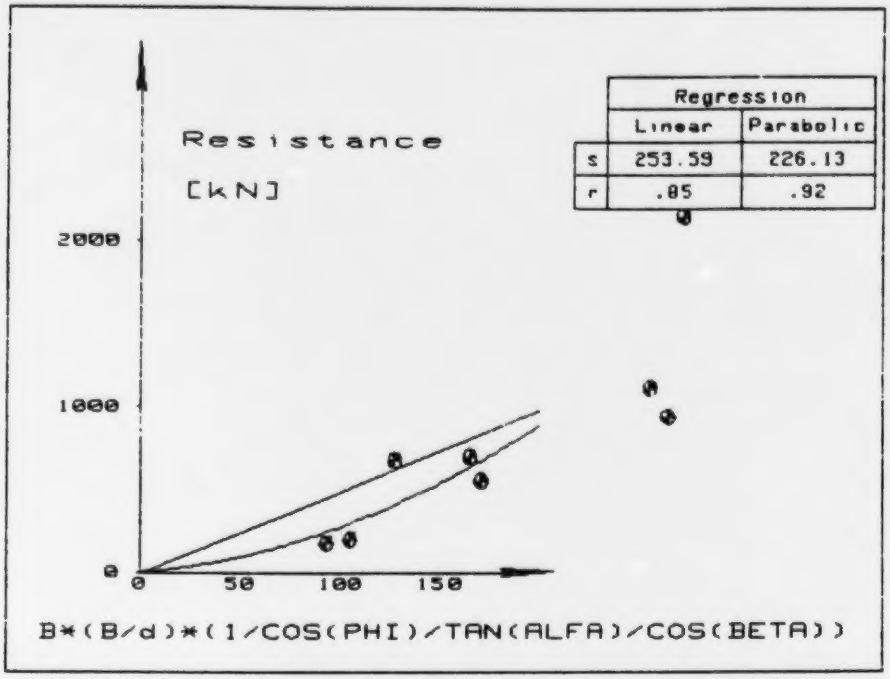

	Regression	
	Linear	Parabolic
s	253.59	226.13
r	.85	.92

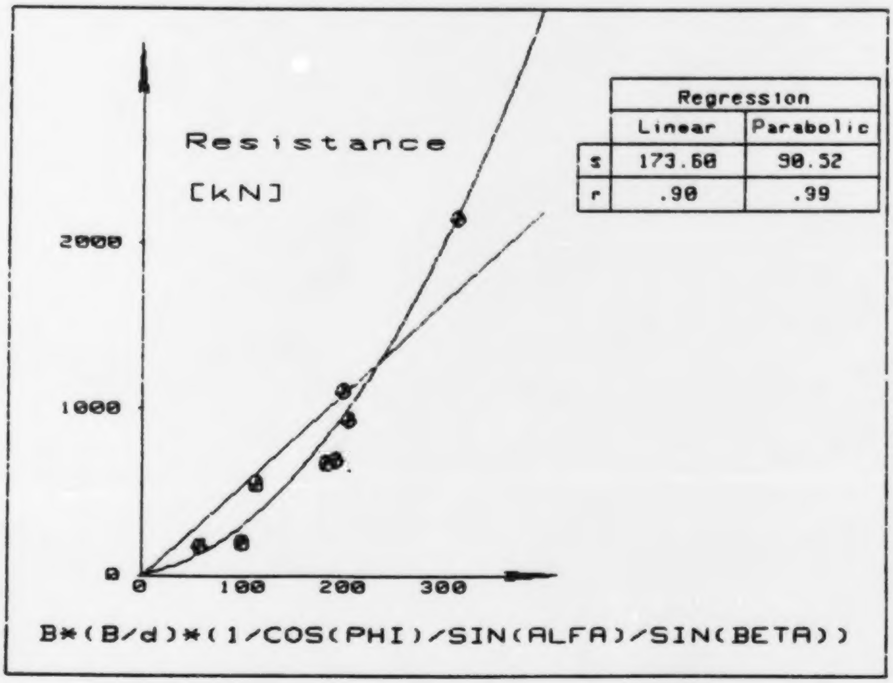

	Regression	
	Linear	Parabolic
s	173.60	90.52
r	.90	.99

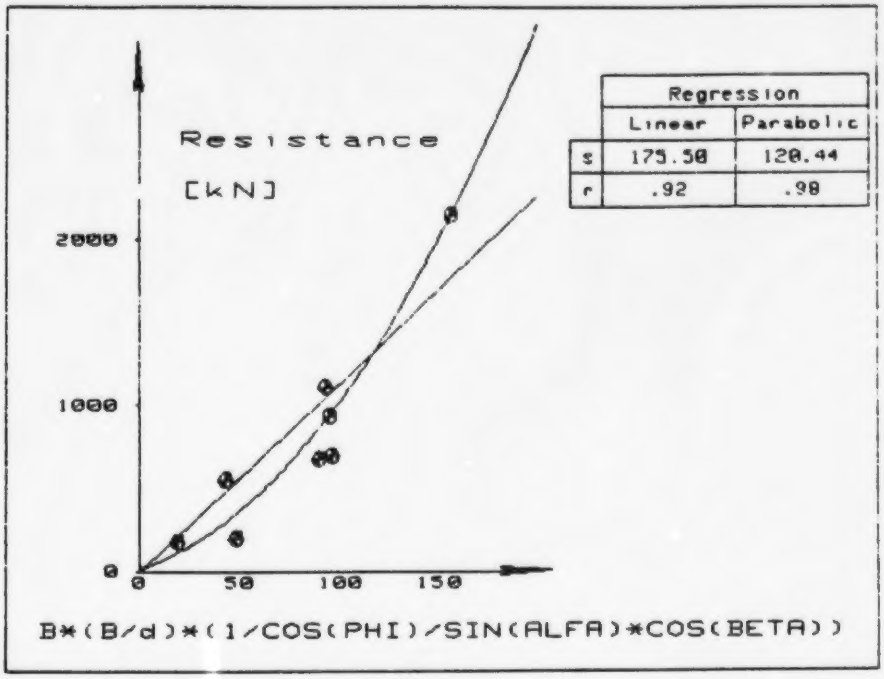

	Regression	
	Linear	Parabolic
s	175.50	120.44
r	.92	.98

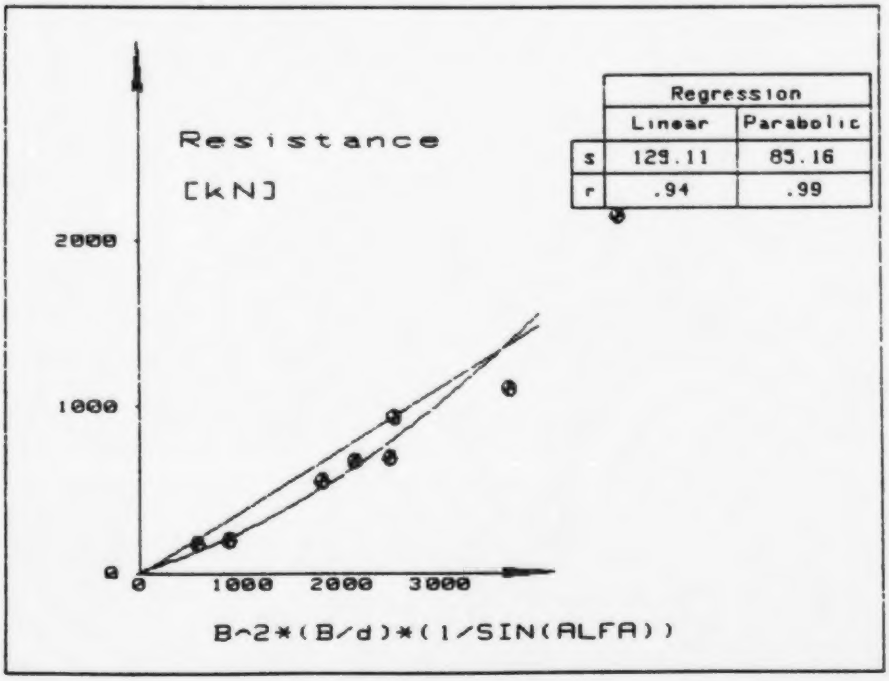

	Regression	
	Linear	Parabolic
s	129.11	85.16
r	.94	.99

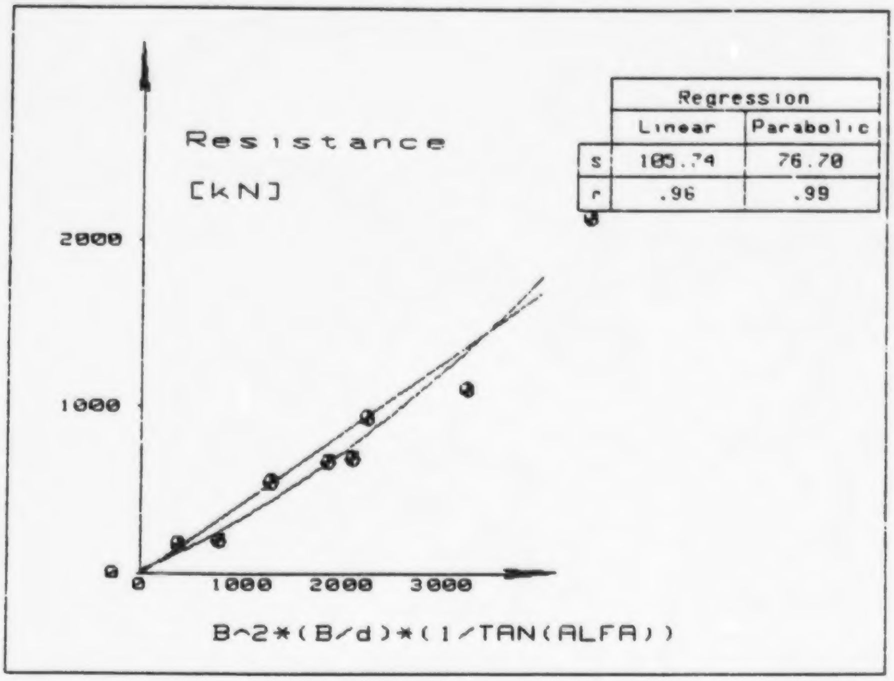

	Regression	
	Linear	Parabolic
s	105.74	76.70
r	.96	.99

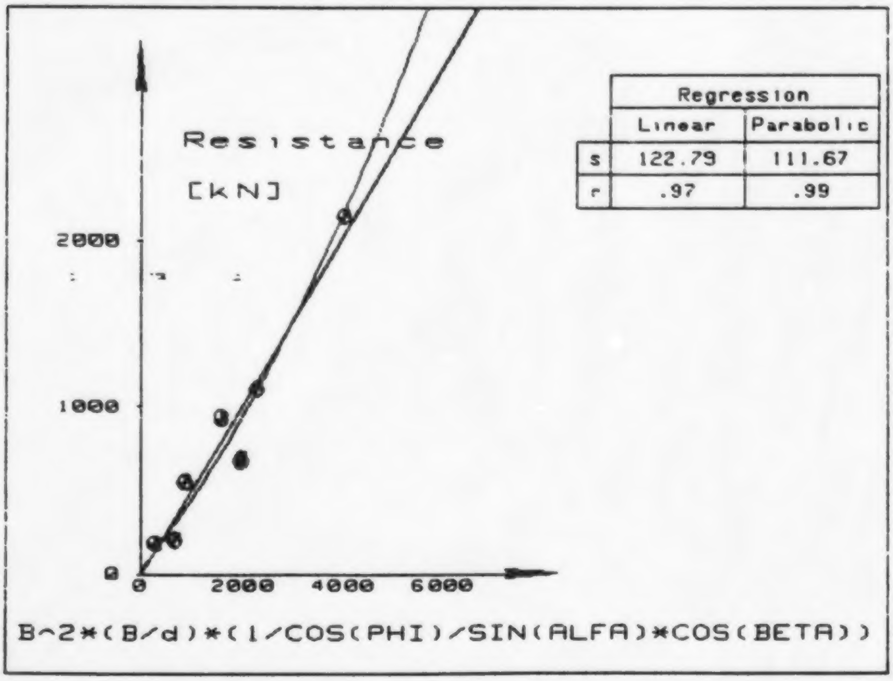

	Regression	
	Linear	Parabolic
s	122.79	111.67
r	.97	.99

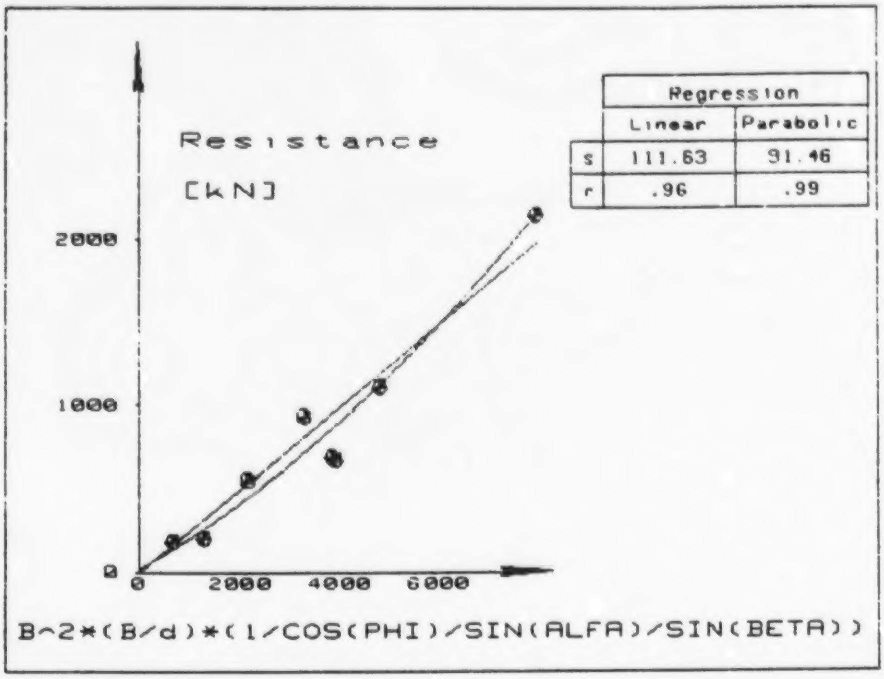

	Regression	
	Linear	Parabolic
s	111.63	91.46
r	.96	.99

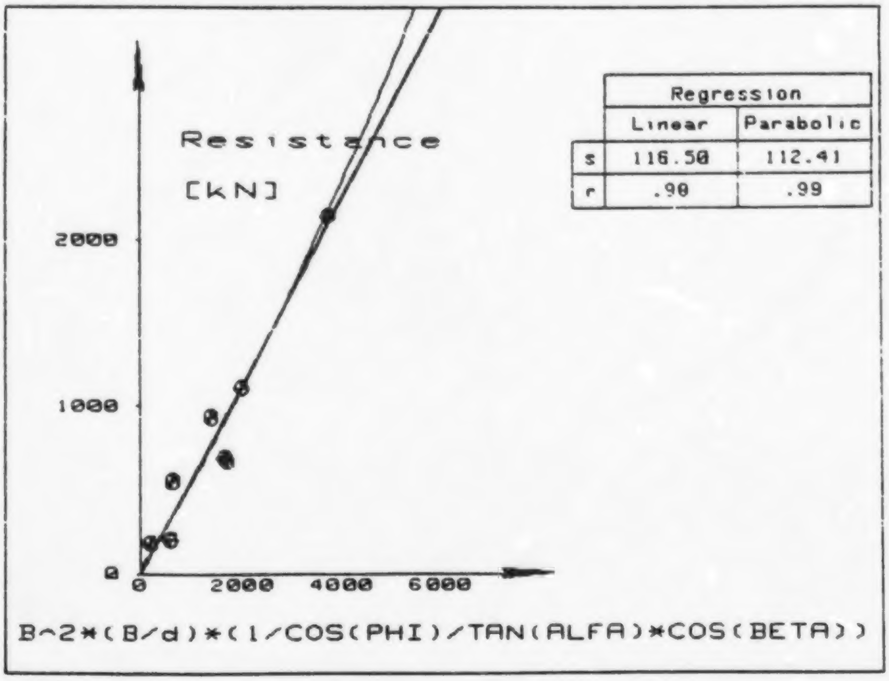

	Regression	
	Linear	Parabolic
s	116.50	112.41
r	.90	.99

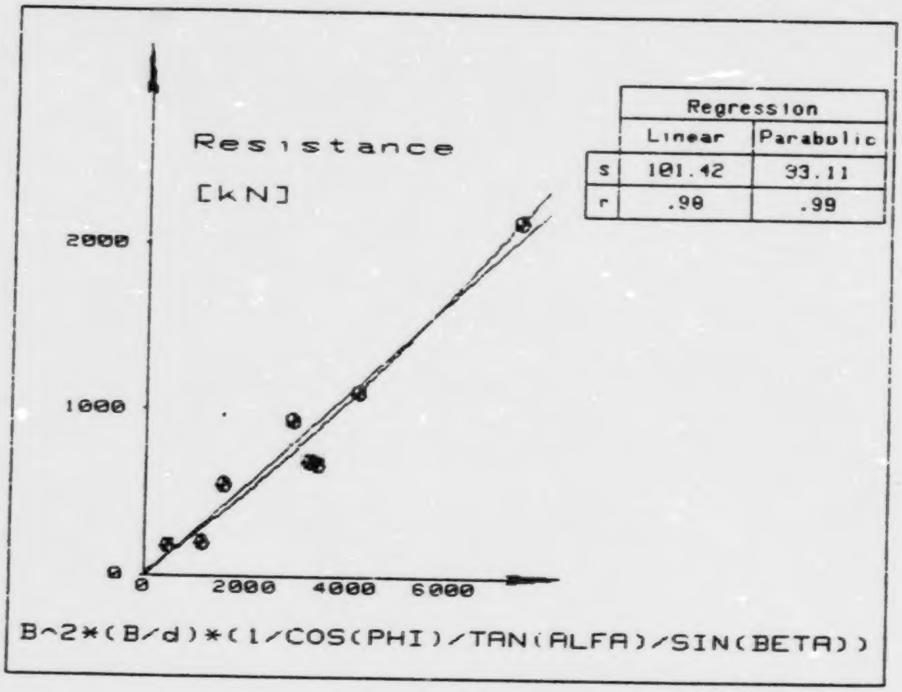

	Regression	
	Linear	Parabolic
s	101.42	93.11
r	.98	.99

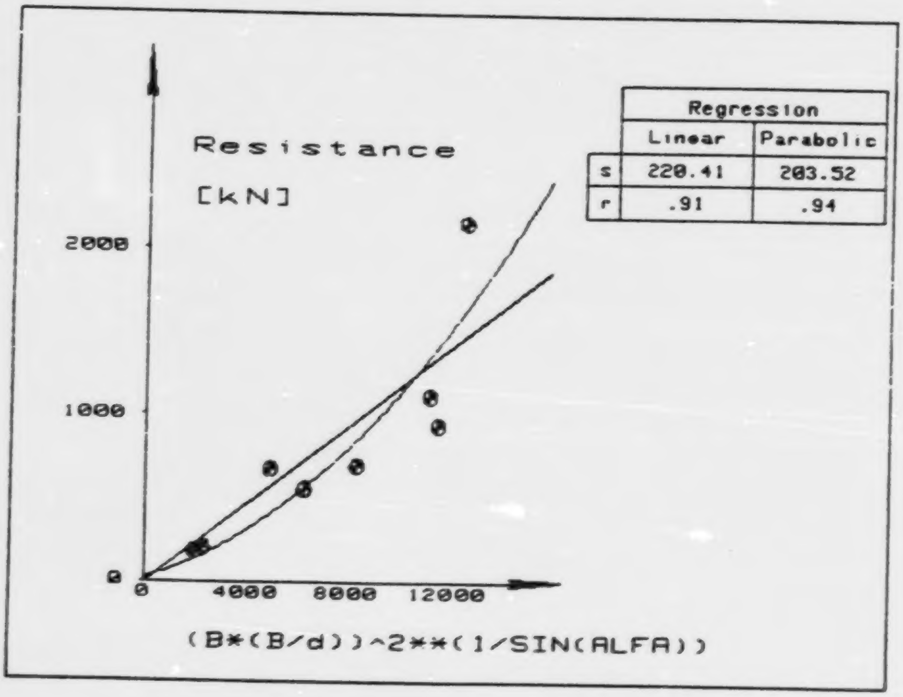

	Regression	
	Linear	Parabolic
s	220.41	203.52
r	.91	.94

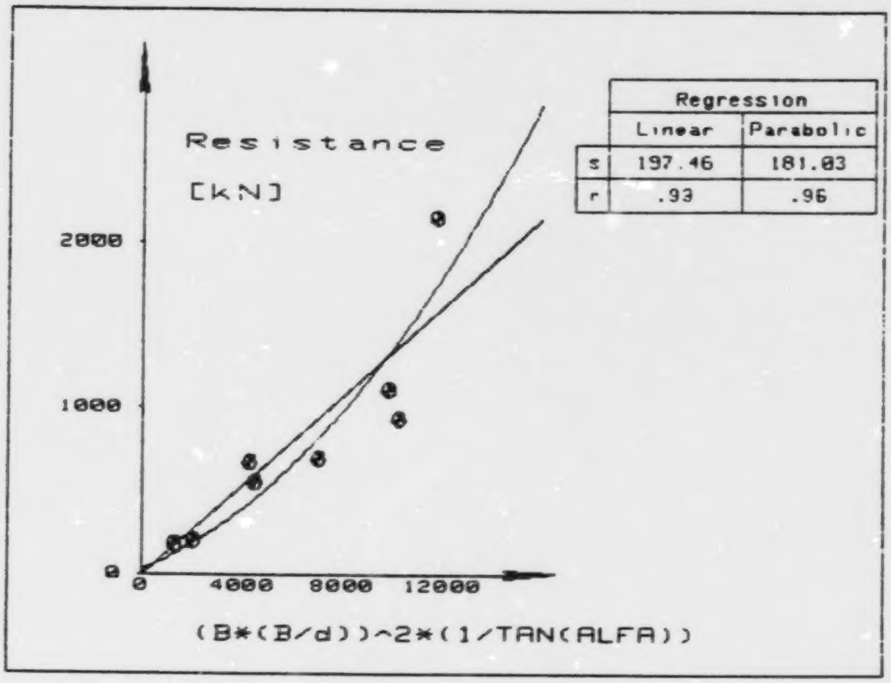

	Regression	
	Linear	Parabolic
s	197.46	181.03
r	.93	.96

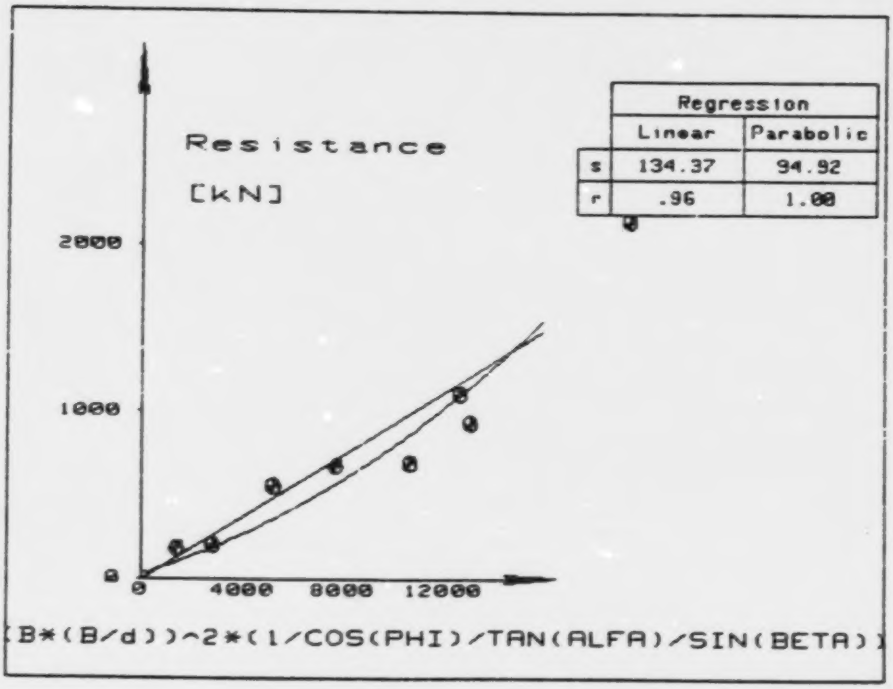

	Regression	
	Linear	Parabolic
s	134.37	94.92
r	.96	1.00

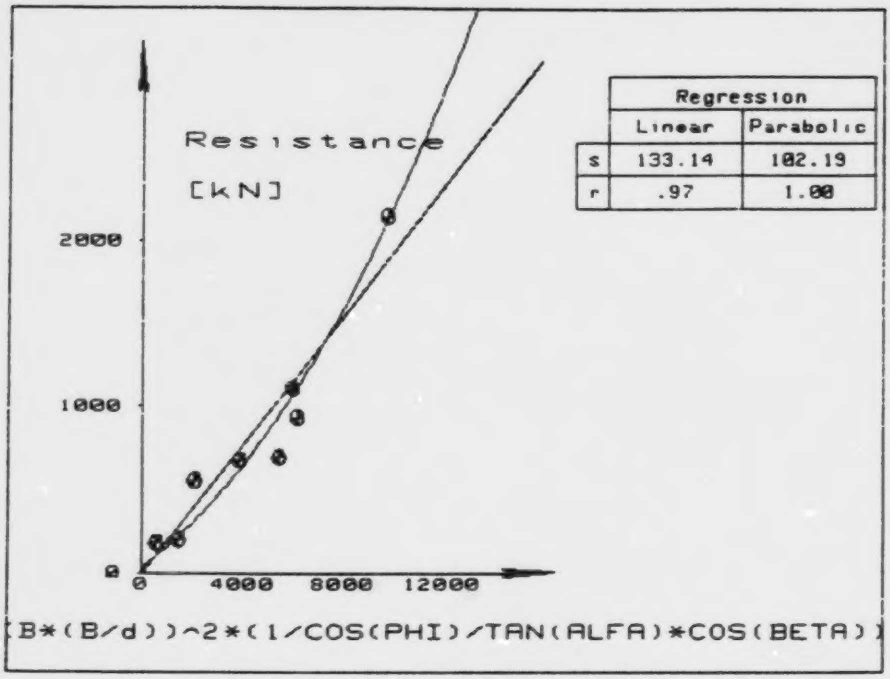

	Regression	
	Linear	Parabolic
s	133.14	102.19
r	.97	1.00

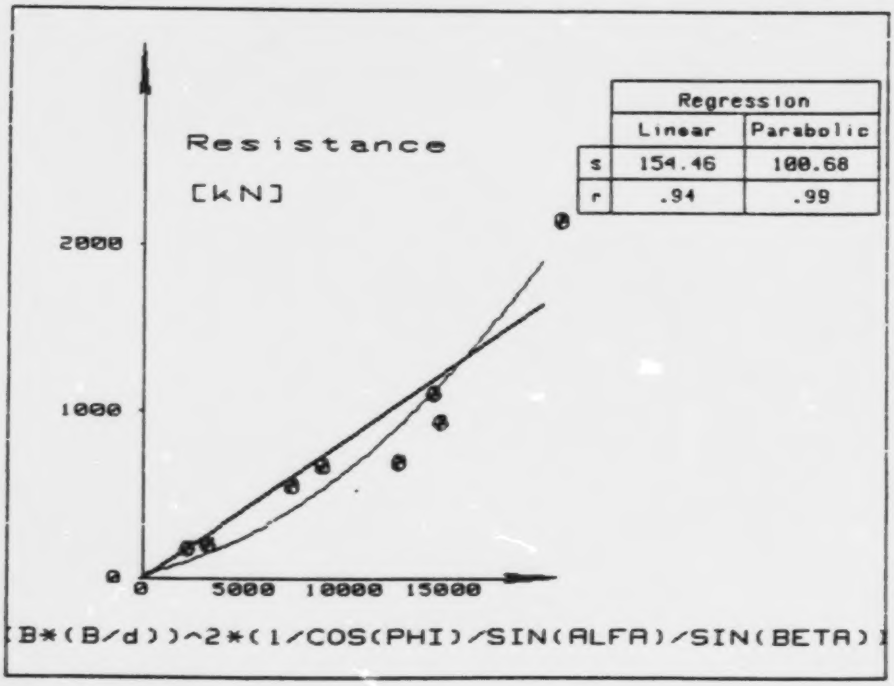

	Regression	
	Linear	Parabolic
s	154.46	100.68
r	.94	.99

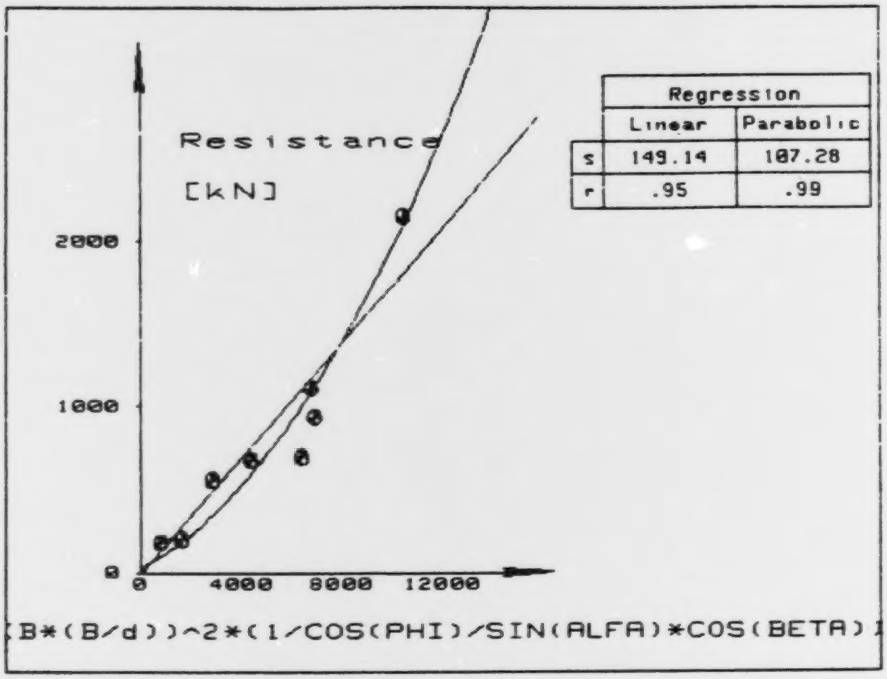

	Linear	Parabolic
s	149.14	107.28
r	.95	.99

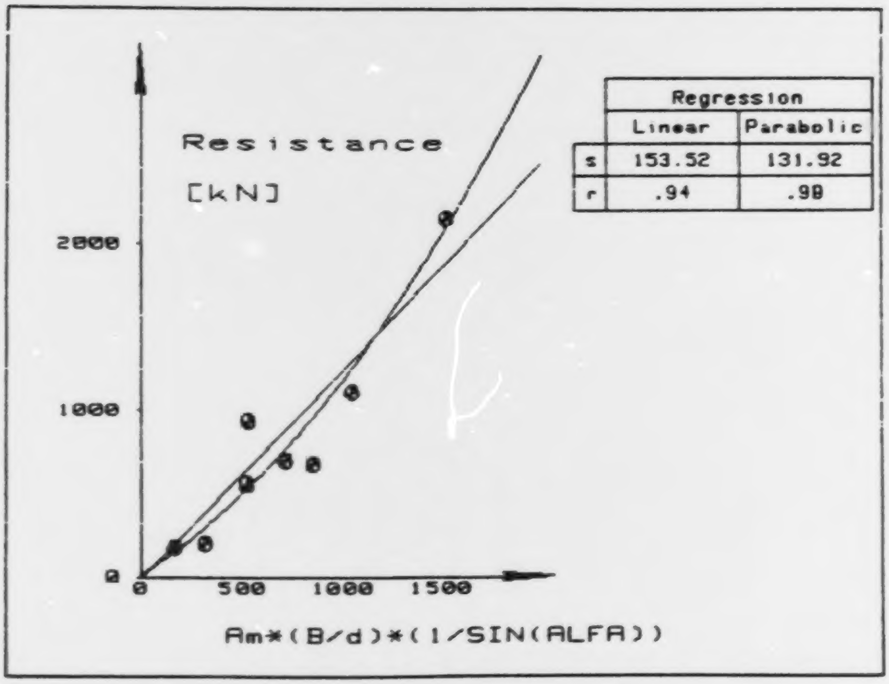

	Linear	Parabolic
s	153.52	131.92
r	.94	.98

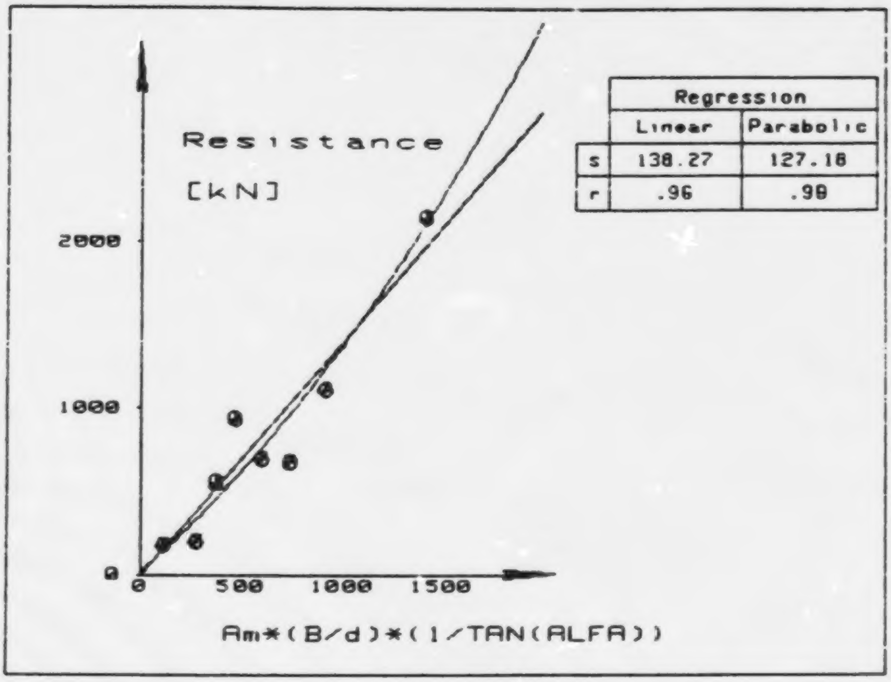
Regression
Linear
Parabolic
s 138.27 127.18
r .96 .98
Resistance
[kN]
2000
1000
0
0
500
1000
1500
Am*(B/d)*(1/TAN(ALFA))

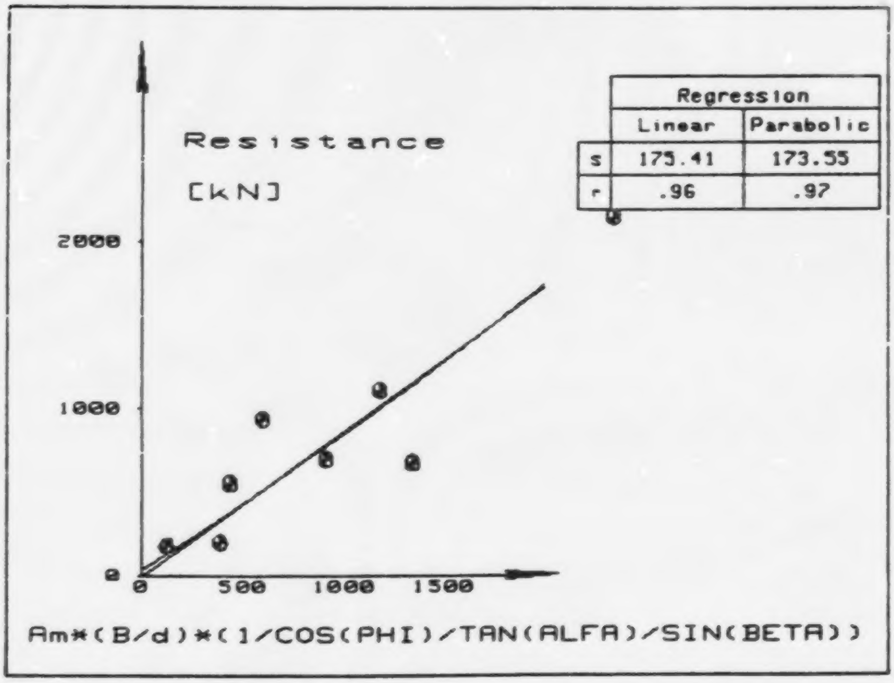
Regression
Linear
Parabolic
s 175.41 173.55
r .96 .97
Resistance
[kN]
2000
1000
0
0
500
1000
1500
Am*(B/d)*(1/COS(PHI)/TAN(ALFA)/SIN(BETA))

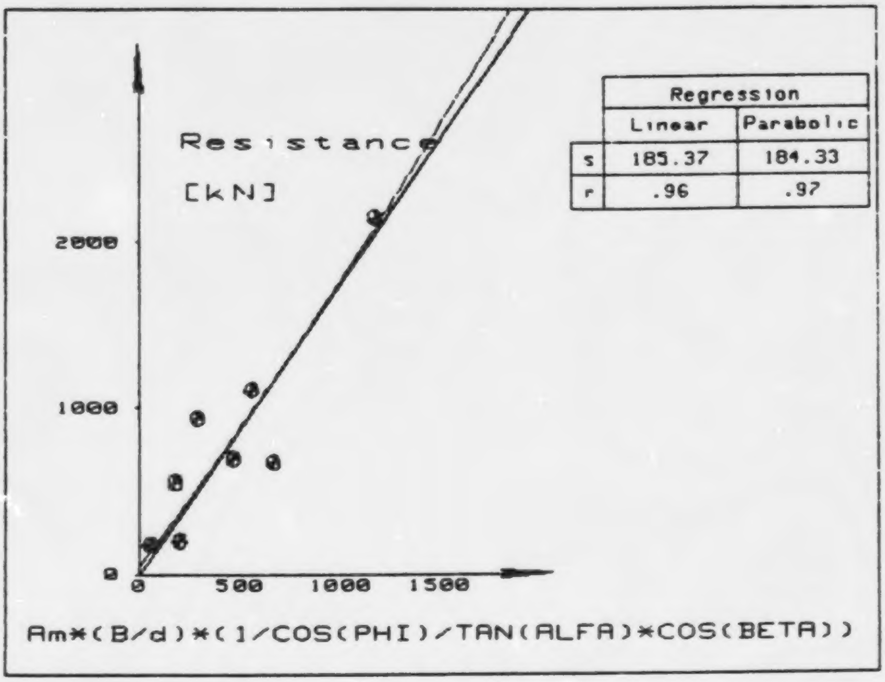
Regression
Linear
Parabolic
s 185.37 184.33
r .96 .97
Resistance
[kN]
2000
1000
0
0
500
1000
1500
Am*(B/d)*(1/COS(PHI)/TAN(ALFA)*COS(BETA))

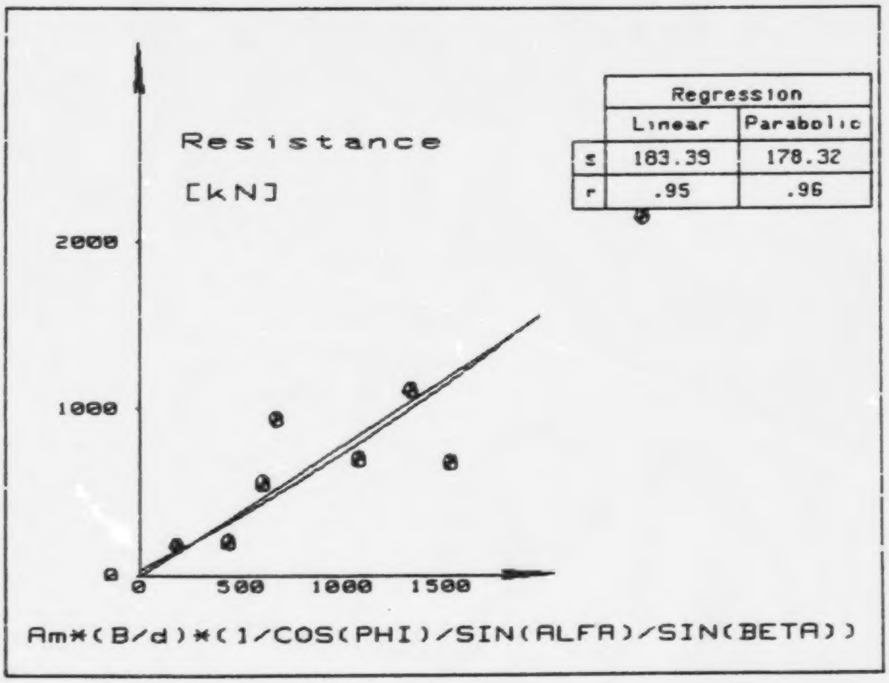
Regression
Linear
Parabolic
s 183.39 178.32
r .95 .96
Resistance
[kN]
2000
1000
0
0
500
1000
1500
Am*(B/d)*(1/COS(PHI)/SIN(ALFA)/SIN(BETA))

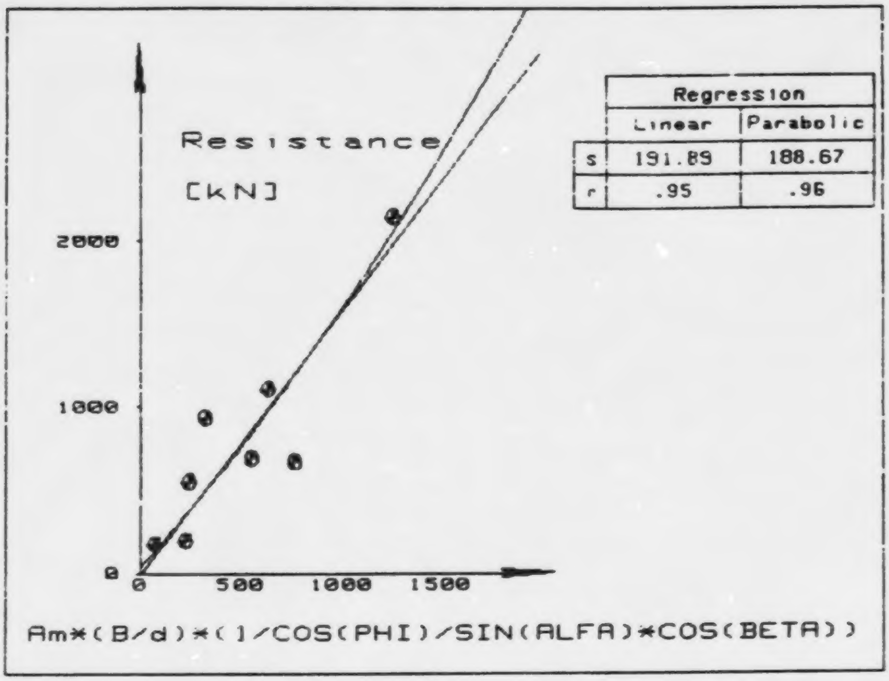

	Regression	
	Linear	Parabolic
s	191.89	188.67
r	.95	.96

APPENDIX B.4

Sensitivity of Ridge Resistance Formula to Changes in H_R

Equation (5-2) from Section 5 for the calculation of ridge resistance in first year ice was developed for a selected value of H_R. To investigate scatter and correlation over a wide range of H_R this appendix applies Equation (5-2) for a wide range of H_R with $0 < H_R < 10$ m. The following Table and Figures show that the absolute values for the standard error s increases over the tested range of H_R by a factor of 10. Compared to the measured and calculated resistance values the relationship between scatter and resistance is almost a constant :

$$\frac{R_{Ridge} \quad (H_R = 1)}{s \quad (H_R = 1)} \approx \frac{R_{Ridge} \quad (H_R = 10)}{s \quad (H_R = 10)}$$

The correlation coefficients indicate for the full range of H_R a good fit between the regression lines and the data.

```
Hr = 1.0  Slope =  .113      Slope/Hr :  .113

Hr = 1.5  Slope =  .153      Slope/Hr :  .102

Hr = 2.0  Slope =  .193      Slope/Hr :  .0965

Hr = 2.5  Slope =  .233      Slope/Hr :  .0933

Hr = 3.0  Slope =  .273      Slope/Hr :  .0911

Hr = 3.5  Slope =  .313      Slope/Hr :  .0896

Hr = 4.0  Slope =  .354      Slope/Hr :  .0884

Hr = 4.5  Slope =  .394      Slope/Hr :  .0875

Hr = 5.0  Slope =  .434      Slope/Hr :  .0868

Hr = 5.5  Slope =  .474      Slope/Hr :  .0862

Hr = 6.0  Slope =  .514      Slope/Hr :  .0857

Hr = 6.5  Slope =  .554      Slope/Hr :  .0853

Hr = 7.0  Slope =  .594      Slope/Hr :  .0849

Hr = 7.5  Slope =  .635      Slope/Hr :  .0846

Hr = 8.0  Slope =  .675      Slope/Hr :  .0843

Hr = 8.5  Slope =  .715      Slope/Hr :  .0841

Hr = 9.0  Slope =  .755      Slope/Hr :  .0839

Hr = 9.5  Slope =  .795      Slope/Hr :  .0837

Hr = 10   Slope =  .835      Slope/Hr :  .0835
```

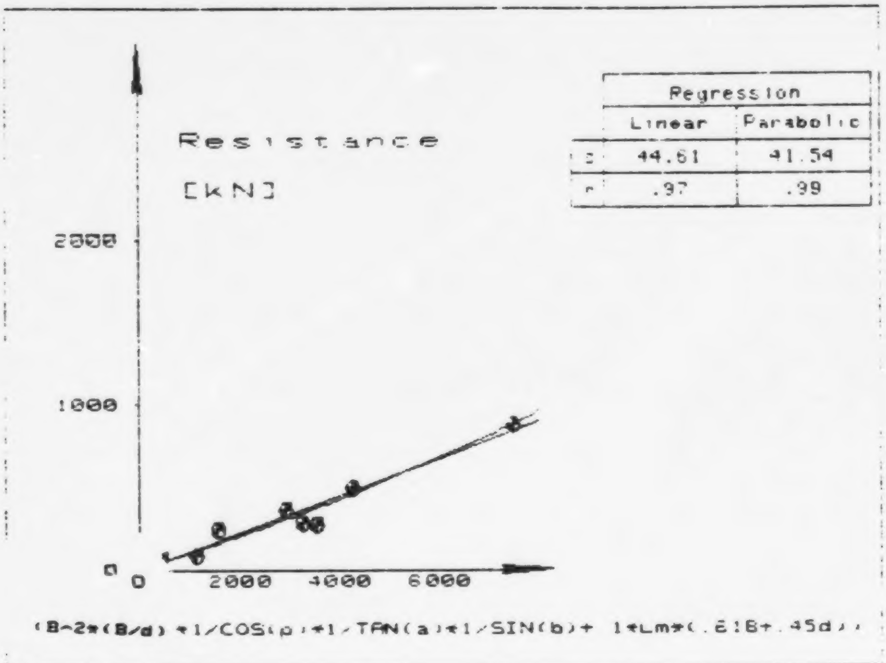

	Regression	
	Linear	Parabolic
s	44.61	41.54
r	.97	.99

HR : 1 [m]

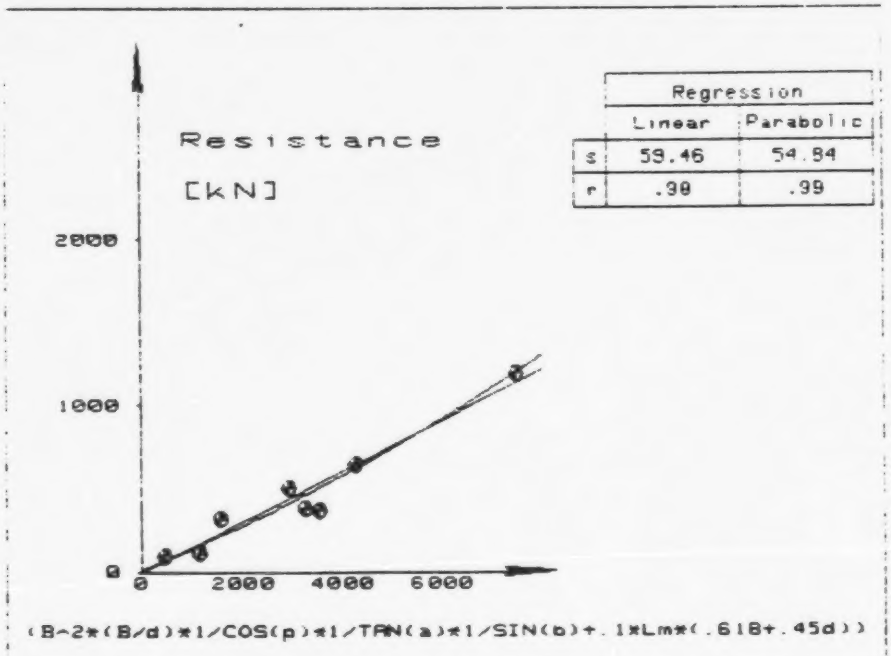

	Regression	
	Linear	Parabolic
s	59.46	54.84
r	.98	.99

HR : 1.5 [m]

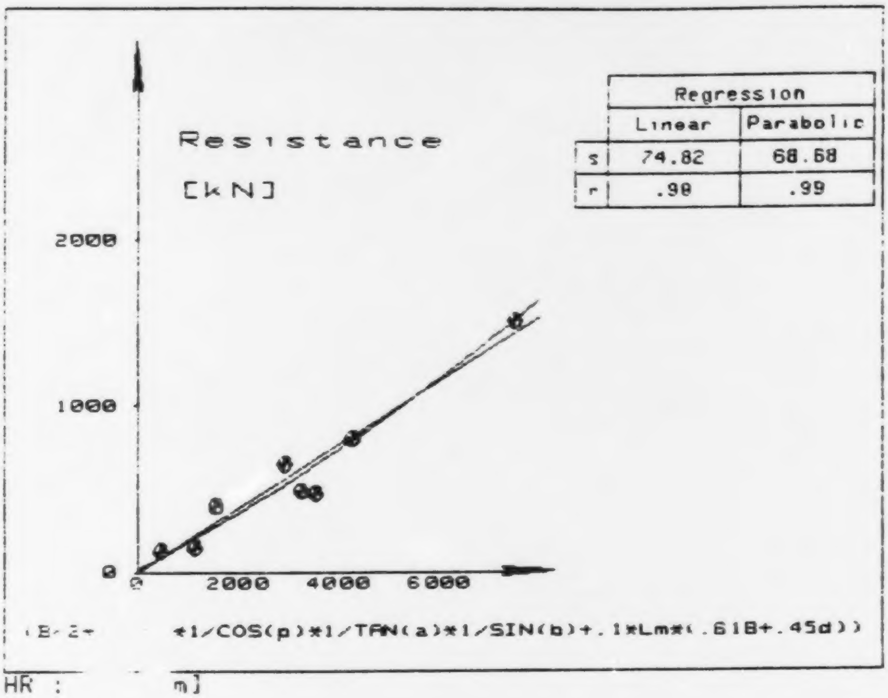

	Regression	
	Linear	Parabolic
s	74.82	68.68
r	.98	.99

(B^2+ *1/COS(p)*1/TAN(a)*1/SIN(b)+.1*Lm*(.61B+.45d))

HR : m]

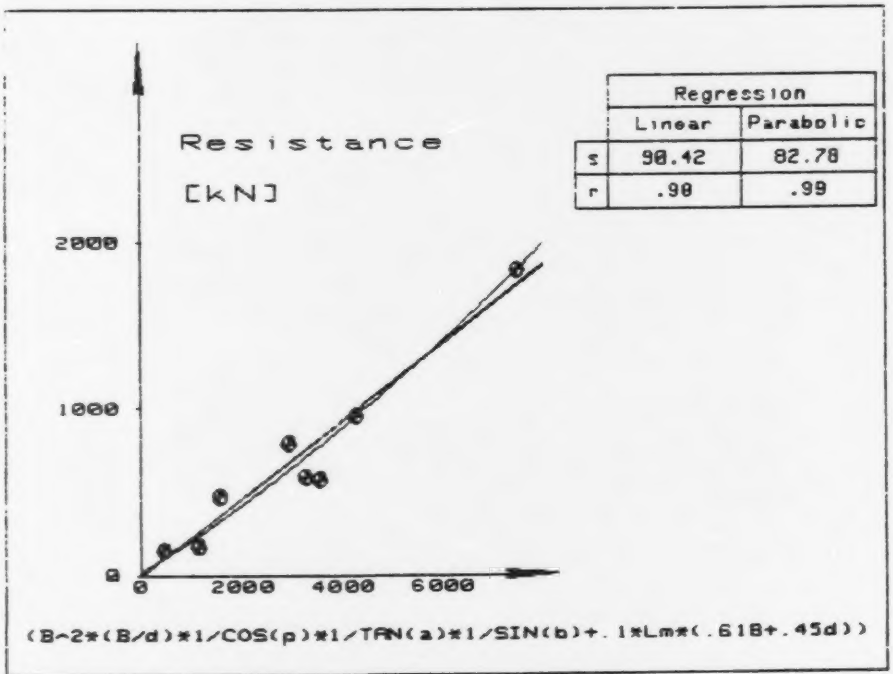

	Regression	
	Linear	Parabolic
s	90.42	82.78
r	.98	.99

(B^2*(B/d)*1/COS(p)*1/TAN(a)*1/SIN(b)+.1*Lm*(.61B+.45d))

HR : 2.5 [m]

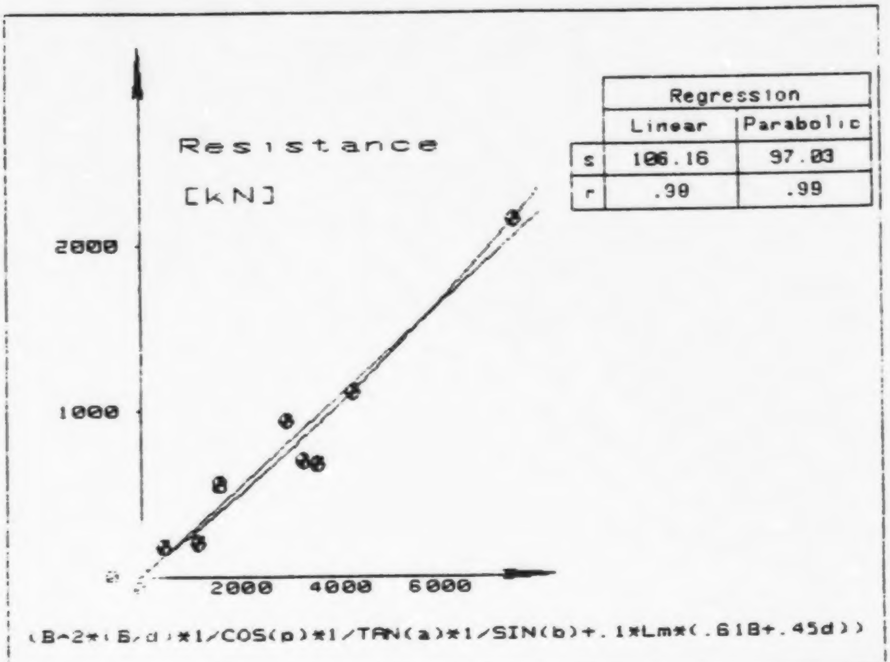

	Regression	
	Linear	Parabolic
s	106.16	97.03
r	.98	.99

HR : 3 [m]

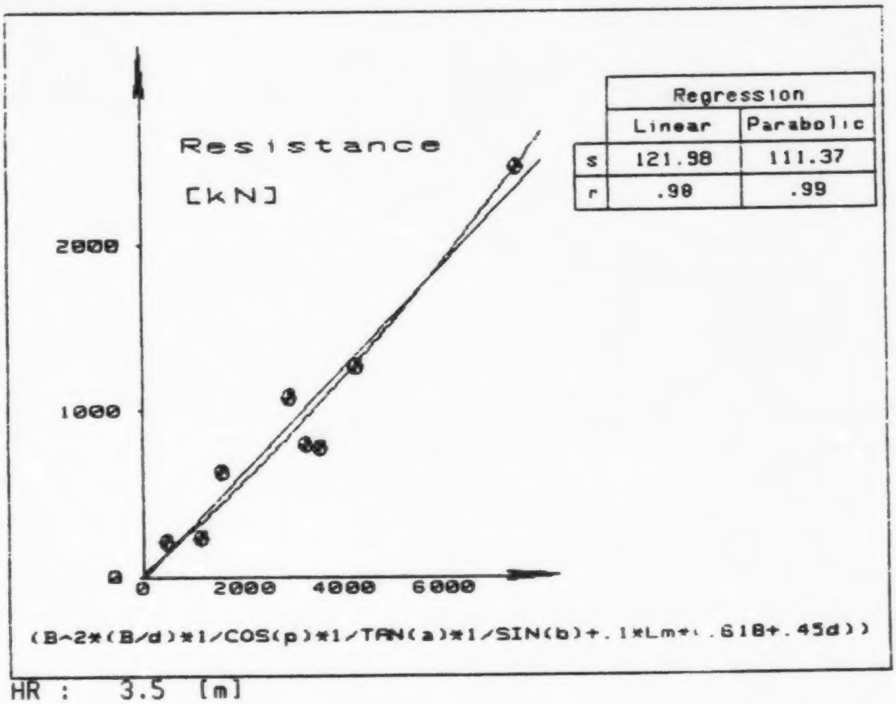

	Regression	
	Linear	Parabolic
s	121.98	111.37
r	.98	.99

HR : 3.5 [m]

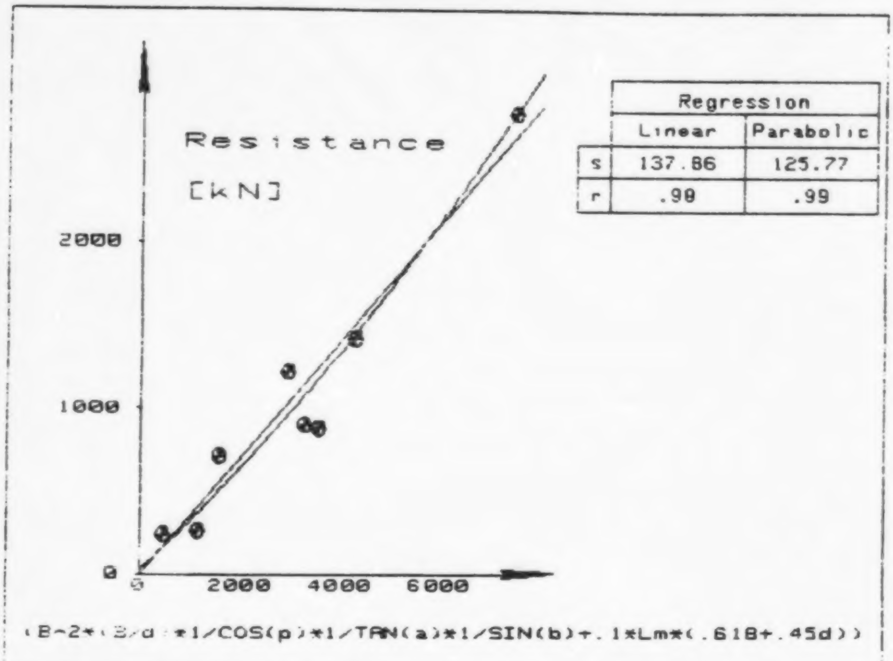

	Regression	
	Linear	Parabolic
s	137.86	125.77
r	.98	.99

HR :   4 [m]

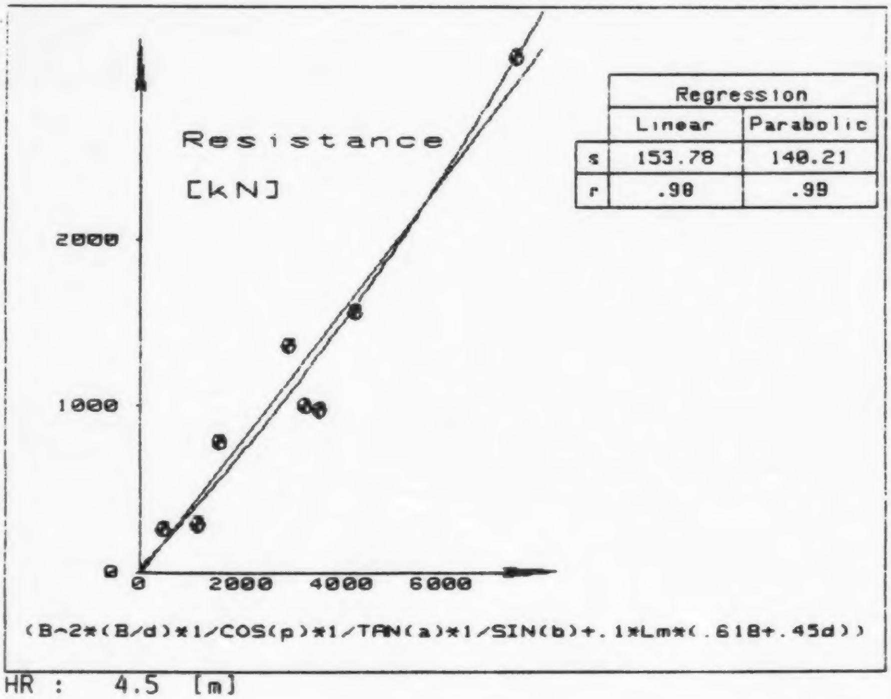

	Regression	
	Linear	Parabolic
s	153.78	140.21
r	.98	.99

HR :   4.5 [m]

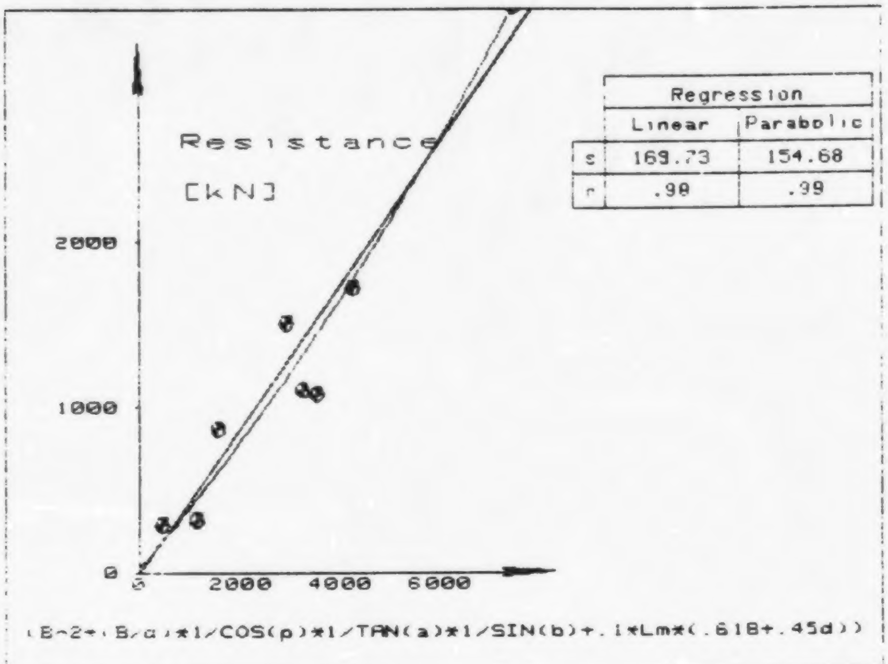

	Regression	
	Linear	Parabolic
s	169.73	154.68
r	.98	.99

HR : 5 [m]

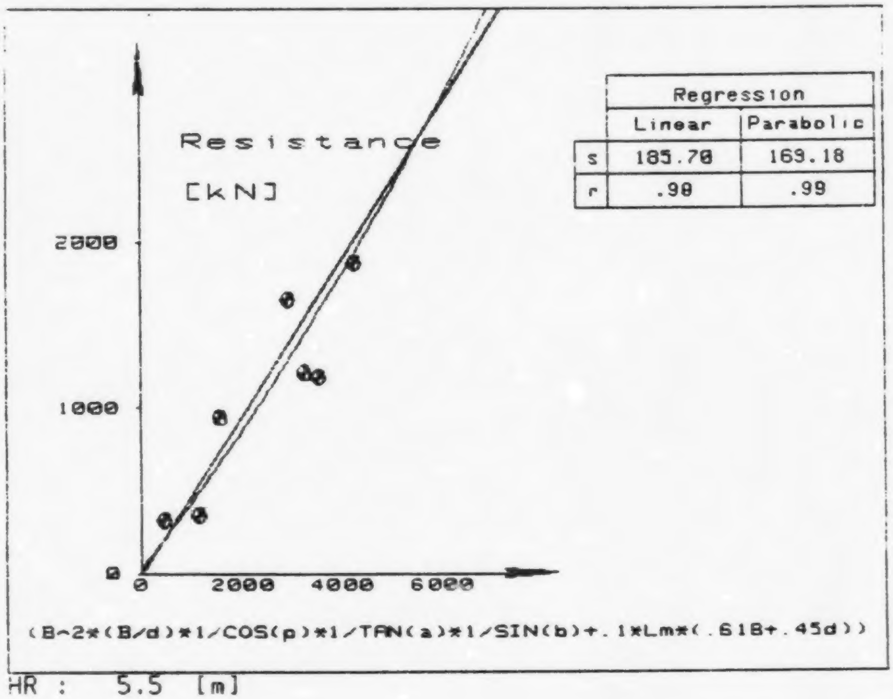

	Regression	
	Linear	Parabolic
s	185.70	169.18
r	.98	.99

HR : 5.5 [m]

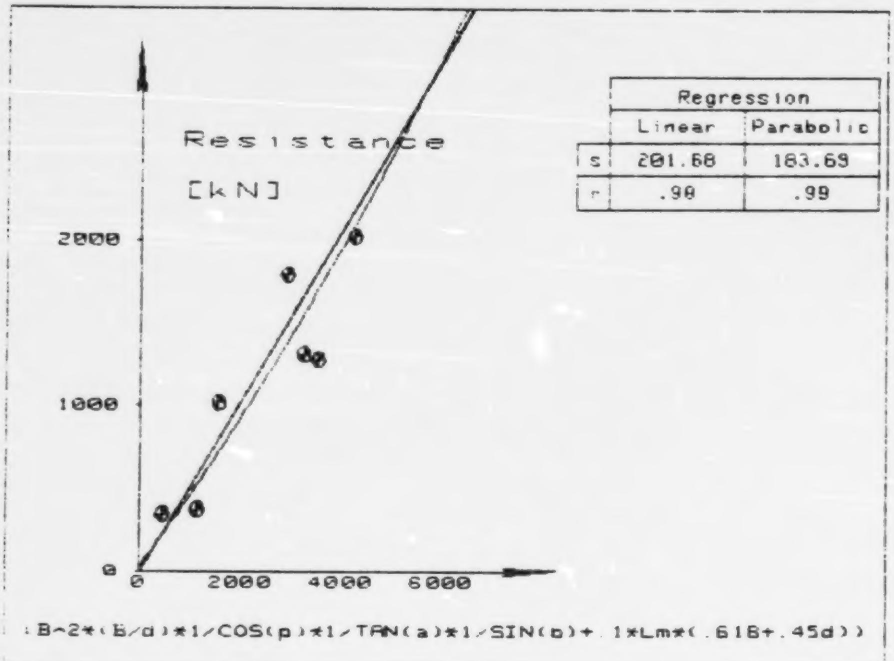
Resistance
[kN]
2000
1000
0
0
2000
4000
6000
(B^2*(B/d)*1/COS(p)*1/TAN(a)*1/SIN(b)+.1*Lm*(.618+.45d))
Regression
Linear
Parabolic
s
201.68
183.69
r
.98
.99

HR : 6 [m]

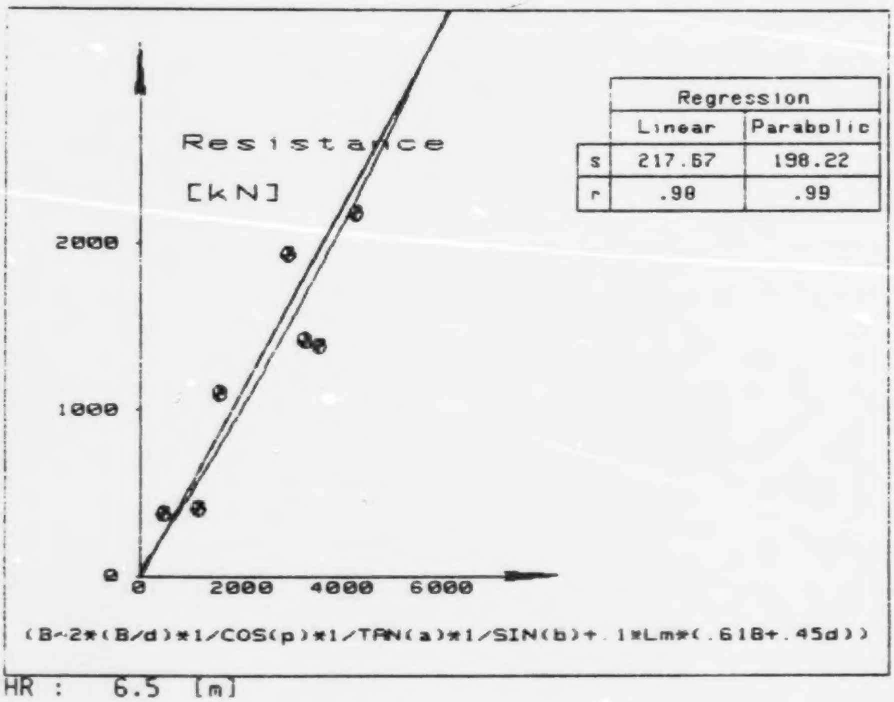
Resistance
[kN]
2000
1000
0
0
2000
4000
6000
(B^2*(B/d)*1/COS(p)*1/TAN(a)*1/SIN(b)+.1*Lm*(.618+.45d))
Regression
Linear
Parabolic
s
217.67
198.22
r
.98
.99

HR : 6.5 [m]

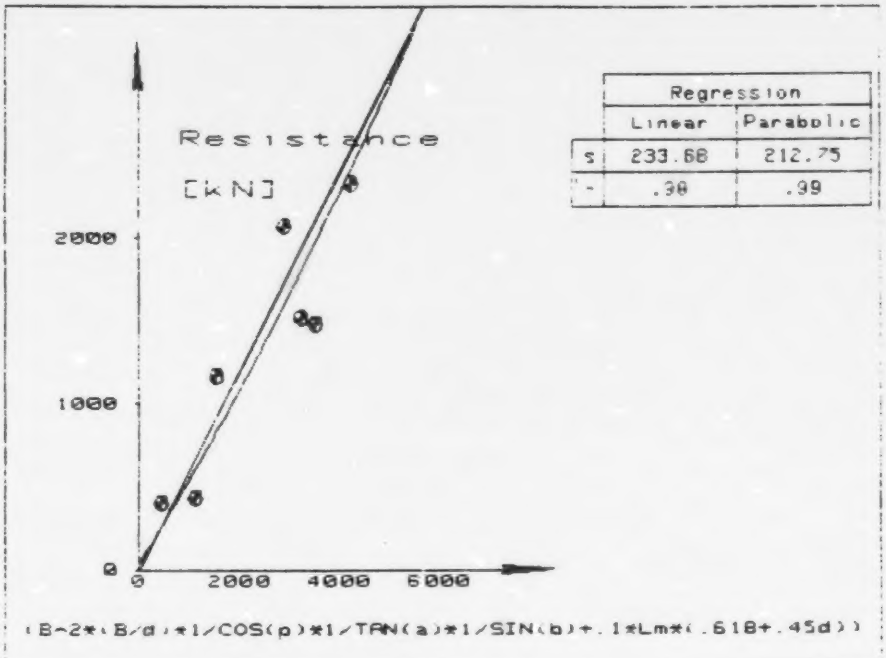

	Regression	
	Linear	Parabolic
s	233.68	212.75
r	.90	.99

HR : 7 [m]

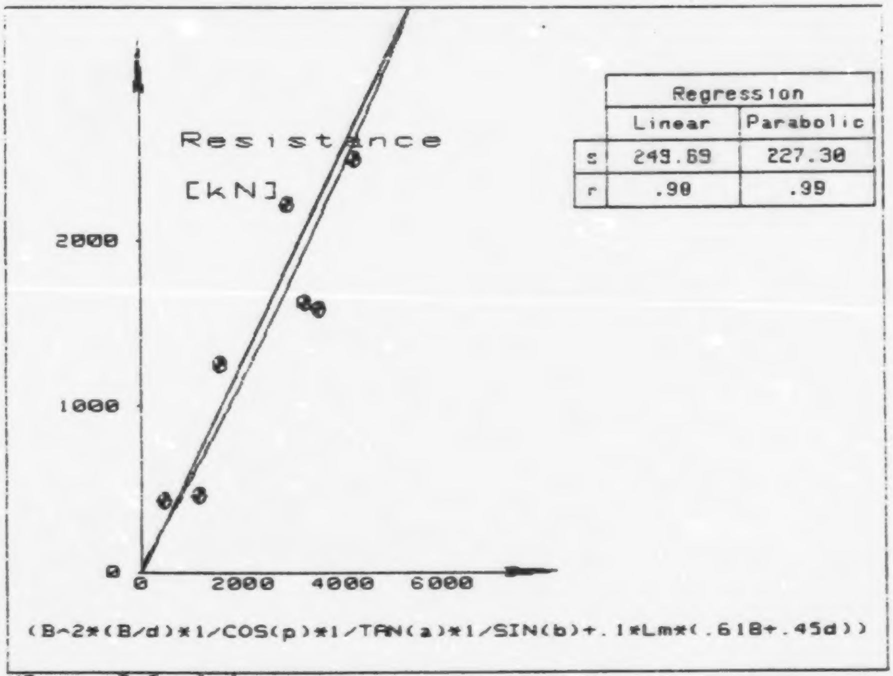

	Regression	
	Linear	Parabolic
s	249.69	227.30
r	.90	.99

HR : 7.5 [m]

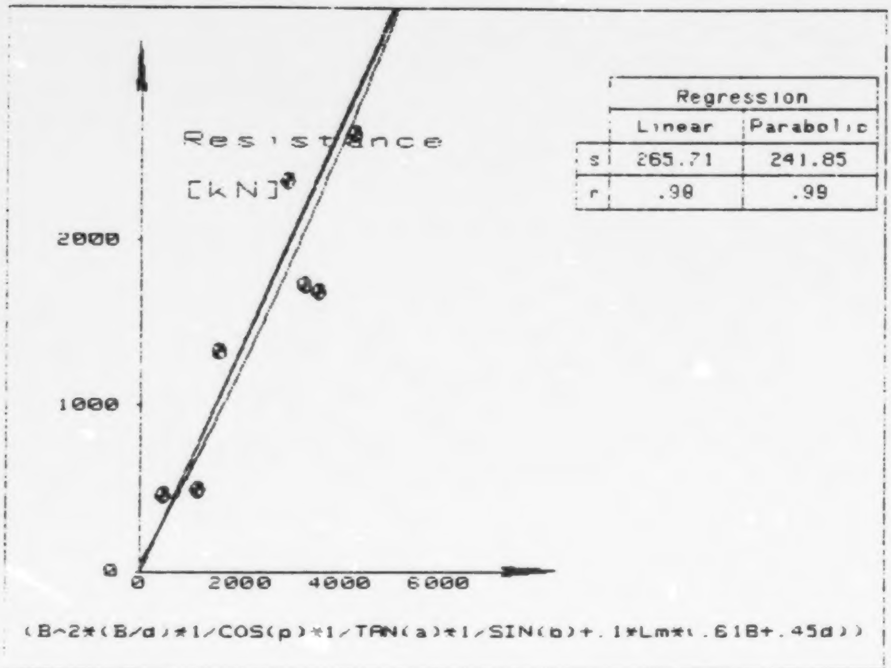

Resistance [kN]
2000
1000
0
0
2000
4000
6000
Regression
Linear
Parabolic
s
265.71
241.85
r
.98
.99
(B^2*(B/d)*1/COS(p)*1/TAN(a)*1/SIN(b)+.1*Lm*(.61B+.45d))

HR : 8 [m]

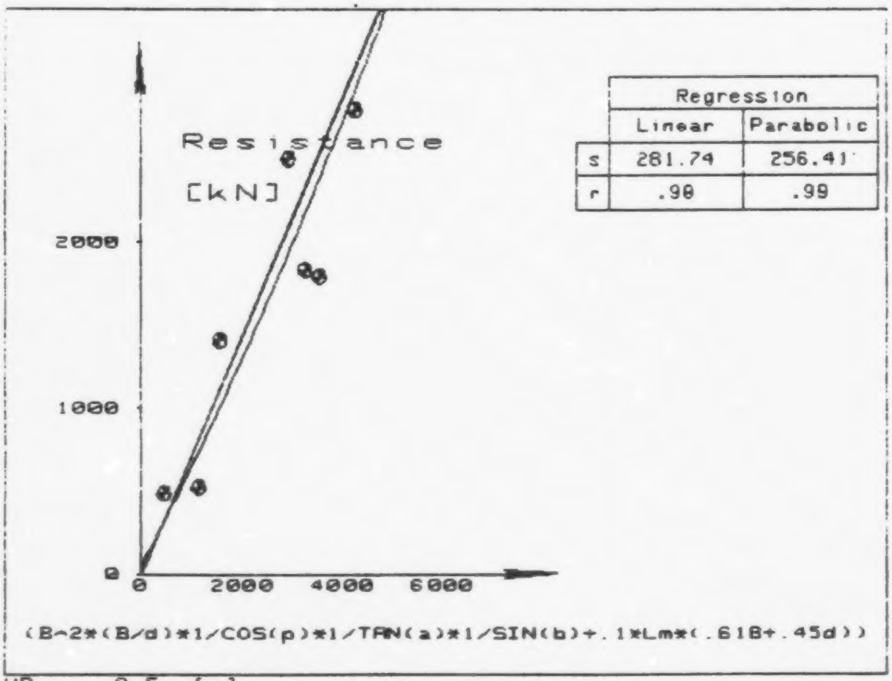

Resistance [kN]
2000
1000
0
0
2000
4000
6000
Regression
Linear
Parabolic
s
281.74
256.41
r
.98
.99
(B^2*(B/d)*1/COS(p)*1/TAN(a)*1/SIN(b)+.1*Lm*(.61B+.45d))

HR : 8.5 [m]

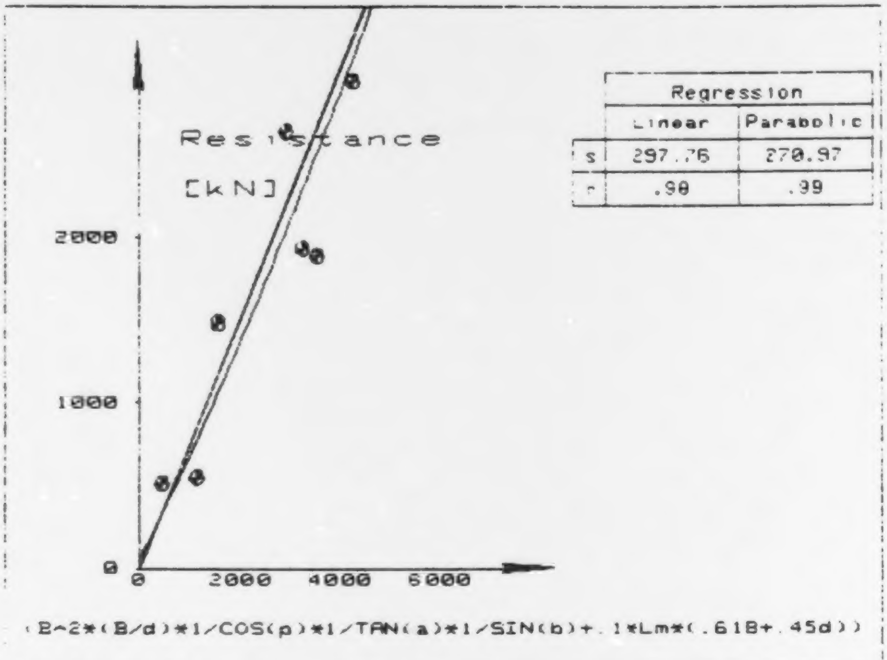

	Regression	
	Linear	Parabolic
s	297.76	270.97
r	.98	.99

HR : 9 [m]

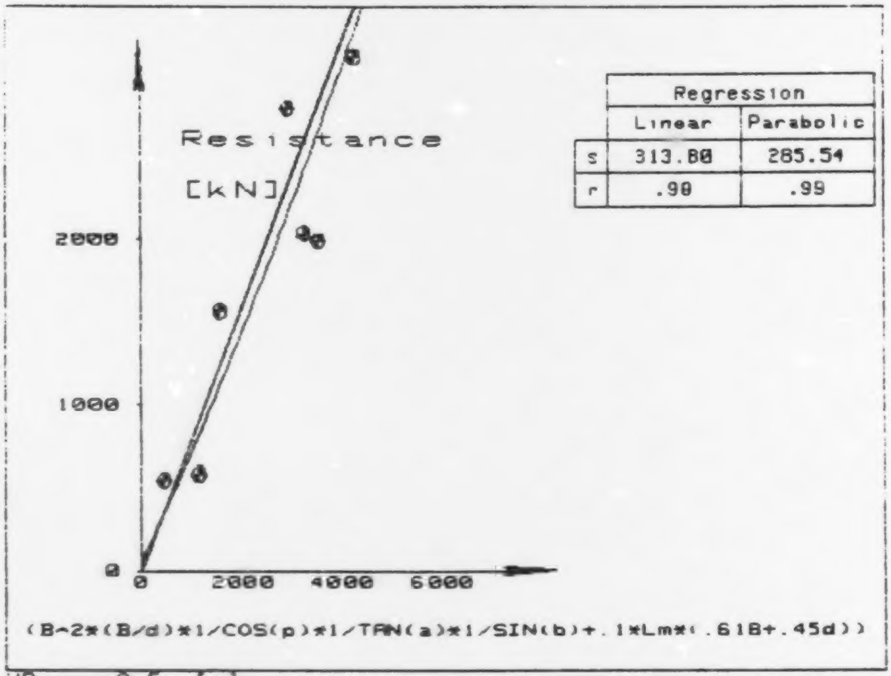

	Regression	
	Linear	Parabolic
s	313.80	285.54
r	.98	.99

HR : 9.5 [m]

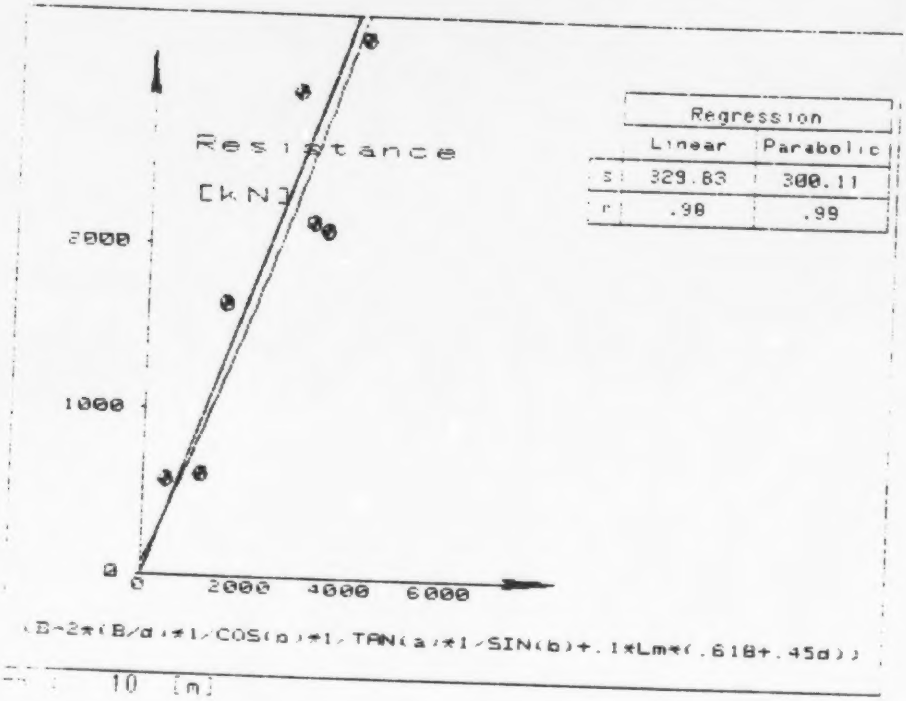

	Regression	
	Linear	Parabolic
s	329.83	300.11
r	.98	.99

APPENDIX C

The contents of this Appendix describes the principles of the computer simulations carried out in connection with the penetration analysis in Section 7. The program applied in the simulation was developed independently of the present work and is proprietary to Wartsila Arctic Inc.

Principles of Simulation

The application of Newton's second law of motion controls the progress of the vessel, i.e.

$$m.\vec{a} = \sum \vec{F} = \vec{R}_{OW} + \vec{R}_{ice} + \vec{R}_{Ridge} + \vec{T}$$

Where:

m = Mass of the ship;

$\vec{a} = \frac{d\vec{v}}{dt} = \frac{d^2\vec{s}}{dt^2}$ = acceleration vector;

$\vec{R}_{OW}$ = Resistance force due to open water;

$\vec{R}_{ice}$ = Resistance force due to unbroken level ice or the consolidated layer with ridges;

$\vec{R}_{Ridge}$ = Pure ridge resistance; and,

$\vec{T}$ = Thrust force

Thrust and resistance components during the penetration phase are shown in Figure C.1.

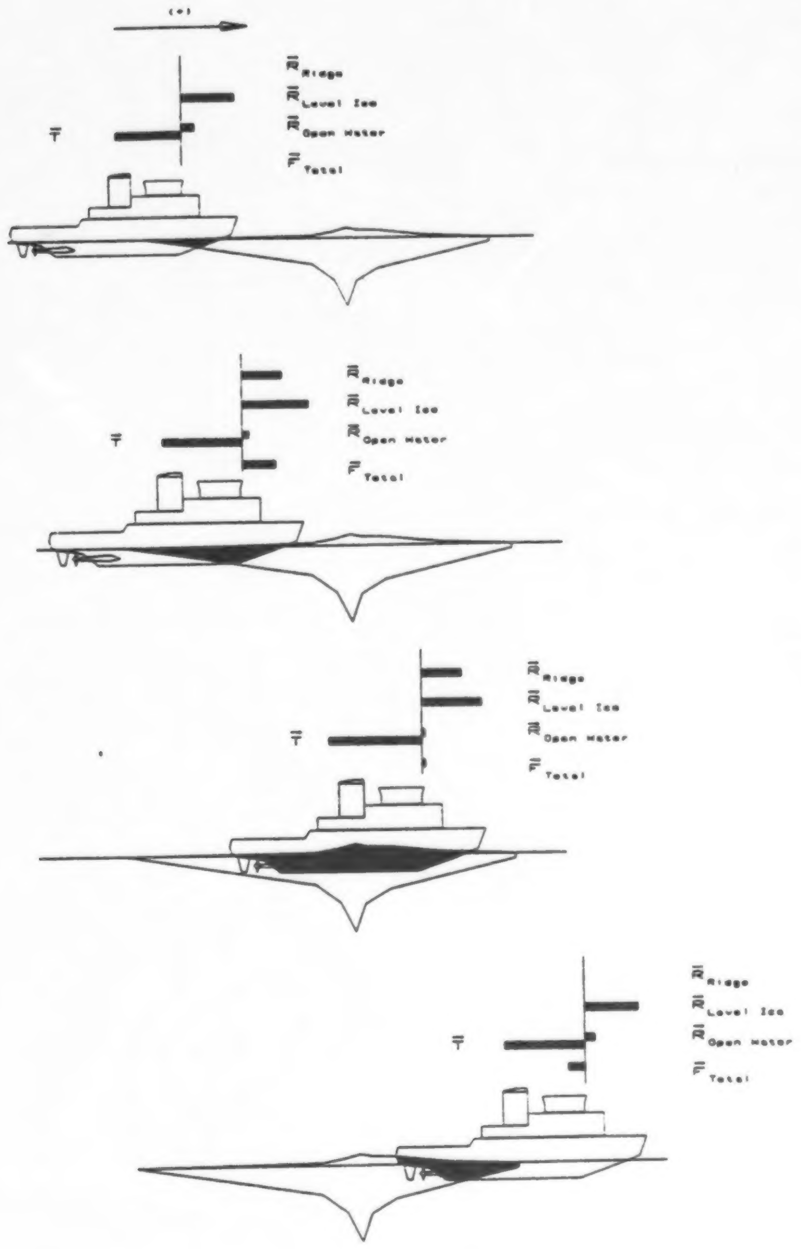

(+)
R Ridge
R Level Ice
R Open Water
F Total
T
R Ridge
R Level Ice
R Open Water
F Total
T
R Ridge
R Level Ice
R Open Water
F Total
T
R Ridge
R Level Ice
R Open Water
F Total
T

Figure C.1 Thrust and Resistance Components During Penetration Phase

The balance of inertia and resistance forces is calculated in intervals of one second steps. The individual resistance components are calculated applying the following methods:

Pure Ridge Resistance:

The formula developed in Section 5 was used to calculate the ridge resistance component. As described, the formula calculates the average resistance experienced during the penetration phase as a function of ship ridge characteristics. In the simulation routine this resistance component is considered from the beginning of the penetration up to the point where the parallel or effective midbody has transitted the ridge.

Level Ice Resistance:

Level ice resistance during the penetration phase is due to the consolidated ice layer. The plot of level ice resistance over ice thickness for a range of bow forms in Figure C.2 indicates the importance of the bow geometry.

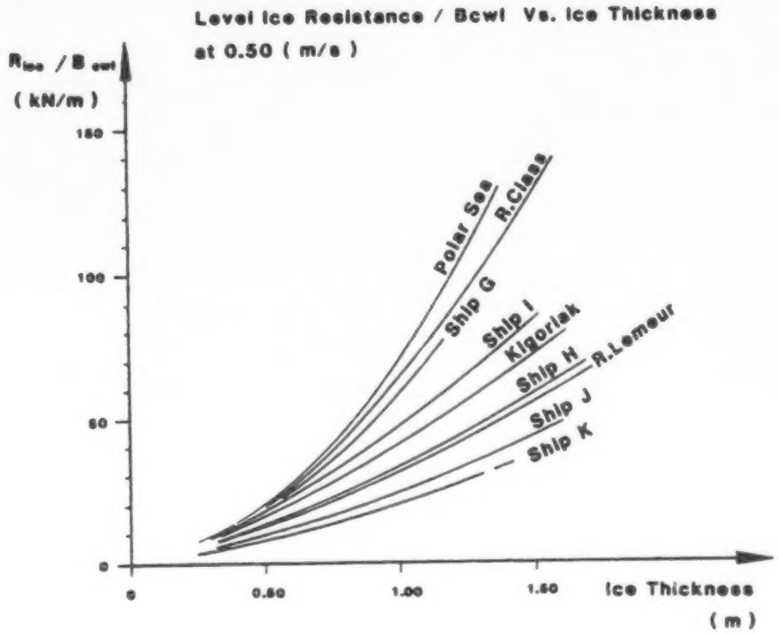

Figure C.2 Significance of Bow Geometry for Level of Ice Resistance

From the above results the following relationship was developed:

$$R_{ice} = 1.29\,\psi \cdot B \cdot t^{1.4}$$

where:

ψ = bow angle (as defined in Figure 5.1);

B = breadth in waterline; and,

t = thickness of consolidated layer.

Open Water Resistance:

The resistance due to open water was calculated according to the method developed by Guldhammar and Harvald. *

Guldhammer, H.E., Harvald, S.A., Ship Resistance, Effect of Form and Principal Dimensions, Akademisk Forlag, Copenhagen, 1965.